April 2009

Submicron Structures from Organometallic Precursors

Benjamin R. St. James
Worcester Polytechnic Institute

Peter Charles Eliopoulos
Worcester Polytechnic Institute

Project Number: ME-SYS-2009

SUBMICRON STRUCTURES FROM ORGANOMETALLIC PRECURSORS

A Major Qualifying Project Report

Submitted to the Faculty

of the

WORCESTER POLYTECHNIC INSTITUTE

in partial fulfillment of the requirements for the

Degree of Bachelor of Science

in Mechanical Engineering

by

Peter Eliopoulos panayiot@wpi.edu
Mechanical Engineering
WPI Class of 2009

Benjamin St. James stjamesb@wpi.edu
Mechanical Engineering
WPI Class of 2009

Date: April 30, 2009

Approved:

Prof. <S. Shivkumar>, Major Advisor

keywords
1. Organometallic
2. Chemical Vapor Deposition
3. Submicron Alloy

Abstract

The goal of this project was to fabricate submicron alloy structures by thermal degradation of organometallic compounds, specifically iron pentacarbonyl and nickelocene. Organometallic compounds were degraded at temperatures of 80, 100, 200, 300 and 400^{o}C to determine ideal mass loss. Structures were analyzed before and after degradation using XRD and SEM. XRD of iron pentacarbonyl identified Fe_3O_4, Fe_2O_3 and Fe. XRD of nickelocene identified NiO and Ni. XRD of iron pentacarbonyl/nickelocene mixtures identified Fe_3O_4, Fe_2O_3, NiO and Ni based on organometallic precursor ratio. SEM of degraded iron pentacarbonyl and iron pentacarbonyl/nickelocene mixtures show fiber structures with diameters in the submicron range. Through the use of higher quality organometallics it is feasible that submicron fiber alloy structures can be generated through thermal degradation of organometallic compounds.

Table of Contents

Table of Figures

List of Tables

List of Equations

1.0 Introduction

Multi-phase alloys with sub-micron structure characteristics have generated a great deal of attention in recent times. It is known that minimization of structural properties of engineering components can lead to significant gains in their performance. Critical engineering parameters such as melting point, thermal conductivity, electrical conductivity, and magnetic properties at the submicron scale differ greatly from properties observed of bulk materials. Concurrently, alloyed materials at the submicron scale, such as spinel ferrites of the form MFe_2O_4, exhibit novel properties that are not demonstrated by individual species of their respective constituents.

Low dimensional metal complexes have significant potential in application for chemical sensors, catalysis, energy storage and conversion, biomedical engineering, and separation technologies with implications towards water and air purification. Magnetic properties of nanoparticles have significant prospects in products magnetic products such as magnetic recording, high density data storage, magneto-caloric refrigeration, contrast enhancement in magnetic resonance imaging and magnetically guided drug delivery. Specifically, research promoting iron nanowires as a possible electromagnetic wave absorber has been studied due to the wires high permeability and shape anisotropy. In applications that are volume dependent, such as fuel cell technologies, solar cell photocollectors and volatile organic compound catalyst, submicron two dimensional structures offer the benefit of having a larger surface area to mass ratio, which allows them to perform more effectively. Investigations of low dimensional bismuth oxide fibers synthesized by electrospinning have been established as a material useful in the reduction of methyl orange pollutants in water by photocatalysis under UV and visible light sources.

Investigators have conducted experiments examining the utilitization of metal-organic precursors in the formation of metal complexes at the submicron level. Notable attention has been given to

organometallic complexes formed with transition metals due to their nature their existence as a low-melting crystal, liquid or gas at ambient temperature. Several techniques that have been reported successful in the formation of submicron metal structures from organometallic precursors include electrospinning, high temperature chemical vapor deposition, laser assisted chemical vapor deposition, plasma enhanced chemical vapor deposition, vapor-liquid-solid method, sol-gel technique and metal organic vapor phase epitaxy. Although these methods have been tested to be appropriate in metal deposition, excessive capital investment and operating costs are preventative factors in the widespread use of these techniques. Previous investigations of organometallic deposition techniques are generally limited to single metal species. Experimental studies have established interest for applications involving catalyst metals, such as nickel and platinum, but research is largely undeveloped for binary metal complexes.

If established as a means of producing alloyed deposition products, organometallic deposition could significantly improve industrial processes that are used to produce thin films, nanoparticles, and fiber complexes in engineering components. High temperature chemical vapor deposition of organometallic compounds offers a straightforward method of isolating metal species from organometallic reagents that can be conducted without the necessity of highly monitored reaction atmospheres or excessively high temperature. Additionally, this technique is well suited for scalability to industrial large scale applications.

This study investigated the fabrication of alloyed metal/metal-oxide compounds by means of thermally degrading an organometallic compound by direct heating. The degradation properties of the chosen organometallic were analyzed by determination of weight loss at various graduation temperatures and sample masses, x-ray diffraction, scanning electron micrograph, energy

dispersive x-ray spectroscopy, and x-ray diffraction. Structures were benchmarked against steel 1018 whose chemical composition was known.

2.0 Background

2.1 Alloyed Components

An alloy can be defined as a substance that has metallic properties and is composed of two or more chemical elements where at least one element is a metal. (1). Alloys composed of two elements are known as binary alloy systems. From 45 of the most common metals, 990 possible binary combinations can be generated. Alloys may exist in either homogeneous solution or as a mixture; homogeneous solutions are constituted by one phase, where in a mixture multiple phases will be observed. In the solid state, three possible phases may be observed: [1] Pure-metal, [2] Intermediate alloy phase or compound, and [3] solid solution. (1).A solution is composed of two parts: Solvent and a Solute. The solute is the minor part of a solution or the material that is dissolved. A solid solution is a solution that exists in the solid state consisting of two kinds of atoms within one type of space lattice. (1). Metal alloy casting can be traced back as far as 6000 B.C, with existing bronze pieces dating back to around 3000 B.C. (2). In this process, liquid metals are poured into a form and are allowed to cool. Powder metallurgy is another process developed by the Egyptians around 3000 B.C. (3).

Superior engineering characteristics have lead to the widespread use of alloys. These new age techniques have been developed to more effectively take advantage of the ameliorative properties alloys imbue onto engineering components. Modern techniques for generation of alloys include vacuum deposition, chemical vapor deposition, electrospinning and electroplating. These techniques focus primarily on the surface of the material, as the environment-surface interactions control many engineered parameters, such as wear resistance, corrosion, and other important surface phenomena.

2.2 Conventional Methods for Development of Alloyed Submicron Structures

Alloyed materials have superior properties when compared to the constituent metals that they consist of. At submicron architectures, alloyed components often exhibit better physical characteristics than alloys formed by traditional methods. A variety of strategies have been developed to generate

submicron alloy architectures for applications engineered components. These methods include electrospinning, electrodeposition, and thermal spraying.

2.2.1 Electrospinning

Electrospinning is an intimate process which spins fibers of various diameters, ranging from 10nm to several hundred nanometers (4). A diagram of electrospinning is shown in Figure 1 (5)

.

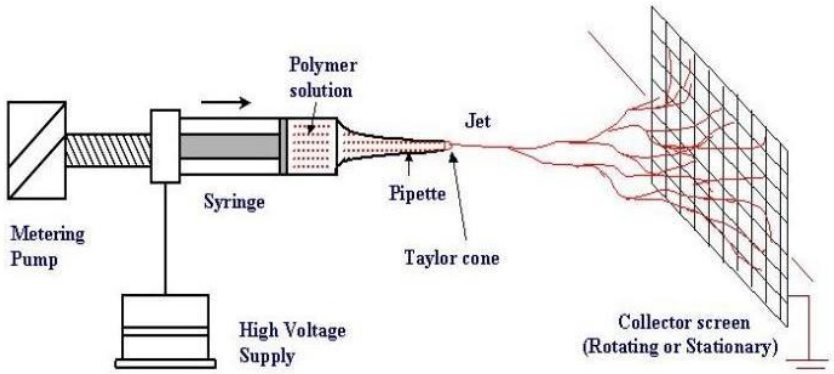

Figure 1: Schematic of Electrospinning Apparatus

Through the process of electrospinning, a high voltage electric field is formed between a polymer solution enclosed in a glass syringe and a collection target. As the voltage gradient increases it comes to a critical value, after which surface tension of the droplet is overcome causing the solution to jet across to the collector plate (4). From the time the droplet leaves the pipette until it reaches the collector plate, it undergoes stretching due to electrical instabilities that cause it to bend and deform. In addition to stretching, the liquid solvent begins to evaporate causing the diameter of the jet to decrease (4).

Electrospinning has been established as a method of producing nanocrystalline ferrites; electrospinning has been used to produce $NiFe_2O_4$, $CoFe_2O_4$, $MnFe_2O_4$, and $BiFe_2O_4$ compounds (6). These materials are

significant for their magnetic properties which lends to application in semiconductor materials. These materials exhibit novel magnetic properties at small architectures. Studies conducted by Ponhan et al. have documented successful attempts in fabricating submicron fibrous structures that exhibit enhanced magnetic properties when organized as nanorods and nanowires (7). Use of electrospinning is primarily limited to the production of polymer and ceramic fibers as precise solution viscosity of precursor solution must be achieved to form fibrous architectures (6). Sample SEM pictures of electrospun $CuFe_2O_4$matrices can be viewed in the Figure 2 (6).

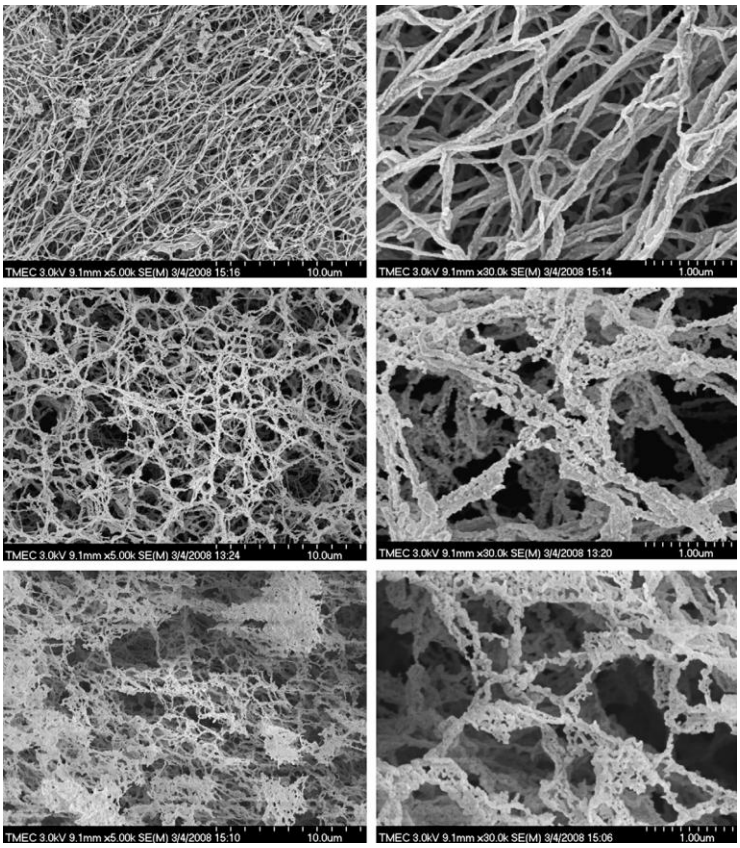

Figure 2: SEM of Submicron CuFe2O4 Fibers Generated by Electrospinning

$NaCo_2O_4$ materials have been investigated via electrospinning for the application of waste-heat recovery in electronic devices. In this material, the CoO_2 allows for electrical conduction, where an insulating layer of Na works as a charge reservoir to stabilize the crystal structure that unlike other candidates remains resistant to oxidation and efficiency loss at high temperatures. (8)

2.2.2 Electrodeposition

Electrodeposition is a surface process in which metal ions suspended in solution are drawn to a desired substrate by means of dissimilar charges. When deposited, metals act as seed crystals from which other metal species may agglomerate either by nucleation or surface diffusion. Figure 3 displays the basic mechanisms associated with electrocrystalization that occurs during the electrodeposition process (9).

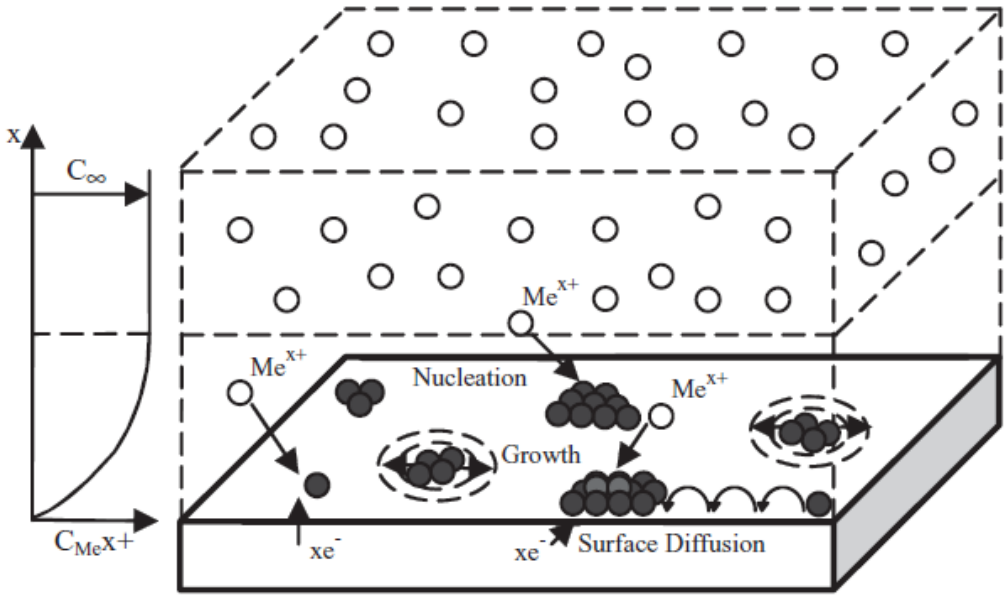

Figure 3: Schematic Describing Methods of Crystal Growth in Electrodeposition

Electrodeposition has been reported successful in producing metal and metal alloys including Ni, Co, Pd, Cu, Zn, Ni-P, Ni-Fe, Ni-Zn, Co-W, Co-Fe, Pd-Fe, Ni-Fe-Cr, and Fe-Co-Ni (9).

2.2.3 Thermal Spraying

Thermal Spraying, or Flame spraying, is a process where thin layers of metal are applied to a substrate material, such carbon steel, by means of atomizing a liquid metal onto a substrate. This process is desirable over other deposition methods for its higher throughput when compared to physical and chemical vapor deposition techniques (10). This process creates an outer coating onto a component that brings the benefit of imbuing the steel piece with resistance to oxidation by completely isolating the base metal from the environment it is placed in. Commonly Zinc, Aluminum and alloys are commonly applied to steel parts as protective coatings. Aluminum alloys are desired for their formation of an

insoluble hydrated aluminum oxide film which forms on the top most surface of aluminum materials that guard against atmospheric corrosion, even in acid media. Al-Zn coatings add the benefit of outstanding atmospheric protection with added galvanic protection. These materials provide increased longevity when compared to pure-zinc films while providing resistance in marine environments that surpasses that the pure-aluminum coating (11). Studies performed by de Rincon et al. determined that alloy materials provided via thermal spray methods were superior to traditional methods of hot dipping and electroplating (11).

2.3 Organometallic

An organometallic is a compound that contains (at least one) direct carbon-metal linkages (13). Most organometallic compounds resemble organic compounds in their physical properties, rather than inorganic compounds. Organometallic compounds can often exist as a low-melting crystal, liquid or gas because of the discrete molecular structures that can be formed by these compounds. These complexes are often soluble in a wide variety of weakly polar solvents (14). Two types of metal-metal bonding can be distinguished: homopolar bonding between metals of very similar electronegativities, typified by $R_3Si\text{-}SiR_3$, $R_3Sn\text{-}PbR_3$ and $R_2As\text{-}AsR_2$; and heteropolar bonding between very dissimilar metals. Examples of systems containing multiple Tin atoms in a chain have been demonstrated (15).

2.3.1 Metal Carbonyls

The class of binary metal carbonyl compounds, which exist in the general form $M_x(CO)_y$ has been studied extensively (15). These complexes are generally formed in a direct synthesis reaction involving a transition metal powder in an excessive carbon monoxide (CO) environment under appropriate heating (1). This method is most appropriate for the formation of nickel and iron carbonyls; nickel will form carbonyl complexes at near ambient pressure and temperature (estimated 30°C, 1 atm for Nickel Tetracarbonyl). Iron and Nickel carbonyl species are volatile at room temperature (16).

Base metal atoms that have been documented include those from the 3d (Sc, Ti, V, Cr, Mn, Fe, Co, Ni) 4d (Y, Zr, Nb, Mo, Tc, Ru, Rh, Pd, and Ag) and 5d (Hf, Ta, W, Re, Os, Ir, Pt, Au) groups. Metals can form with one or multiple metal atoms at the center of the molecule; 1, 2, 3, and 4 metallic atoms within a compound have been reported.

2.3.2 Metallocene Complexes

Another common organometallic ligand is the cyclopentadienyl ligand, C_5H_5. For electron-counting purposes, a C_5H_5 ligand can be considered to be either an aromatic anion, $C_5H_5^-$, or a neutral radical, C_5H_5 (15). A cyclopentadienyl ligand can coordinate to a metal atom in two principle structural arrangements: a metal can form a shared π-bond acting as a pentahapto ligand or the metal can forma a localized cyclopentadiene σ-bonding within the ring (15).

2.3.2.1 Ferrocene

Ferrocene (dicyclopentyl iron) is an organometallic compound with bonding sites between the cyclopentadienyl group(s) and the iron atom. This compound is resistant to hydrolytic and oxidative cleavage. It is oxidizable reversibly to the ferricinium ion ($^+$), and as an unsaturated organic derivative it goes through substitution rather than addition, reactions. The rotational barrier of the two rings about the C_5H_5-Fe- C_5H_5 axis is low, but at ordinary temperatures, the ring of hydrogens is staggered. The molecular orbital accounting for these structural data involves not only bonding of π-electrons from the cyclopentadienyl group to the hybridized d-orbital's of the iron, but the back donation of electrons from the filled d-orbital's of the iron to the unoccupied ant bonding π-electrons of the hydrocarbon rings. In addition to Iron (II) and Iron (III), titanium (IV), Chromium (II) cobalt (II), nickel (II), and Copper (I) appear to form complexes of the sandwich or half-sandwich type (15).

2.3.2.2 Nickelocene

Unlike ferrocene, nickelocene does not satisfy the 18-electron rule; this compound remains stable with an outer valence of 20 electrons (17). This compound is easily oxidized into the nickelocenium ion (19

VE), which is probably due to the electronic structure of the molecule; there is a general agreement that the highest molecular orbitals have mainly 3d character with unpaired electrons occupying the antibonding e_{1g} orbitals (17). Studies have investigated the feasibility of Nickel deposition from Nickelocene precursor on Silver and Copper substrates (18).

2.4 Degradation Mechanisms in Organometallic Compounds

Organometallic compounds have been reported to degrade by various mechanisms determined by experimental approach. In general terms, Reactions can be classified as thermal decomposition (pyrolysis) reactions, hydrogen reduction and coreduction, oxidation and hydrolysis, and carbidization and nitridation reactions.

2.4.1.1 Thermal-Decomposition (Pyrolysis) Reactions

Thermal decomposition reactions involve the denaturing of reactants into more elementary molecules: their respective metals and ligand groups. Due to the chemical structure of the free metal, a solid powder is deposited and gas molecules are left maintained within the environment (19). An explanation of decomposition reactions can be viewed in Equations 1, 2, 3, 4.

Hydrocarbon Decomposition

$$CH_4(g) \rightarrow C(s) + 2H_2(g) \quad (1)$$

Halide Decomposition

$$WF6(g) \rightarrow W(s) + 3F_6(g)$$

$$TiI_4(g) \rightarrow Ti(s) + 2I_2(g) \quad (2)$$

Carbonyl Decomposition

$$Ni(CO)_{4(g)} \rightarrow Ni(s) + 4CO(g) \quad (3)$$

Hydride Decomposition

$$SiH_4(g) \rightarrow Si(s) + 2H_2(g)$$

$$B_2H_6(g) \rightarrow 2B(s) + 3H_2(g) \quad (4)$$

2.4.1.2 Hydrogen Reduction Reactions

Chemical reduction is the result of an element lowering its oxidation state by gaining an electron. This is done by the reaction of a precursor molecule with a gas, usually hydrogen for halide complexes due to its ability to perform decompositions at low temperatures. Equation 5 depicts the reagents and final products of the reaction. It should be noted that often intermediate reactions will occur; these reactions were omitted for the sake of simplicity.

Hydrogen Reduction

$$WF_6(g) + 3H_2(g) \rightarrow W(s) + 6HF(g)$$
$$SiCl_4(g) + 2H_2(g) \rightarrow Si(s) + 4HCl(g) \quad (5)$$

2.4.1.3 Hydrogen Coreduction Reactions

Similarly to (singular) reduction reactions, coreduction reactions can be observed by using two reagents of similar morphology, which reduce to form an intermetallic compound and a byproduct gas. This reaction is outlined in Equation 6.

Coreduction Reduction

$$TiCl_4(g) + 2BCl_3(g) + 5H_2(g) \rightarrow TiB_2(s) + 10HCl(g) \quad (6)$$

2.4.1.4 Oxidation and Hydrolysis Reactions

Oxidation and Hydrolysis reactions are the result of nucleophillic attack by oxygen present in air or water. These reactions are outlined in Equations 7 and 8.

Oxidation Reaction

$$SiH_4(g) + O_2(g) \rightarrow SiO_{2(s)} + 2H_2(g)$$
$$SiCl_4(g) + 2CO_2(g) + 2H_2(g) \rightarrow SiO_2(s) + 4HCl(g) + 2CO(g) \quad (7)$$

Hydrolysis Reaction

$$2AlCl_3(g) + 3H_2O(g) \rightarrow Al_2O_3(s) + 6HCl(g) \quad (8)$$

2.4.1.5 Carbidization and Nitridation Reactions

Carbidization reactions are most commonly achieved as the result of the reaction of a metal halide complex with a gaseous hydrocarbon such as methane. Similarly, Nitridation can be developed as the

result of a reaction of a metal halide with ammonia due to its positive free energy of formation. These reactions are being summarized in Equations 9 and 10. (19)

Carbidization Reaction

$$TiCl_4(g) + CH_4(g) \rightarrow TiC(s) + 4HCl(g) \quad (9)$$

Nitridation Reaction

$$3SiCl_4(g) + 4NH_3(g) \rightarrow Si_3N_4(s) + 12HCl(g) \quad (10)$$

2.5 Metal-organic Chemical Vapor Deposition

Metal-organic chemical vapor deposition (MOCVD) is a process that refers to the deposition of thin layers of compound material by co-pyrolysis of combinations of organometallic compounds and hydrides. Particular interest has been leant to this method the formation of alloyed semiconductor materials as well as doping additives due to its high quality yield and growth rate, which can be controlled within the nanometer range; deposits of less than 10nm in thickness have been reported (19). Additionally, MOCVD has been documented as a method alloy aluminum/copper complexes for semiconductor metallization in efforts to reduce electromigration in aluminum semiconductors. (19).

A variety of mechanisms have been studied in the pursuit of forming high purity metal films. These techniques primarily focus on the thermal degradation of an organometallic species to adsorb elemental metals onto the surface of a desired substrate. These techniques include high temperature organometallic chemical vapor deposition, laser induced chemical vapor deposition, laser ablation chemical vapor deposition, ultraviolent induced chemical vapor deposition, plasma enhanced chemical vapor deposition, focused ion chemical vapor deposition, electron beam chemical vapor deposition, fluidized bed chemical vapor deposition, atomic layer deposition, and organometallic vapor phase epitaxy.

2.5.1 High Temperature Organometallic Chemical Vapor Deposition

The principle of organometallic chemical vapor deposition is to vaporize a metal containing precursor, organometallic compounds, which undergo thermal decomposition at higher temperatures. Metal

precipitate is then deposited to form a thin metallic layer on a given substrate material. Deposition is initiated on the substrate material by heating the organometallic compound to a temperature beyond the stability of the organometallic compound, there by forming decomposition products. Due to the instability of organometallic compounds, OMCVD can be performed at temperature ranges hundreds degrees Celsius lower than methods that rely on other techniques. (20)

This method is not without drawbacks, as there is an associated likelihood of the inclusion of impurities due to the non-combustion of organometallic constituents. A diagram describing the process of OMCVD can be viewed in Figure 4. Numbers included in the diagram refer to the different stages of the decomposition process. These steps are:

1. Convection of gaseous reagents
2. Diffusion of reagents towards the substrate
3. Adsorption of the reagents onto the substrate
4. Chemical reaction of the adsorbed species producing nuclei and reaction to give a metal
5. Desorption of the gas products of the reaction
6. Diffusion of these gas products through the boundary layer
7. Gas evacuation of the system.
   (20)

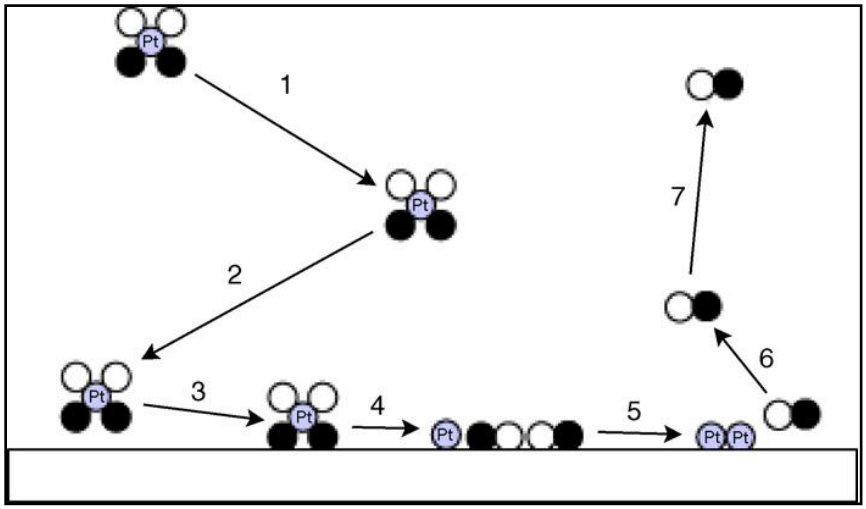

Figure 4: Degradation for Organometallic Species by Chemical Vapor Deposition

2.5.2 Laser Induced Chemical Vapor Deposition

Laser induced chemical vapor deposition (LICVD) is a process that is similar to OMCVD in that organometallics are deposited via degradation onto a desired substrate. The difference in this process is that a low or high powered laser (depending on application) is used to initiate the degradation mechanism of organic precursor.

Because of the controlled aperture of the laser, tight control of deposition of material onto the surface can be achieved. Additionally, because the reaction is catalyzed by the laser, lower substrate temperatures, generally 30-100°C can be used. Growth characteristics of materials generated in this process are generally faster than traditional OMCVD. Higher vapor pressure can be used in this technique (20).This process has documented problems with photolysis due to light exposure as well as overheating of the substrate which can lead to laser desorption (20). The Figure 5 describes the generalized laser-substrate interaction for different laser powers.

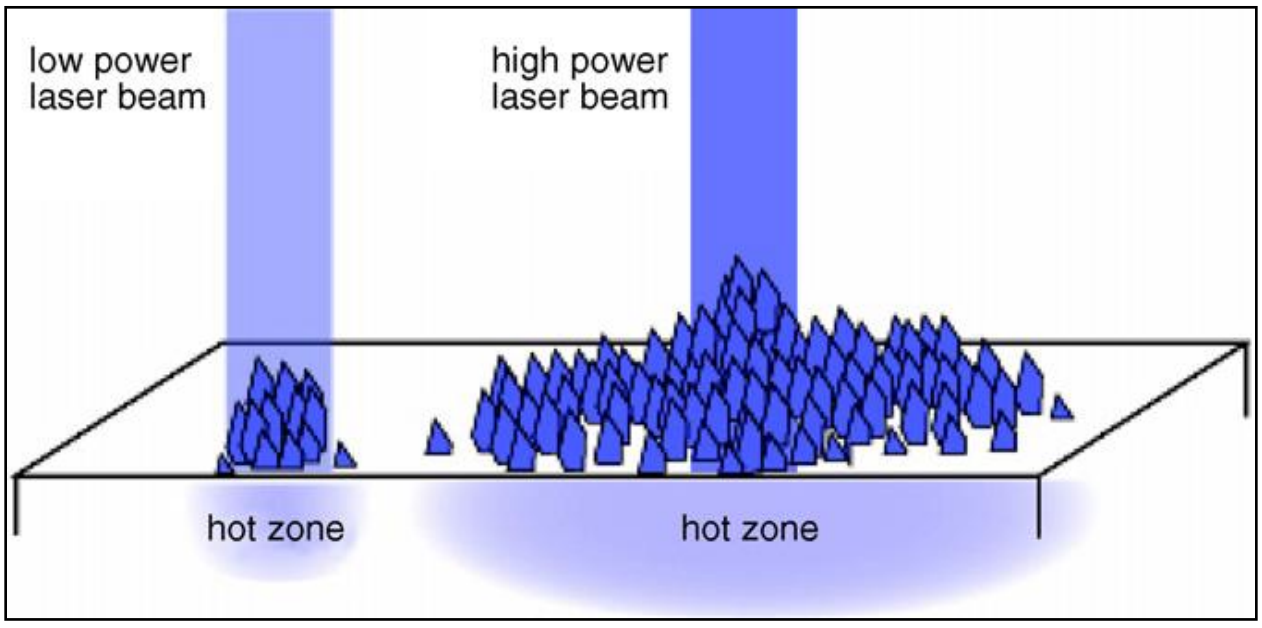

Figure 5: Deposition of Metal by Low and High Powered Laser Induced Chemical Vapor Deposition

2.5.3 Laser Ablation Chemical Vapor Deposition

Laser pyrolysis has been successful in producing magnetic iron oxides from organometallic precursors. In this process a gaseous species is excited by laser radiation acting as a catalyst. Nucleated particles formed by the gas stream are collected at the exit. This process is discrete from laser induced chemical vapor deposition because particles are formed in a dynamic process without substrate. In this method, Iron pentacarbonyl is a common precursor material (decomposition into iron carbon monoxide), using ethylene as a carrier gas. Iron particles are then oxidized in air resulting in the formation of iron oxide particles (21). A schematic describing this process can be viewed in Figure 6.

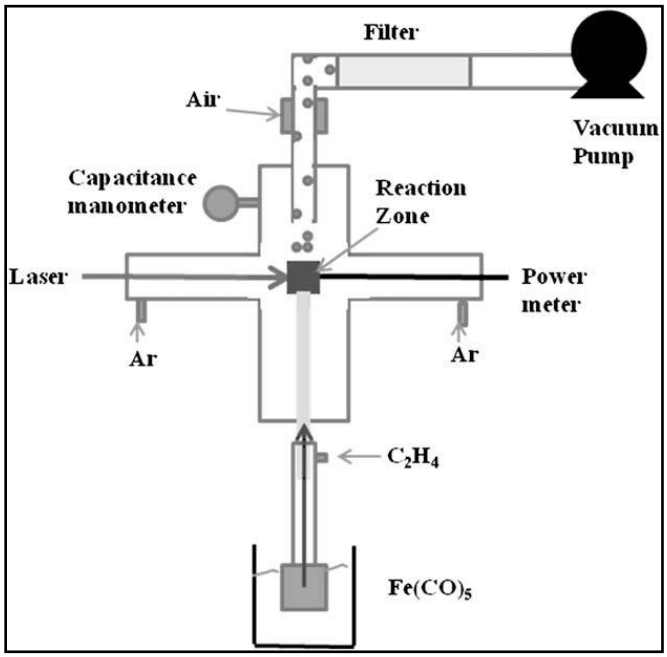

Figure 6: Iron Oxide Formation by Laser Pyrolysis

2.5.4 Ultraviolent Induced Chemical Vapor Deposition

A process similar to Laser induced chemical vapor deposition is UV assisted Chemical Vapor deposition. In this process a UV lamp can be used to improve the nucleation process of deposited metals while lowering the operational decomposition temperature. This process can be separated into two discrete steps: deposition onto substrate surface and UV assisted decomposition via adsorption of

organometallic to produce elemental metals. Marsh et al. were successful in producing a 6nm thin film using this technique using a cyclopentyl trimethyl platinum solution as a precursor material (20).

2.5.5 Plasma Enhanced Chemical Vapor Deposition

Film purities approaching 100% have been achieved through the use of radio frequency generated plasma. Degradation temperatures are low ~70°C at 600m Torr vapor pressure with a substrate temperature of 300°C. (20) .This mechanism uses energy imparted by radio waves to generate degradation of precursors in a controlled manner, similar to that of laser induced chemical vapor deposition (20).

2.5.6 Focused Ion Chemical Vapor Deposition

Ion beams have been used to deposit elemental platinum from organometallic precursors with a resulting resistivity 10-5000 times higher than that of pure platinum due to elemental impurities trapped within the deposited structure. Impurities range from Carbon from organic precursor component, oxygen from reaction in gas environment and metal ions residually imparted onto the substrate from the ion beam. Platinum (deposited) content was reported to be 46% in experimental study performed by Telari et al. (20).

2.5.7 Electron Beam Chemical Vapor Deposition

Electron Beam Chemical vapor deposition is a technology that uses a focused electron beam to degrade organometallic precursors. This is not done by the primary beam, but by the secondary electrons emitted from the substrates surface that cause dissociation of reagent molecules. In this manner, quantum dots can be grown if the electron beam is not moved, similar to the deposition characteristics of rapid prototyping on the macro scale. Because of the high aspect ratio, growth rates have been highest reported at 9µm/min. Similar to focused ion-assisted chemical vapor deposition, organic reagent precursors are often included in produced structures. In spite of this, this technique is favored over

other methods due to its relatively low level of impurities (~60%) and tendency not to degrade the substrate material as in other techniques.

2.5.8 Fluidized Bed Chemical Vapor Deposition

In fluidized bed chemical vapor deposition, gas containing organometallic species is flown upwards through a powder material allowing the degradation of the specified reagents allowing them to collect as a surface coating on the powder material. This technique is generally transport limited and growth has been shown to be consumed within a few centimeters of the gases inlet. This however is mitigated by the high degree of gas-solid mixing during the process allowing for isothermal composition and uniform distribution.

2.5.9 Atomic Layer Deposition

In this process, high temperature conditions are initiated through a substrate material which is contained in an environment mixed with precursor organometallics and air oxygen. The benefit of this method is the controlled deposition which occurs layer by layer due to the limited supply of gaseous reactants. Gas pulses thus control growth through this auto-limited growth mechanism.

2.6 Technological Significance of Work

Extensive research has been carried out in many fields pertaining to submicron structures. Chemical vapor deposition holds special interest in its technological importance in the fabrication of opto-electronic, high speed electronic devices, lasers, PIN photodetectors, solar cells, phototransistors, photocathodes, field effect transistors, and modulation doped field effect resistors (22).

Though individual metal deposition by chemical vapor deposition has been studied, degradation mechanisms are poorly understood for many organometallic compounds (23). Investigation of metal chemical vapor deposition of multiple metals has not identified this technique as an established process that can be used to produce novel alloy structures. Many processes undertaken to better understand deposition procedures are often costly and do not lend well to being scaled to industrial applications.

This report aims to address problems currently experienced in the field of developing alloyed materials through examination of degradation products of organometallic compounds and their precursor materials.

3.0 Objectives

- Investigate degradation characteristics of two organometallic compounds via mass loss using sample mass and degradation temperature as variables.
- Characterize degradation products of a degraded mixture of Iron Carbonyl and Nickelocene using scanning electron microscope, electron dispersive x-ray spectroscopy, and x-ray diffraction
- Establish feasibility of using high temperature degradation of organometallic compounds as a means of forming submicron alloy structures

4.0 Experimental Design

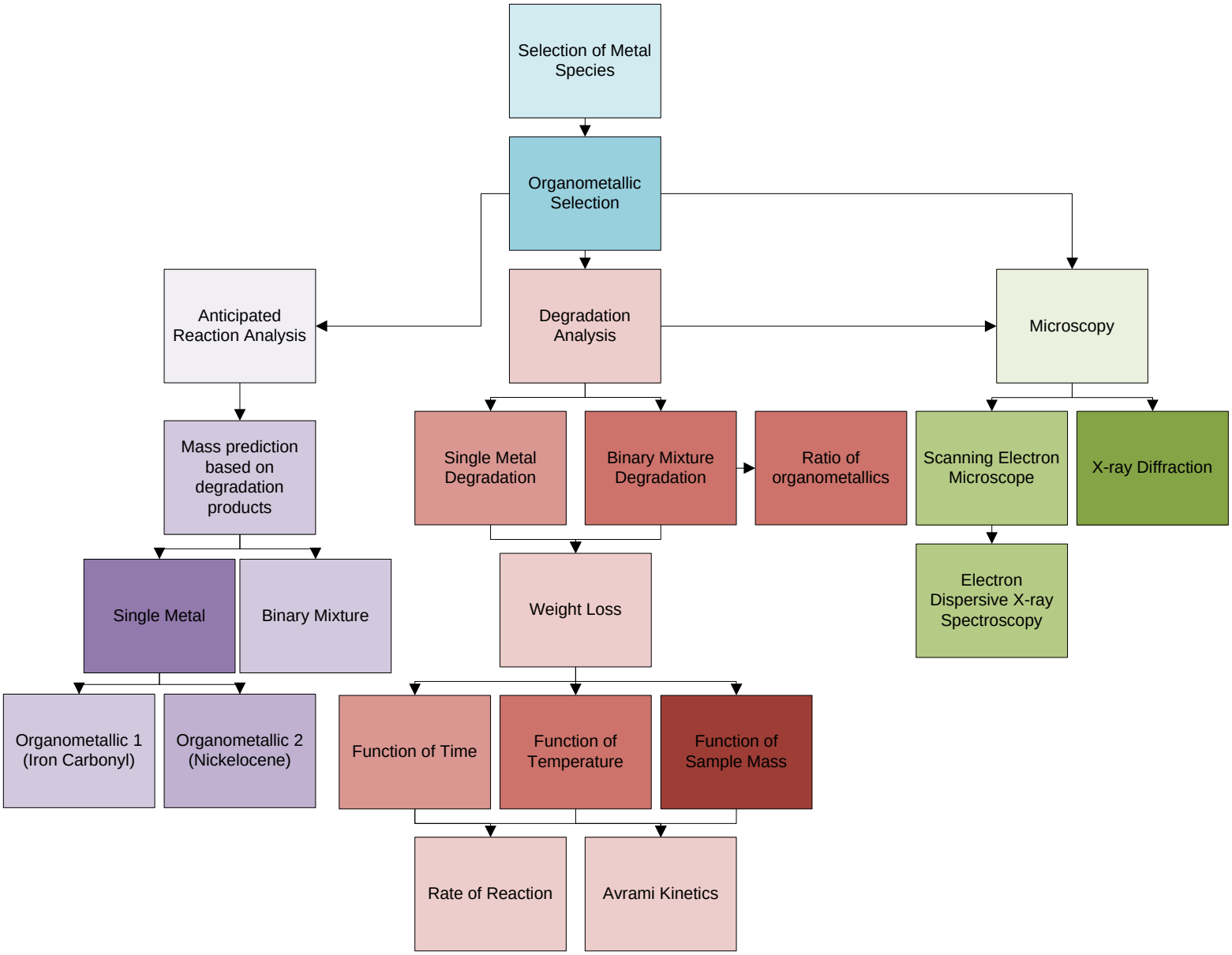

Figure 7 describes the experimental design used for this study.

Figure 7: Experimental Design Flow Chart

4.1 Selection of Precursor Metals

Identification of possible precursor metals for investigation was necessary in determining appropriate organometallic complexes for investigation. Manufacturing Engineering Technology 6th Ed. was consulted in order to generate a possible list of alloying elements that form low temperature alloys.

Binary alloy formation was considered as appropriate for the scope of the project. Literature documenting binary phase diagrams was consulted, including Smithell's Metal Reference Book and Handbook of Binary Phase Diagrams.

Metal pairs with mutual solubility of >2% were identified. These metal pairs include Tin/Indium, Lead/Tin, Lead/Tellurium, Zinc/Gold, Zinc/Silver, Zinc /Cadmium, Iron/Gold, Iron/Cobalt, Iron/Vanadium, Iron/Rhodium, Iron/Chromium, Iron/Platinum, Iron/Manganese, Iron/ Rubidium, Iron/Nickel, and Iron/Osmium. Figures describing these phase diagrams can be viewed in the appendix of this report. This preliminary list was then focused to metal combinations that had lead, zinc, tin or iron as the metal solvent based on pricing and availability. A list potential organometallic candidates and their relative cost can be found in Table 1.

Table 1: Potential Organometallic Candidates

Organometallic	Price (USD)	Relative cost per gram(USD)
Iron Pentcarbonyl	46.90/250g	0.19
Tin (II) 2-ethylhexanoate	19.10/100g	0.19
Ferrocene	24.20/50g	0.48
Tributyltin methoxide	33.40/25g	1.34
Tributyltin hydride	24.90/10g	2.49
Tetrabutyl tin	16.10/5g	3.22
Tributyl(phenylethynyl)tin	36.90/10g	3.69
Tetraphenyltin	25.30/5g	5.06
Dibutylmethoxidetin	34.10/5g	6.82
Nickelocene	36.90/5g	7.38
Tetraphenyllead	19.30/1g	19.30

4.2 Selection of Organometallic Compounds

The selection process was continued based availability of organometallic compounds available within the prescribed $320 budget afforded to the project from suppliers Fischer Scientific and Sigma-Aldrich. Price for organometallic compounds can vary greatly based on stochiometry and potential use;

inexpensive metal compounds often can be found in complex, expensive morphologies as organometallics. In addition to price, molecular structure and degradation temperature were also relevant parameters. Experimental procedure was conducted to determine degradation characteristics of selected organometallic complexes. As a guideline, material flash point was used as an indicator of degradation temperature; two organometallics with similar flash points were chosen based on data provided in material data sheets. Initial candidates for investigation were limited by the selection criteria of being less than fifty dollars for 5 gram quantities, existence as a low melting crystal or liquid at ambient temperature, with similar morphologies.

It was determined that Iron Pentacarbonyl and Nickelocene would be suitable candidates for alloy formation. The binary phase diagram shows limited mutual solubility, the compounds similar chemical structures, and the two organometallics have similar degradation temperatures. These compounds can be purchased for a relatively low amount of money; 250g of iron pentacarbonyl was purchased for $49.60 with additional shipping costs; 5g nickelocene was purchased for $36.90 with additional shipping costs. The molecular weights of the two organometallics are 195.90 g/mol for Iron Pentacarbonyl and 188.88 g/mol for Nickelocene. The chemical structures of these two compounds can be viewed in Figures 8 and 9.

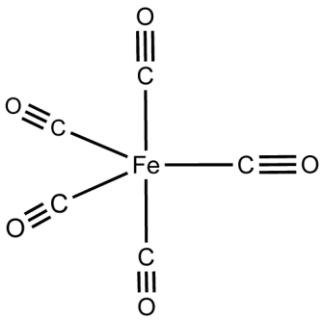

Figure 8: Chemical Structure of Iron Pentacarbonyl

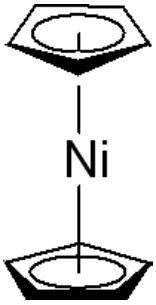

Figure 9: Chemical Structure of Bis(dicyclopentadienyl)nickel II: Common Name Nickelocene

4.3 Selection of Experimental Procedures

The selected organometallics were intended to be used to develop an alloy, so experimental procedures were created to attempt to develop the alloy. Experimental procedures were fashioned to eliminate the organic components in the organometallics. As stated previously the materials' flash points were used to determine the degradation temperature of each of the organometallics and thermal degradation experiments were fabricated.

Solubility experiments were developed in order to establish the mutual solubility of the organometalllics within each other. The phase diagram was consulted to determine the theoretical solubility. The theoretical solubility was used to develop the experimental procedures used to create suitable solubility experiments. Once the degradation and solubility experiments were developed, the two experiments could be combined to develop the alloy.

4.4 Selection of Analytical Experiments

After obtaining adequate experiments to create the sought after sample, analytical experimental procedures needed to be developed in order to determine what was contained in the generated sample. Many different analytical techniques were considered, although in the end only three were accepted. Scanning electron microscopy was used to determine the molecular structure of the generated samples, Energy dispersive x-ray spectroscopy was used to determine the elements contained in the generated samples. X-ray diffraction was used to further determine the identity of the sample by comparing experimental data against a set of standard data for all compounds.

4.5 Design of optimized sample holder for XRD

To address concerns of background peak detection during XRD scans, a design for an x-ray diffraction sample holder made of a non crystalline plastic was designed. This sample holder was made to maintain the 25x15x5mm specifications that are generally used in x-ray diffraction data collection and work with existing lab equipment. A CAD rendering of this fixture can be viewed in Figure 10.

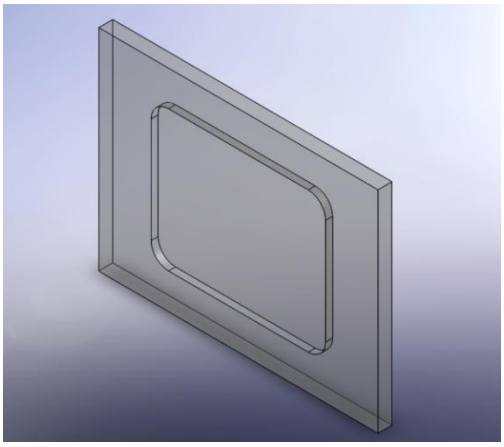

Figure 10: Polystyrene XRD Sample Plate

Detailed drawing specifications can be viewed in Appendix 11.10

5.0 Methodology

In this study, degradation mechanisms for various organometallic compounds were considered. Due to associated variables with each process, high temperature chemical vapor deposition was identified as a logical solution for degrading organometallic species, and was best suited to the scope of this investigation. High temperature chemical vapor deposition will be implemented as method to isolate metal species from organometallic precursors.

Various experiments were conducted to study the effects of degradation on organometallics and to discover if mixing different organometallics and thermally degrading them could possibly produce an alloy. This section will describe the experiments conducted throughout this study.

5.1 Materials and Equipment

A variety of materials were used throughout this study. The organometallics needed for this study were iron pentacarbonyl ($Fe(CO)_5$) and bis(cyclopentadienyl)nickel, also known as nickelocene ($C_{10}H_{10}Ni$). These organometallics were obtained from Sigma Aldrich Co., St. Louis, MO. The Thermolyne 47900 lab furnace, as seen in Figure 10, was used for all thermal degradation experiments. All degraded samples were measured on a scale to measure mass loss over time. The scale used was a Denver Instrument company A-250 as seen in Figure 11. A JSM-840 scanning electron microscope (SEM) with an energy dispersive X-ray detector (EDX) attachment (Kevex), as seen in Figure 13, was used to gather pictures of the molecular structures of our samples. In order to determine which elements were present in our sample the X-Ray Diffraction Process needed to be completed using a General Electric X-ray Diffractometer as seen in Figure 14.

Figure 11: Thermolyne Furnace

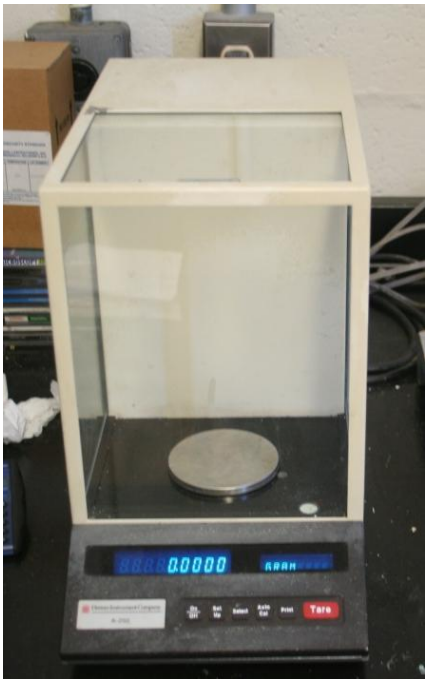

Figure 12: Denver Instrument Company A-250 Scale

Figure 13: JSM-840 Scanning Electron Microscope

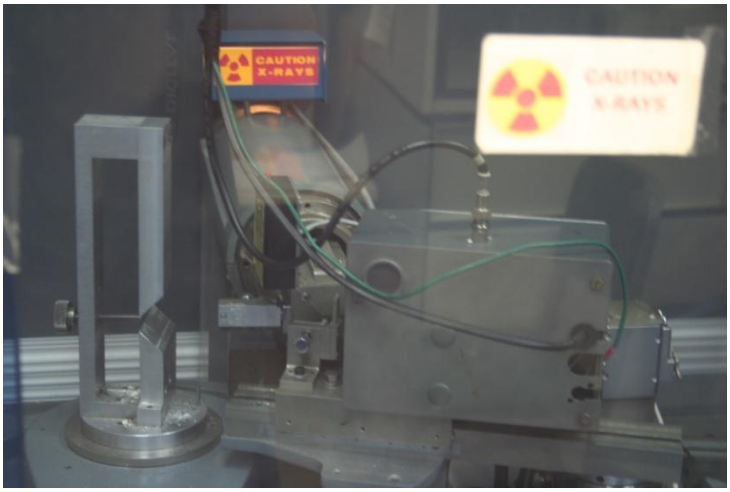

Figure 14: General Electric X-Ray Diffractometer

5.2 Effect of Container on Iron Pentacarbonyl Degradation

Initial experiments were conducted to characterize the degradation behavior of the organometallics. Different crucibles were available for use in the laboratory and it was necessary to determine which crucible was ideal to conduct future experiments. Three different types of crucibles were available for use in the lab, a ceramic crucible as seen in Figure 15, a glass crucible as seen in Figure 16 , and an aluminum foil dish constructed from ordinary household aluminum foil as seen in Figure 17 . 50mg of Iron Pentacarbonyl was placed in each different type of crucible. Three trials for each type of crucible were conducted. The samples were placed in the furnace using metal tongs and were burned in thirty minute intervals for ninety minutes to determine the weight loss over time. The furnace was turned to 200°C; this temperature was chosen because it was well over the boiling point of Iron Pentacarbonyl.

Figure 15: Ceramic Crucible used in High Temperature Degradation

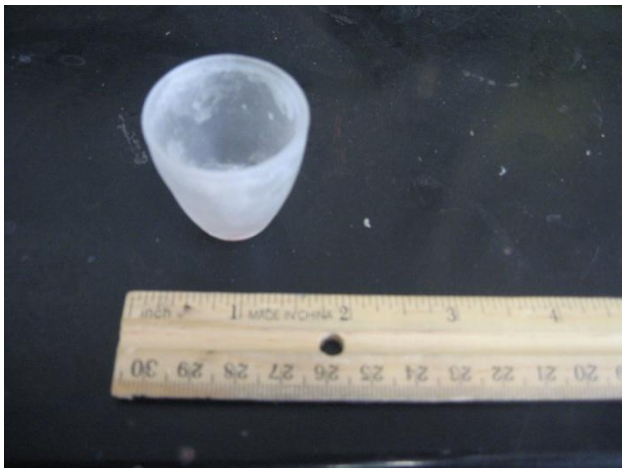

Figure 16: Glass Crucible used in High Temperature Degradation

Figure 17: Aluminum Foil Dish used in High Temperature Degradation

Due to the relative sample weights being studied, it was determined that aluminum foil cups would be more appropriate for degradation investigation. These containers were easier to prepare than the crucibles, were free of residual materials, and provided a more even heating surface to the sample being studied.

5.3 Effect of Time and Temperature on Iron Pentacarbonyl Degradation

For the purpose of this research, it was necessary that we understand degradation mechanisms for each organometallic. The duration of the degradation process needed to be determined to definitively understand degradation mechanisms of reagent materials. The Iron Pentacarbonyl was thermally degraded using the Thermolyne Furnace. Two aluminum foil dishes were made and 200mg samples of Iron Pentacarbonyl were placed in each dish. The samples were placed in the furnace set at 100°C and

were heated directly. The mass loss was measured and recorded after 1 minute, 2 minutes, and 5 minutes. The mass loss vs. time was recorded for each interval and the total mass loss vs. temperature was also recorded. Additional experiments were conducted at 200°C, 300°C, 400°C, and 80°C.

5.4 Solubility of Nickelocene in Iron Pentacarbonyl

The goal of this research was to develop an alloy through thermal degradation of organometallics. In order to develop an alloy using organometallics, two compatible metal elements were necessary. Nickelocene was chosen for this experiment because the Fe – Ni phase diagram, as seen in Figure 18, showed some solubility between nickel and iron. A 10mg sample of nickelocene was added to a small beaker, then the Iron Pentacarbonyl was taken from the container using a pipette and was added to the beaker a few drops at a time, measuring the added mass simultaneously. After every few drops of the Iron Pentacarbonyl, the mixture was stirred. Only a total of 200mg of Iron Pentacarbonyl was added to the 10mg of Nickelocene. Through this procedure a sample containing 200mg of Iron Pentacarbonyl and 10mg of Nickelocene was prepared.

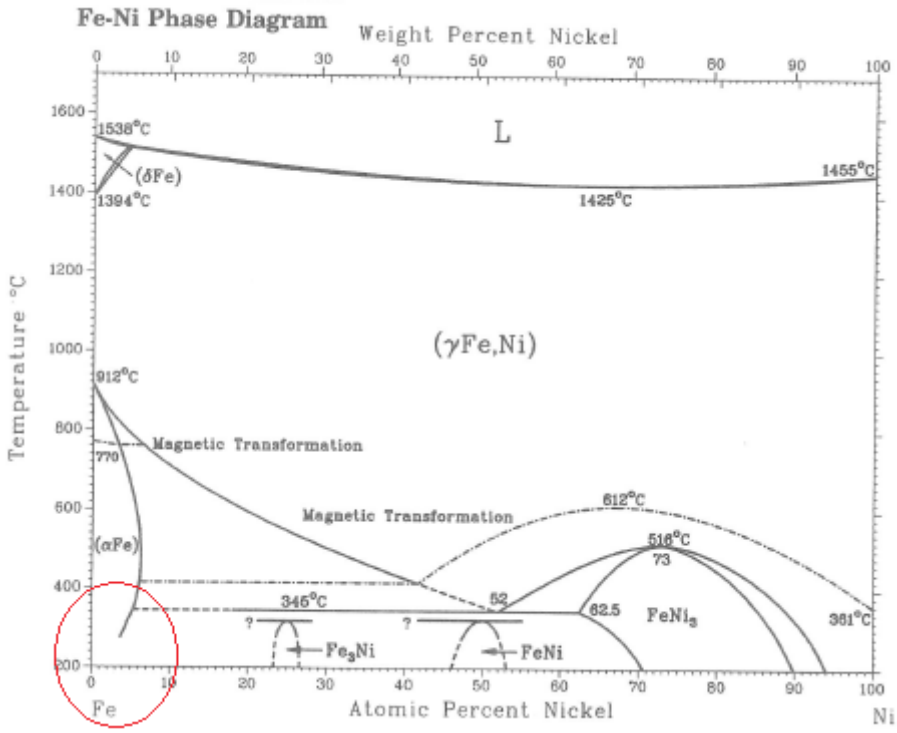

Figure 18: Fe-Ni Phase Diagram Displaying Limited Solubility of Nickel in Iron

5.5 Nickelocene Degradation

Nickelocene samples were prepared using aluminum degradation containers. Experimental procedure was conducted on nickelocene at masses of 200mg and 1g masses at temperatures of 300°C and 400°C.

5.6 Iron Pentacarbonyl/Nickelocene Mixture Degradation

Iron pentacarbonyl/Nickelocene organometallic mixtures were prepared for degradation at 400^{o}C at various ratios. Iron pentacarbonyl mass was maintained at 1.0g and nickelocene mass was tailored to fit the desired ratio for degradation. Ratios of precursor Fe:Ni 40:1, 20:1, 5:1, 2.74:1, 2.59:1, 2.48:1, 1:1 were tested for weight loss over time until samples demonstrated weight loss of less than five percent their undegraded mass.

5.7 Effect of Super Cooling Prior to High Temperature Chemical Vapor Deposition

To better understand the degradation mechanisms of iron pentacarbonyl, experimental procedures were developed to investigate the effect of supercooling organometallic materials using liquid nitrogen immersion of degradation containers. 200mg samples were super cooled for 30 seconds via submerging the degradation container after which samples were placed directly into a 400°C oven. Samples were measured against ambient specimens to determine correlations between weight loss and temperature prior to degradation.

6.0 Results

6.1 Iron Pentacarbonyl Degradation Analysis

It was found that at all temperatures above the boiling point of Iron Pentacarbonyl, a majority of the observed mass loss occurred within the first minute of degradation. According to the MSDS, Iron pentacarbonyl is highly flammable, and rapid degradation was observed within the first ten seconds of heating. Application of heat was often accompanied with an audible noise hinting rapid degradation inside the furnace. A noticeable amount of brick colored fumes that exited the furnace heating vent were also observed. Mass Loss vs. Time graphs for 200mg samples can be seen in Figure 19.

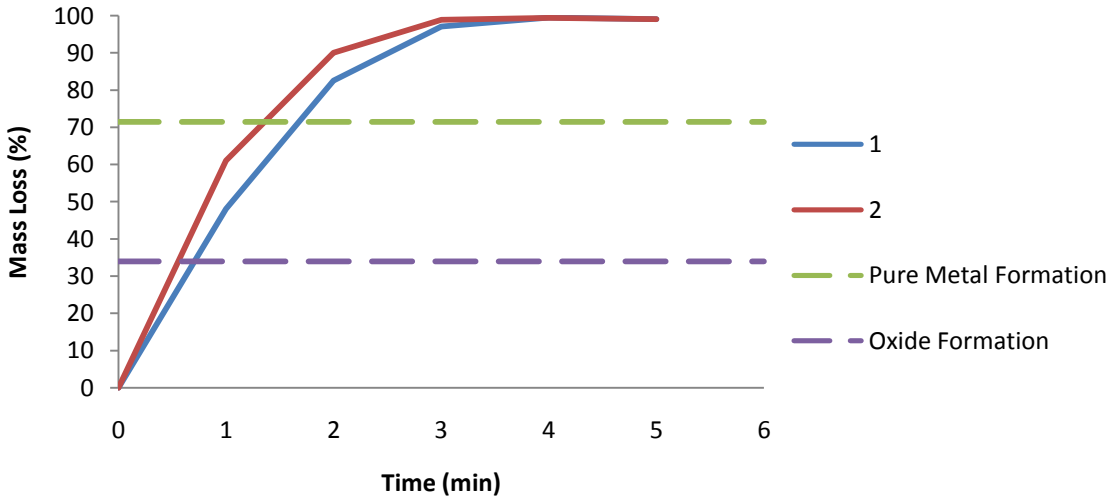

Figure 19: Mass Loss of Degraded Iron Pentacarbonyl at 80°C

At 80°C, after the first minute only between 50% - 60% of the mass loss was lost, although after five minutes almost 100% of the mass was lost. This is a possible result because it was observed that the Iron Pentacarbonyl will evaporate at room temperature. Figure 20 describes data collected during degradation studies conducted at 100°C.

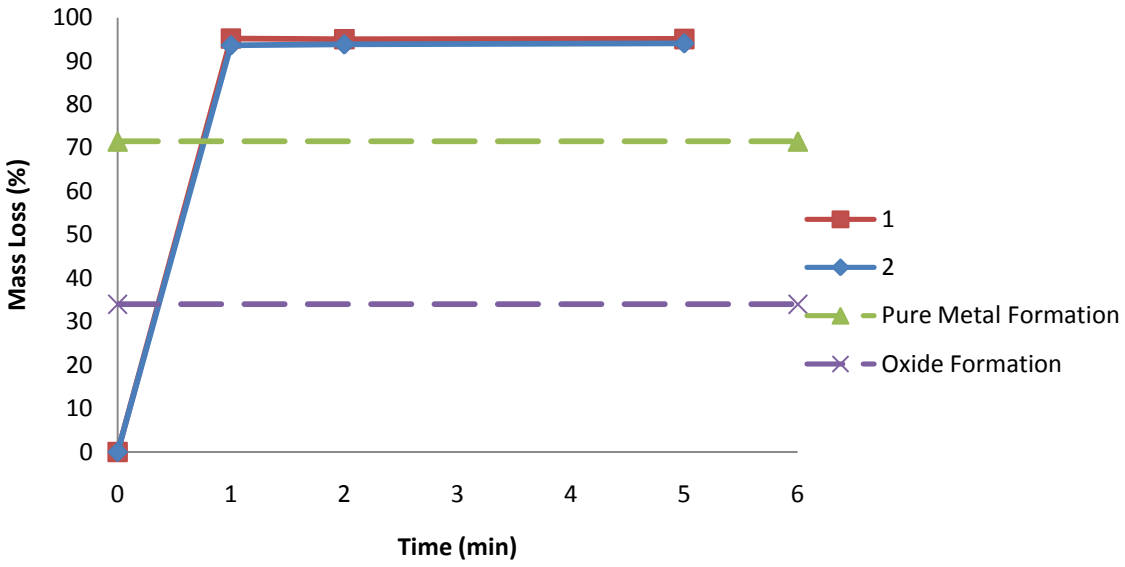

Figure 20: Mass Loss of Degraded Iron Pentacarbonyl at 100°C

Unlike the 80°C trial, at 100°C a majority of the observed mass loss occurred during the first minute. There were negligible mass losses recorded for the duration of heating. Figure 21 describes data collected during degradation studies conducted at 200°C.

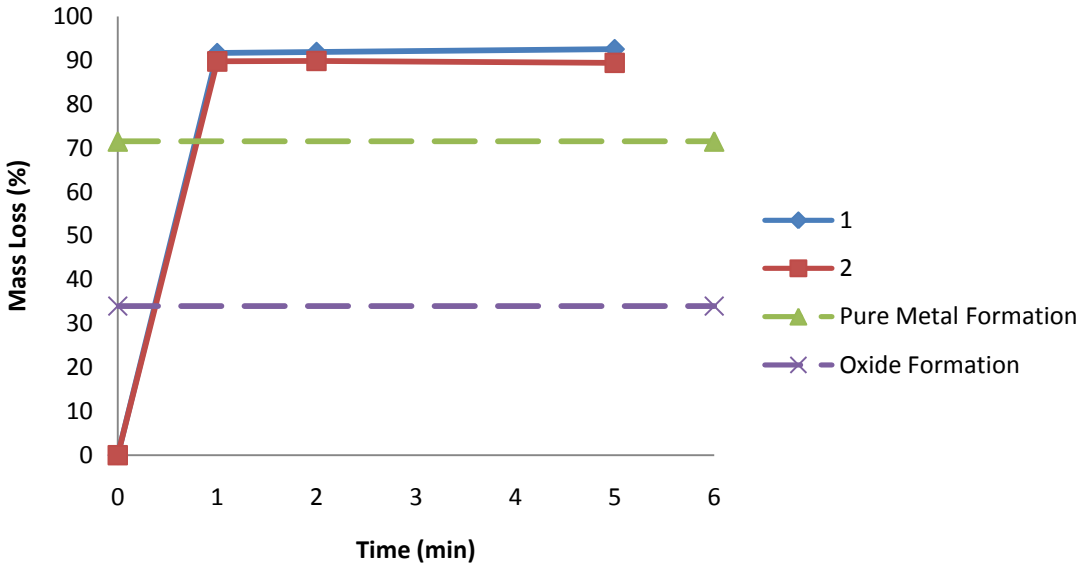

Figure 21: Mass Loss of Degraded Iron Pentacarbonyl at 200°C

Similarly to the 100°C trial, at 200°C, a majority of the observed mass loss occurred during the first minute of heating. Samples heated at 200°C showed a mass retention roughly 3% greater than samples degraded at 100°C. Figure 22 describes data collected during degradation studies conducted at 300°C.

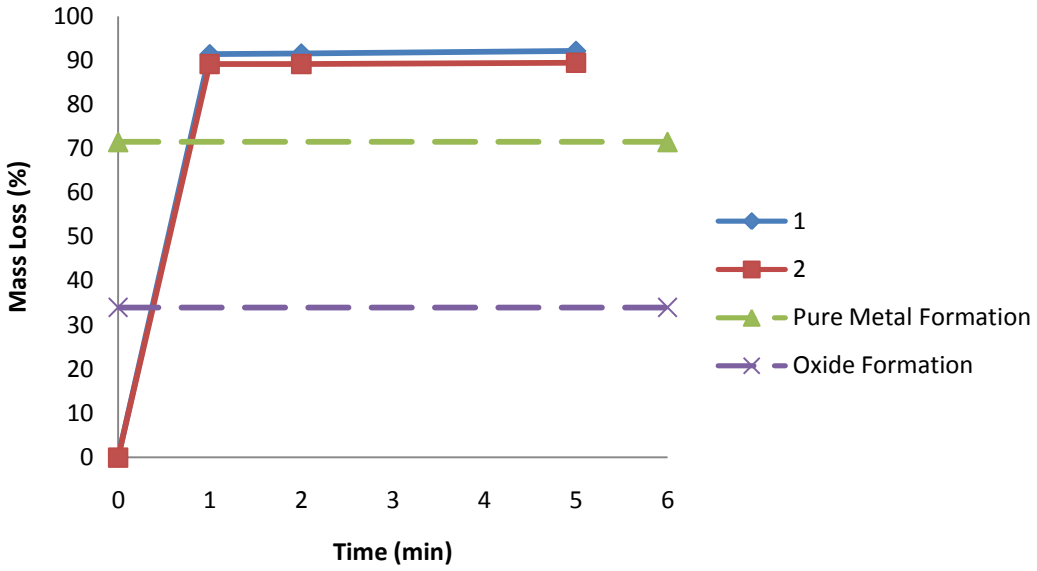

Figure 22: Mass Loss of Degraded Iron Pentacarbonyl at 300°C

For 300°C, a majority of mass loss was observed in the first minute. Mass loss values were comparable to that of 200°C samples. Figure 23 describes data collected during degradation studies conducted at 400°C.

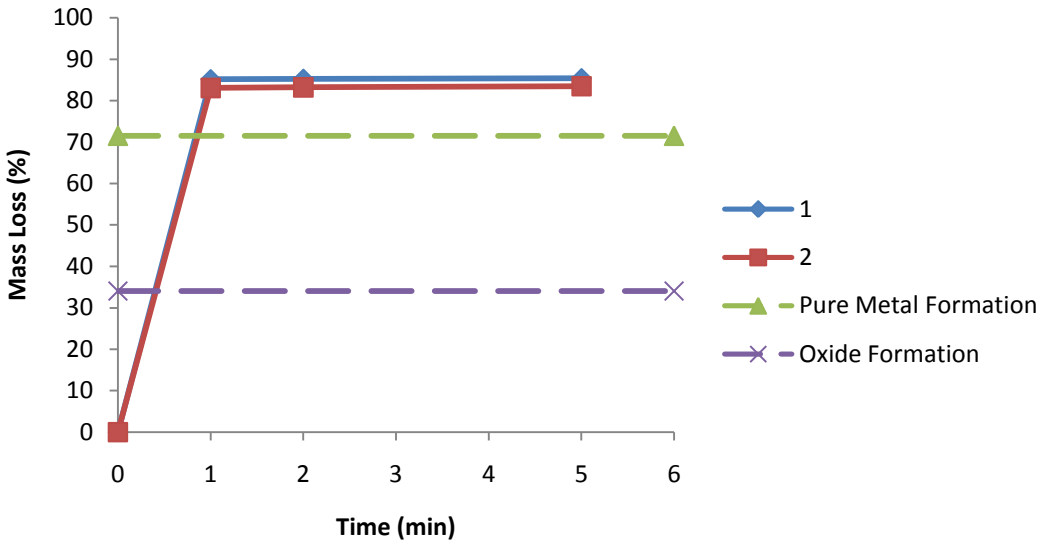

Figure 23: Mass Loss of Degraded Iron Pentacarbonyl at 400°C

At 400°C average mass loss was about 5% less than at 300°C. The 84% average weight loss at 400°C was not accurate because the aluminum foil sample holders did not contain the reaction happening inside the furnace well; all generated reaction product was not contained within the degradation containers. A figure showing the average mass loss vs. temperature can be seen in Figure 24.

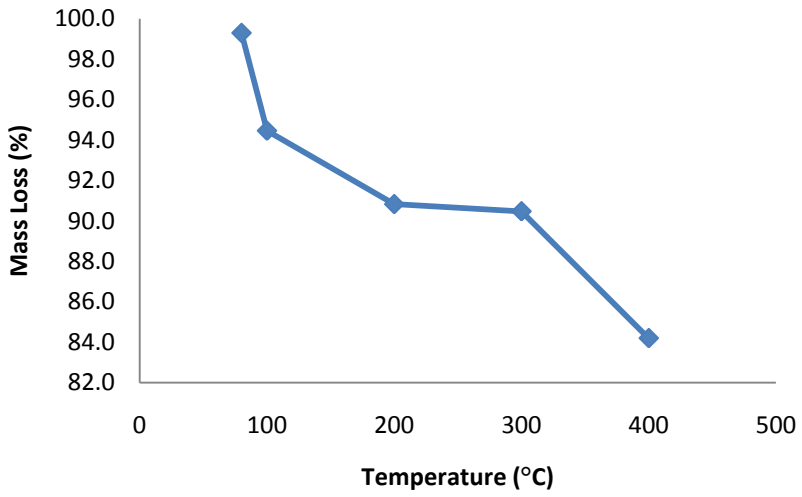

Figure 24: Average Mass Loss of Iron Pentacarbonyl for Degradation Temperatures

It was observed that iron pentacarbonyl applied to different heating temperatures had significant effect on the rate and quality of degradation. The materials data safety sheet (MSDS) for iron pentacarbonyl states that the boiling point of Iron Pentacarbonyl is 103°C. Five different temperatures were chosen for the degradation experiments: 80°C, 100°C, 200°C, 300°C, and 400°C. These temperatures were chosen to determine what would happen to the samples if they were degraded under the boiling point, at the boiling point, and above the boiling point of the Iron Pentacarbonyl. Since the temperature affected the degradation, different results were seen from degradation at different temperatures. The results of degradation at 80°C and 400°C can be seen in Figure 25 and Figure 26 respectively.

Figure 25: Degraded Iron Pentacarbonyl at 80°C

Figure 26: Degraded Iron Pentacarbonyl at 400°C

At 80°C the Iron Pentacarbonyl seemed to just evaporate and leave an orange brown stain on the bottom of the aluminum foil dish. At 400°C the Iron Pentacarbonyl had a chemical reaction of some sort and the result was a blackish reddish fibrous structure reminiscent of soot. 100°C, 200°C, and 300°C degraded samples had appearances that were similar or indistinguishable to the sample generated at 400°C. The most observed was the color was a differed at the different temperatures; samples generated at higher temperatures were found to contain more red fiber structures, while samples degraded at lower temperatures contained hues of indigo and violet. The textural quality of the powder

allowed the material to be compressed while still staying conjoined to the relative fiber network, similar to cotton balls.

6.4 Nickelocene Degradation Analysis

A 400°C degradation temperature for nickelocene was proposed based on experimental results taken from iron pentacarbonyl studies, which was chosen as the given metal solvent for this study. Investigation was undertaken to validate that 400°C would be an appropriate temperature for nickelocene degradation studies.

Degraded samples were observed to show signs of degradation within the first minute of heating; these indicators included a black to emerald green fumes that escaped the ventilation hood accompanied with visible fiber particles as well as a noxious smell that was similar to that of aromatic solvents The mass loss vs. time of two 200mg samples can be seen in Figure 27.

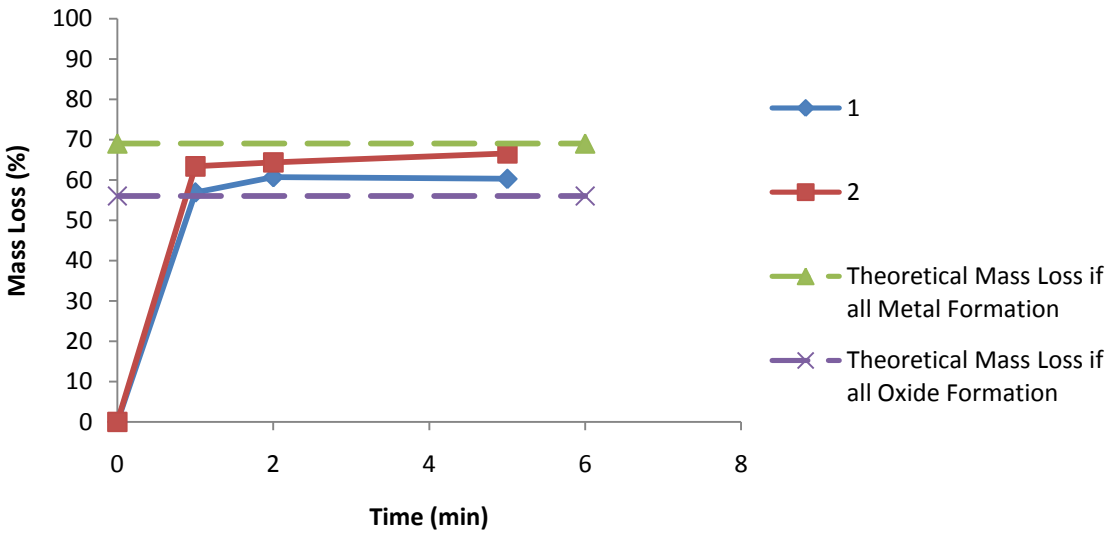

Figure 27: Mass Loss of Degraded Nickelocene at 400°C

Figure 28 shows the degraded Nickelocene in the aluminum foil dish after being degraded for five minutes. The degraded Nickelocene looks clumpy and more like ash than fibrous like the iron

pentacarbonyl. Additionally the quality of the produced fiber had a gritty texture that was dissimilar to the aerated fiber network produced by degrading iron pentacarbonyl.

Figure 28: Degraded Nickelocene at 400°C

6.5 Iron Pentacarbonyl and Nickelocene Mixture Degradation Analysis

Three different ratios were calculated for the organometallic mixture. The iron pentacarbonyl and nickelocene ratios were 2.48:1, 2.59:1, and 2.74:1. Mixtures with these compositions were degraded at 400°C to achieve the least amount of mass loss. Figure 29 shows the mass loss vs. time for the three samples of different ratios.

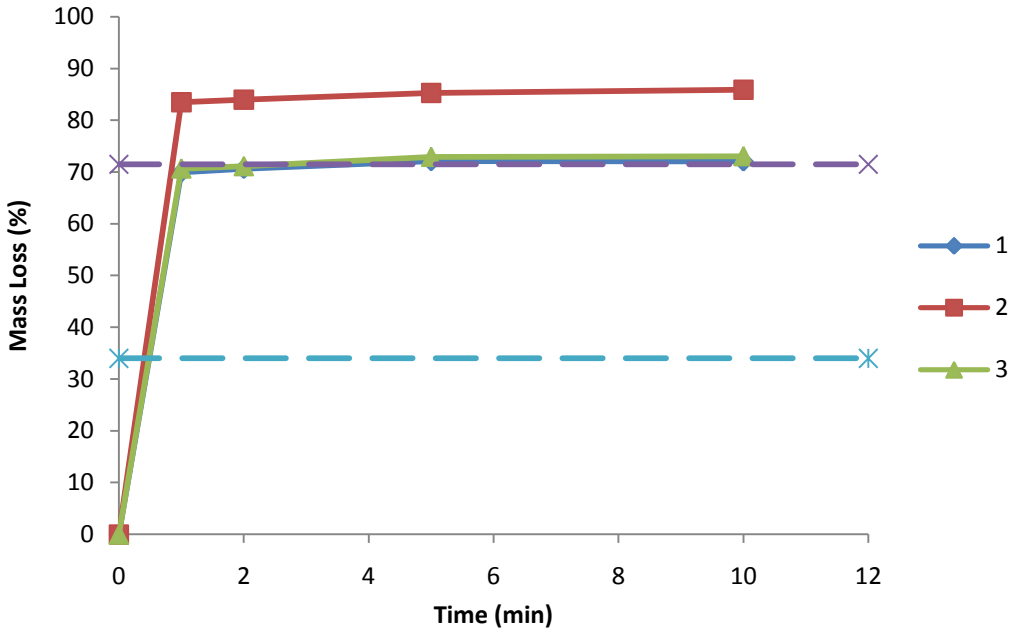

Figure 29: Mass Loss of 20:1 [Fe-P:Ni-C] Mixture Degraded at 400°C

The majority of the mass loss of the degraded mixture occurred within the first minute of heating. Figure 28 show that the 2.59 ratio had more than 10% more mass loss than the other two mixtures. Relative masses of materials are variable as substantial sample mass was lost through fiber structures escaping the ventilation hood of the furnace. Samples appeared as denser versions of the degraded iron pentacarbonyl, but still maintained the pliability and coloration of the degraded iron carbonyl sample. A picture of the degraded mixture at a ratio of 20:1 can be seen in Figure 30.

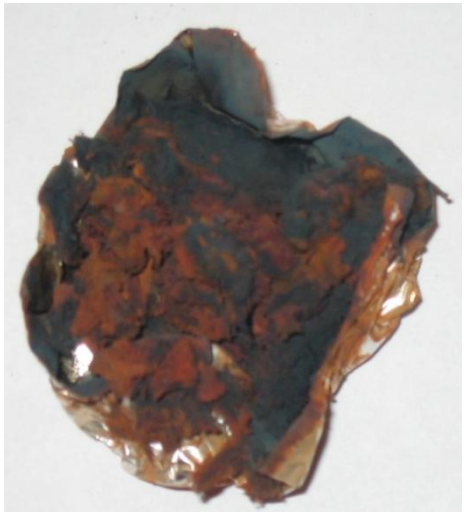

Figure 30: Iron Pentacarbonyl and Nickelocene Mixture Degraded at 400°C

6.2 Iron Pentacarbonyl Rate of Reaction

Rate of reaction can be established through observation experimental data, namely observed mass loss versus time. A best-fit line was implemented to determine the slope of the active region measured where mass loss was most noticeable. This number was then modified through application of molecular weight of the material (Iron Carbonyl) and the Avogadro's number conversion factor to yield a term which reflected mass loss in the unit [molecules/minute]. Application of this method yields the experimental data described in Table 2.

Table 2: Rate of Reaction Iron Carbonyl

Temperature (C)	Rate (g/min)	K value (molecules/min)
80	0.2463	7.5713E+20
100	0.4454	1.36917E+21
200	0.8718	2.67993E+21
300	0.8635	2.65441E+21
400	0.877	2.69591E+21

6.3 Determination of Energy of Activation for Iron Pentacarbonyl

The Arrhenius equation is an empirical relationship that relates the rate of a chemical reaction to the temperature under which the operation is carried out. The unmodified version of this relationship can be defined as:

$$k = Ae^{\frac{Q}{RT}} \tag{11}$$

k represents the rate constant; *A* represents a pre-exponential factor; *Q* represents activation energy; *T* is temperature of reaction (in Kelvins); *R* refers to the molar gas constant [R = 8.314 472(15) J K^{-1} mol^{-1}]. Given corollary values for mass loss given two different temperatures, as was determined by measurement of experimental weights, equations can be developed to reflect the Arrhenius relationship between mass loss and temperature, assuming that the reaction fits this method. The generalized equation that relates mass loss to temperature can be defined as:

$$x_1 = A \cdot e^{\frac{-Q}{R \cdot T_1}} \tag{12}$$

By assuming that for any reaction has the same value constants A, and Q, that is pre-exponential component and energy of activation, a modified for m that relates mass loss values of any two points versus their temperatures can be developed:

$$\frac{x_1}{e^{\frac{-Q}{R \cdot T_1}}} = \frac{x_2}{e^{\frac{-Q}{R \cdot T_2}}} \tag{13}$$

Through algebraic manipulation this equation can be modified to simplified form:

$$Q = \frac{R_1 \cdot \ln\left(\frac{x_1}{x_2}\right)}{\left(\frac{1}{T_2} - \frac{1}{T_1}\right)} \tag{14}$$

Through comparison between two points of known values for temperature and mass loss, as is provided in Table 3, experimental energies of activation can be determined.

Table 3: Calculated Energy of Activation Iron Pentacarbonyl

Temperature 1 (K)	Temperature 2 (K)	Mass loss @ T1 (%)	Mass loss @ T2 (%)	Rate of Reaction (J/mol)
353.15	373.15	99	95	-2259
353.15	473.15	99	91	-975.5
353.15	573.15	99	90	-729
353.15	673.15	99	84	-1015
373.15	473.15	95	91	-631.5
373.15	573.15	95	90	-480.7
373.15	673.15	95	84	-856.6
473.15	573.15	91	90	-249.1
473.15	673.15	91	84	-1060
573.15	673.15	90	84	-213
			Average	-1047

6.2 Architecture Determination by Scanning Electron Microscope

In order to determine the molecular structure of the degraded samples, the samples were run through the Scanning electron microscope (SEM). The SEM provided many pictures at very small scales to give some detailed images of the structure of our samples.

6.2.1 Scanning Electron Microscopy of Degraded Iron Pentacarbonyl

Scanning electron microscope analysis of degraded iron carbonyl at 400°C yielded a micrograph that can be viewed in Figure 31.

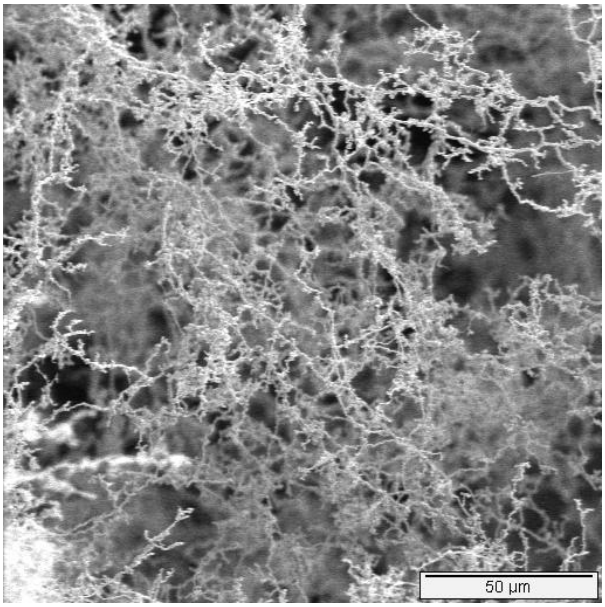

Figure 31: SEM of Degraded Iron Pentacarbonyl degraded at 400°C

At a relatively broad viewing range (50µm) one can view that the degraded organometallic species arranges itself into fiber structures.

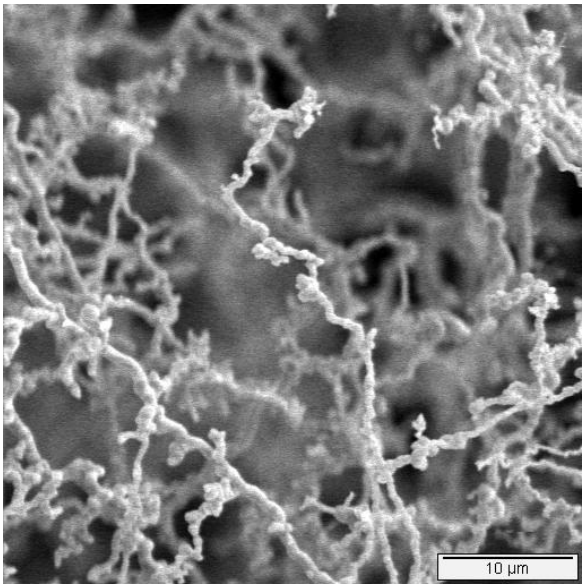

Figure 32: SEM of Degraded Iron Pentacarbonyl degraded at 400°C at Low Magnification

In Figure 32, it can be observed that though linkages between fibers exist, most fibers in the observed samples are nonlinear autonomous structures that exist in a relatively thin, uniform area.

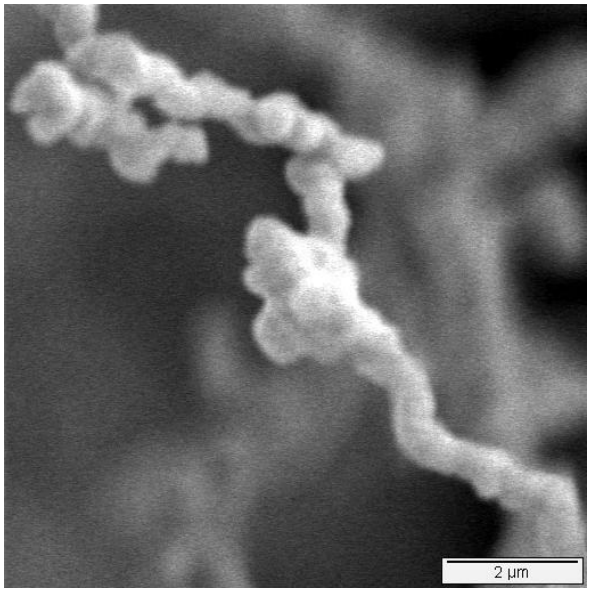

Figure 33: SEM of Degraded Iron Pentacarbonyl degraded at 400°C at High Magnification

At higher magnification, as is observed in Figure 33, we can observe that degraded iron carbonyl structures that are generated are less than 1 micron in diameter.

Due to the conductive nature of the degraded material as is evident in its ability to produce visible images, it can be surmised that metallic compounds are present in the observed sample. SEM, however, cannot be used as a definitive tool to determine the structure of the metal species that is observed in these micrographs.

6.2.2 Scanning Electron Microscopy of Degraded Nickelocene

Scanning electron micrographs of degraded nickelocene heated at 400°C. At a low magnification, it can be observed that the nickelocene when degraded forms a denser powder than the iron when degraded at the same temperature. Figure 34 includes images that were taken in two different spots of the degraded nickelocene sample.

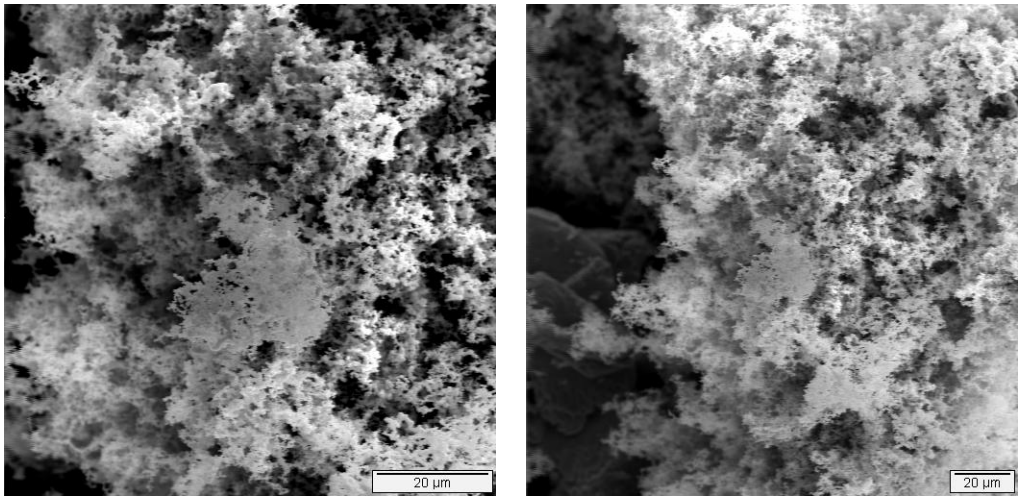

Figure 34: SEM of Degraded Nickelocene degraded at 400°C at Low Magnification

At higher magnifications, it can be observed that the graded material is sufficiently more agglomerated than the degraded iron carbonyl sample. Fiber formations can be viewed off of lumped structures, but diameters of these fibers are irregular and of non uniform diameter. Figure 35 contains images of degraded nickelocene at higher magnification.

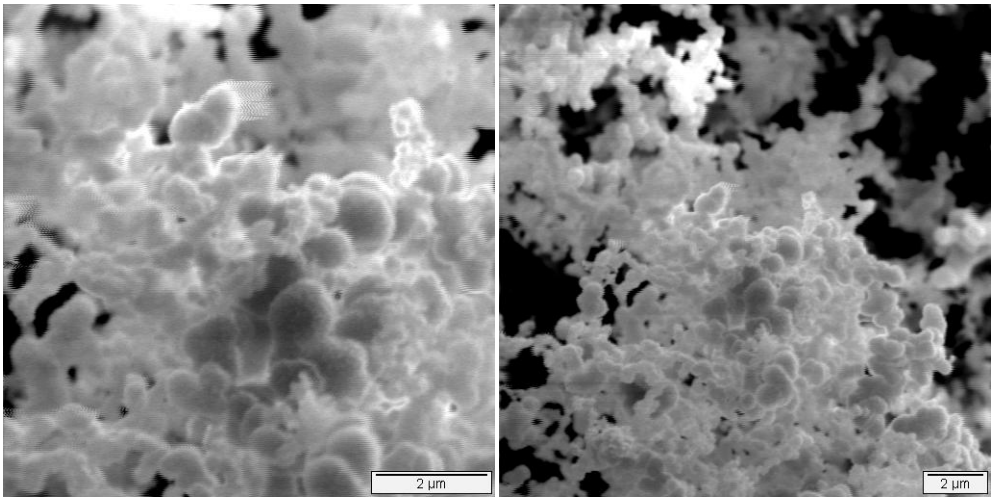

Figure 35: SEM of Degraded Nickelocene degraded at 400°C at High Magnification

6.2.3 Scanning Electron Microscopy of Degraded Iron Pentacarbonyl/Nickelocene Mixture

The mixture of Iron Pentacarbonyl and Nickelocene was also run through the SEM. Figure 36 displays a wide range micrograph of the degraded species. When compared to the species taken of degraded Iron carbonyl at 50µm and 10µm magnifications, it is clear that the resultant structure of mixed organometallics has a different structure observed in the degradation studies of both iron carbonyl and degraded nickelocene. The quality of the degraded mixture appears as a middle ground between the singular fibers as observed in the degraded iron carbonyl and the dense clusters observed in the degraded nickelocene.

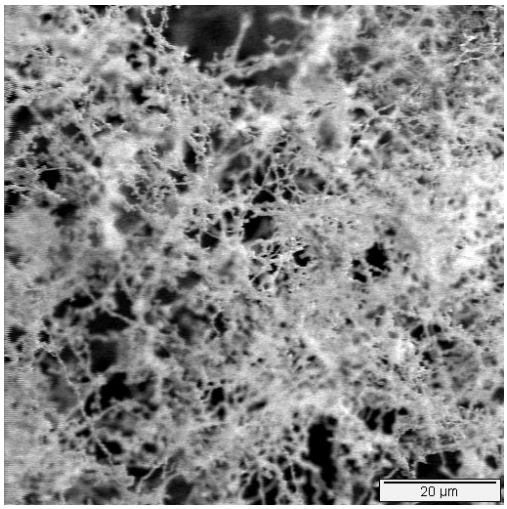

Figure 36: SEM of 20:1 [Fe-P:Ni-C] Mixture degraded at 400°C at Low Magnification

At higher magnifications, such as is observed at Figure 37, one can see that the structure viewed at 2µm is different than that of the degraded iron carbonyl and degraded nickelocene structures at the same magnification. Whereas the individual iron species appeared as isolated fiber particles of relatively constant diameter, the mixture exhibits a tendency to form masses of interconnected dendritic structures that are lumpier with small potato-shaped projections, though fibrous sections are still present. Concurrently, the architecture of the degraded mixture is also significantly less dense than that of the degraded nickelocene.

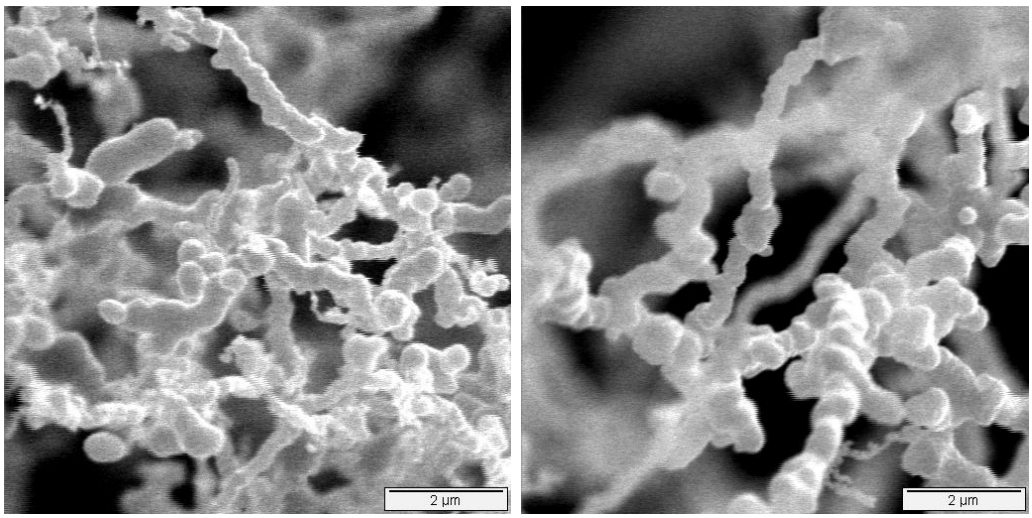

Figure 37: SEM of 20:1 [Fe-P:Ni-C] Mixture degraded at 400°C at High Magnification

Similarly to the degraded iron carbonyl structure, images were able to be generated without the addition of a conductive coating, leading to the inference that this material contains metallic constituents that give it the ability to conduct electricity.

7.0 Analysis

7.1 Estimation of Weight Losses by Assumed Degradation Products

Prior to degradation study simple weight loss mechanisms were developed to model the change of solid mass during degradation reactions. Theoretical data was generated for the two individual organometallic compounds as well as the combined mixture, and was compared to experimental results with the impetus of discovering discernable results from observed degradation process product measurements.

These anticipated degradation patterns can be classified resulting in elemental metal, permutation of possible oxide or as carbide. For simplicity, it was assumed that a complete reaction would be observed and thus theoretical numbers reflect complete degradation. From identification of possible degradation products, the following equations were developed to characterize the different possible routes of degradation as described in Equations 15-31.

$$Fe(CO)_5 = Fe + 5CO \quad (15)$$
$$2Fe(CO)_5 + 5O_2 = 2Fe + 10CO_2 \quad (16)$$
$$2Fe(CO)_5 + 6O_2 = 2FeO + 10CO_2 \quad (17)$$
$$6Fe(CO)_5 + 17O_2 = 2Fe_3O_4 + 30CO_2 \quad (18)$$
$$4Fe(CO)_5 + 13O_2 = 2Fe_2O_3 + 20CO_2 \quad (19)$$
$$2Fe(CO)_5 = 2Fe + 5CO_2 + 5C \quad (20)$$
$$Fe(CO)_5 + O2 = FeO_2 + 5CO \quad (21)$$
$$2Fe(CO)_5 + 7O2 = 2FeO_2 + 10CO_2 \quad (22)$$
$$Fe(CO)_5 = FeO + 2CO_2 + 3C \quad (23)$$
$$2Fe(CO)_5 = Fe_2O_3 + 7CO + 3C \quad (24)$$
$$3Fe(CO)_5 + 14O_2 = Fe_3C + 14CO_2 \quad (25)$$
$$2Fe(CO)_5 = 2FeO_2 + 3CO_2 + 7C \quad (26)$$
$$Ni(C_5H_5)_2 = Ni + 2(C_5H_5) \quad (27)$$
$$2Ni(C_5H_5)_2 + 15O_2 = 2Ni + 20CO_2 + 10H_2O \quad (28)$$
$$6Ni(C_5H_5)_2 + 69O_2 = 2Ni_3C + 54CO_2 + 30H_2O \quad (29)$$
$$2Ni(C_5H_5)_2 + 16O_2 = 2NiO + 20CO_2 + 10H_2O \quad (30)$$
$$4Ni(C_5H_5)_2 + 53O_2 = 2Ni_2O_3 + 40CO_2 + 20H_2O \quad (31)$$

Hypothetical degradation reactions were analyzed for solid mass content in stages prior and post degradation. These numbers were then used to formulate a mass retention percentage which can be

applied to a sample mass (assuming complete reaction). Table 4 reflects the relative percentages of solid mass retention based on the equations given above.

Table 4: Theoretical Mass Retention by Probable Degradation Path

Equation	Theoretical Mass Retention (%)
$Fe(CO)_5 = Fe + 5CO$	28.509
$2Fe(CO)_5 + 5O_2 = 2Fe + 10CO_2$	28.509
$2Fe(CO)_5 + 6O_2 = 2FeO + 10CO_2$	36.677
$6Fe(CO)_5 + 17O_2 = 2Fe_3O_4 + 30CO_2$	39.396
$4Fe(CO)_5 + 13O_2 = 2Fe_2O_3 + 20CO_2$	40.758
$2Fe(CO)_5 = 2Fe + 5CO_2 + 5C$	43.836
$Fe(CO)_5 + O2 = FeO_2 + 5CO$	44.844
$2Fe(CO)_5 + 7O_2 = 2FeO_2 + 10CO_2$	44.844
$Fe(CO)_5 = FeO + 2CO_2 + 3C$	45.873
$2Fe(CO)_5 = Fe_2O_3 + 7CO + 3C$	49.954
$3Fe(CO)_5 + 14O_2 = Fe_3C + 14CO_2$	61.106
$2Fe(CO)_5 = 2FeO_2 + 3CO_2 + 7C$	66.302
$Ni(C_5H_5)_2 = Ni + 2(C_5H_5)$	31.073
$2Ni(C_5H_5)_2 + 15O_2 = 2Ni + 20CO_2 + 10H_2O$	31.104
$6Ni(C_5H_5)2 + 69O_2 = 2Ni_3C + 54CO_2 + 30H_2O$	33.192
$2Ni(C_5H_5)2 + 16O_2 = 2NiO + 20CO_2 + 10H_2O$	39.544
$4Ni(C_5H_5)2 + 53O_2 = 2Ni_2O_3 + 40CO_2 + 20H_2O$	43.782

7.3 Energy-Dispersive X-ray Spectroscopy (EDS)

Degradation products were qualititatively analyzed to determine elemental content using electron-dispersive spectroscopy.

7.3.2 Nickelocene Degraded at 400°C

To determine elemental content of the degraded organometallics, energy-dispersive x-ray spectroscopy was conducted on the degraded nickelocene sample as viewed in the scanning electron micrographs above. Two spots were analyzed for elemental content. Figure 38 and 39 identify that the primary element of the observed material as nickel with secondary elements oxygen and carbon also being present.

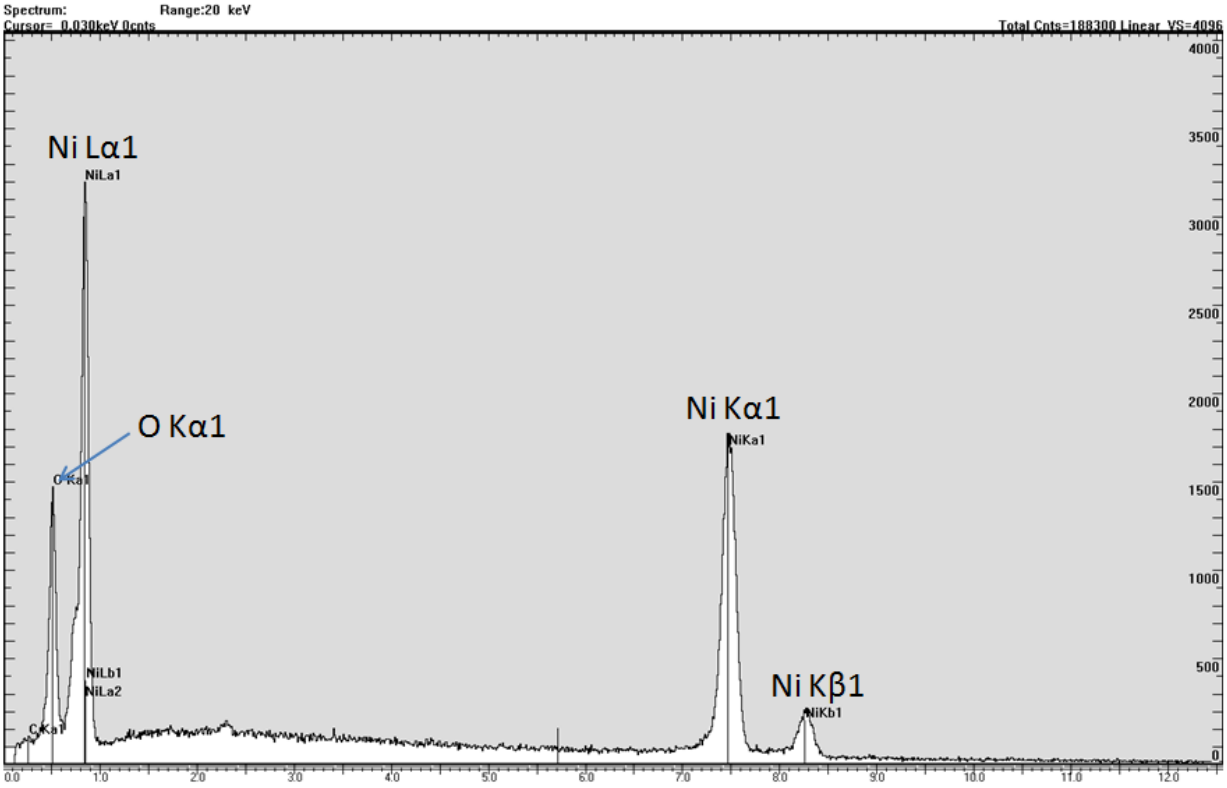

Figure 38: EDS of Nickelocene Degraded at 400°C Narrow Scan

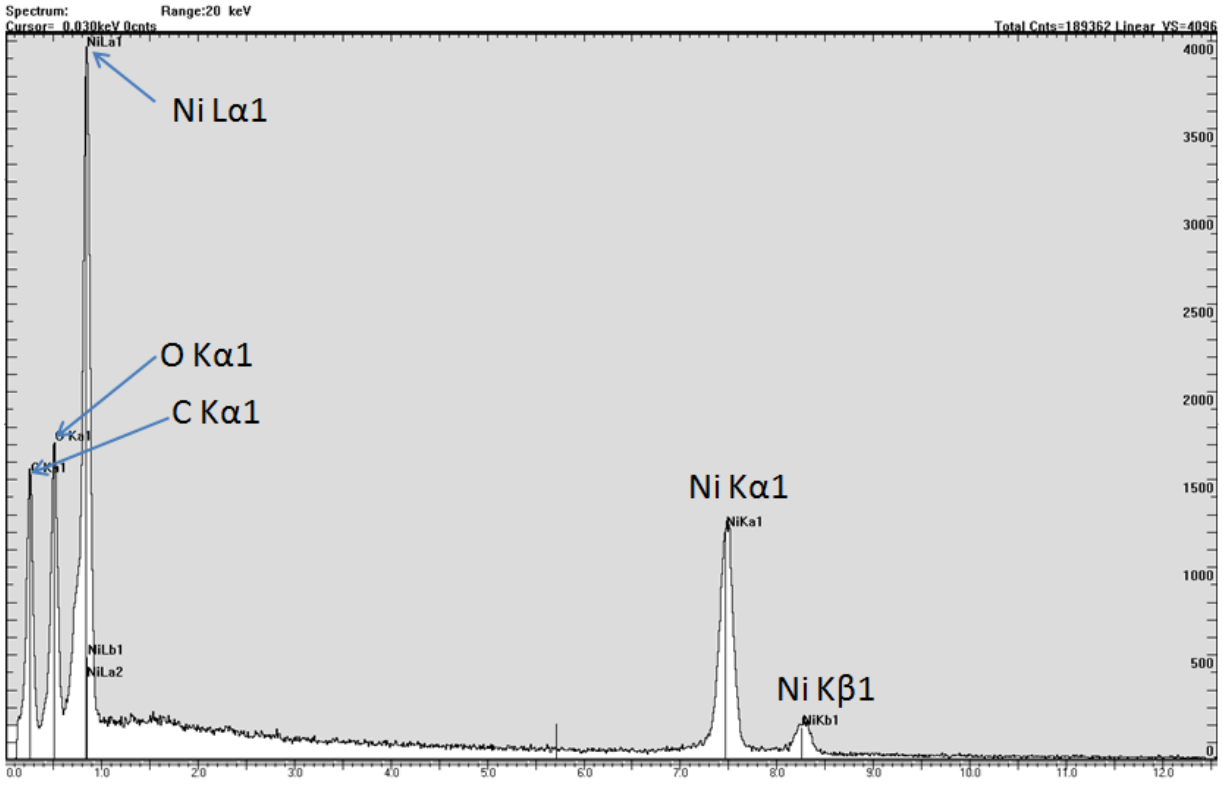

Figure 39: EDS of Nickelocene Degraded at 400°C Wide Scan

7.3.2 Iron-Nickel Mixture Degraded at 300°C

Figure 40 represents data taken from a large area scan of a sample prepared from Iron-Nickel mixture prepared by degradation at 300°C. In this diagram, a trace amount of nickel can be observed. Strong carbon peaks are present, though carbon associated with the adhesive tape used to prepare the sample could contribute to this peak; when thicker areas of the sample were viewed, carbon peak was shown to be less prominent.

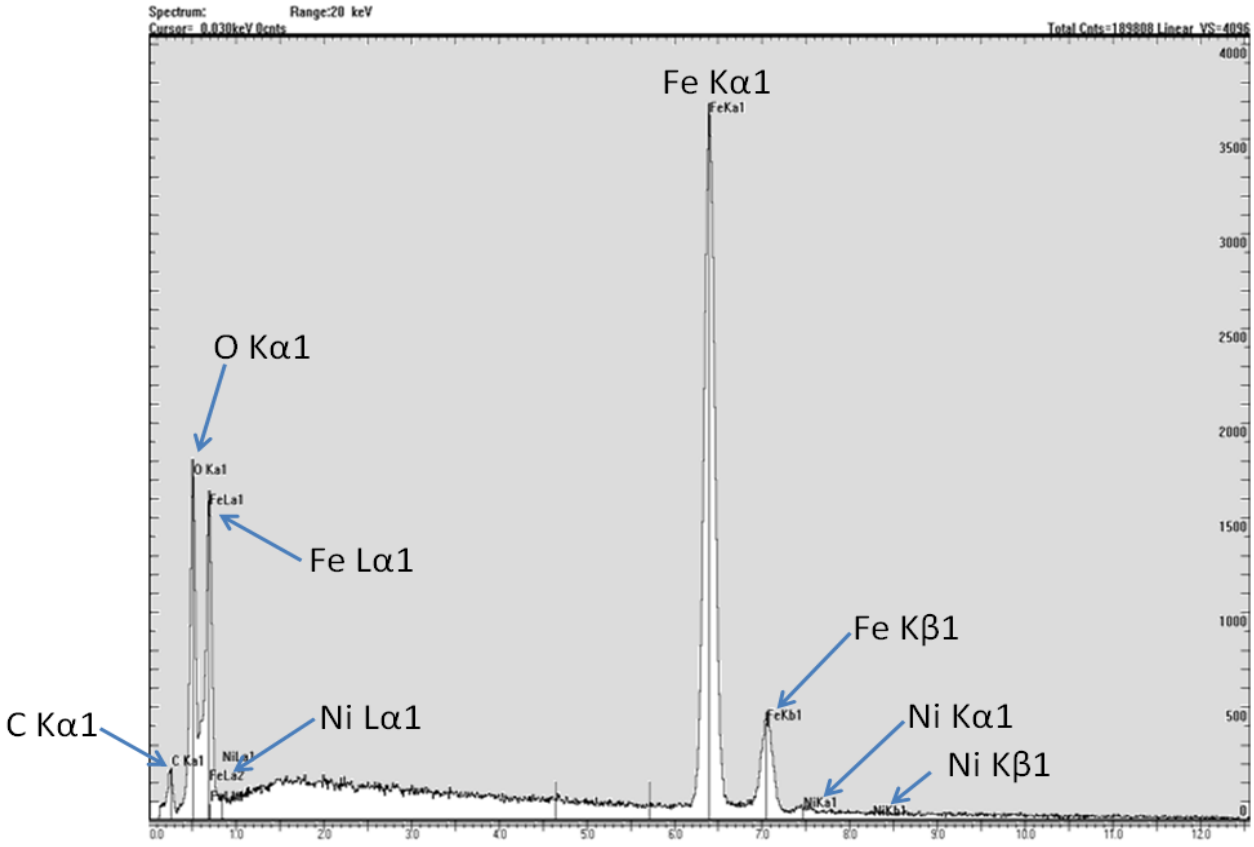

Figure 40: EDS of 20:1 [Fe-P:Ni-C] Mixture Degraded at 300°C

7.3.3 Iron-Nickel Mixture Degraded at 400°C

Figure 41 represents data taken from an area scan of a sample prepared from Iron-Nickel mixture prepared by degradation at 400°C. From this graph, it can be clearly established that by degrading mixture samples in this way, compounds that form consisting of iron and nickel can be formed.

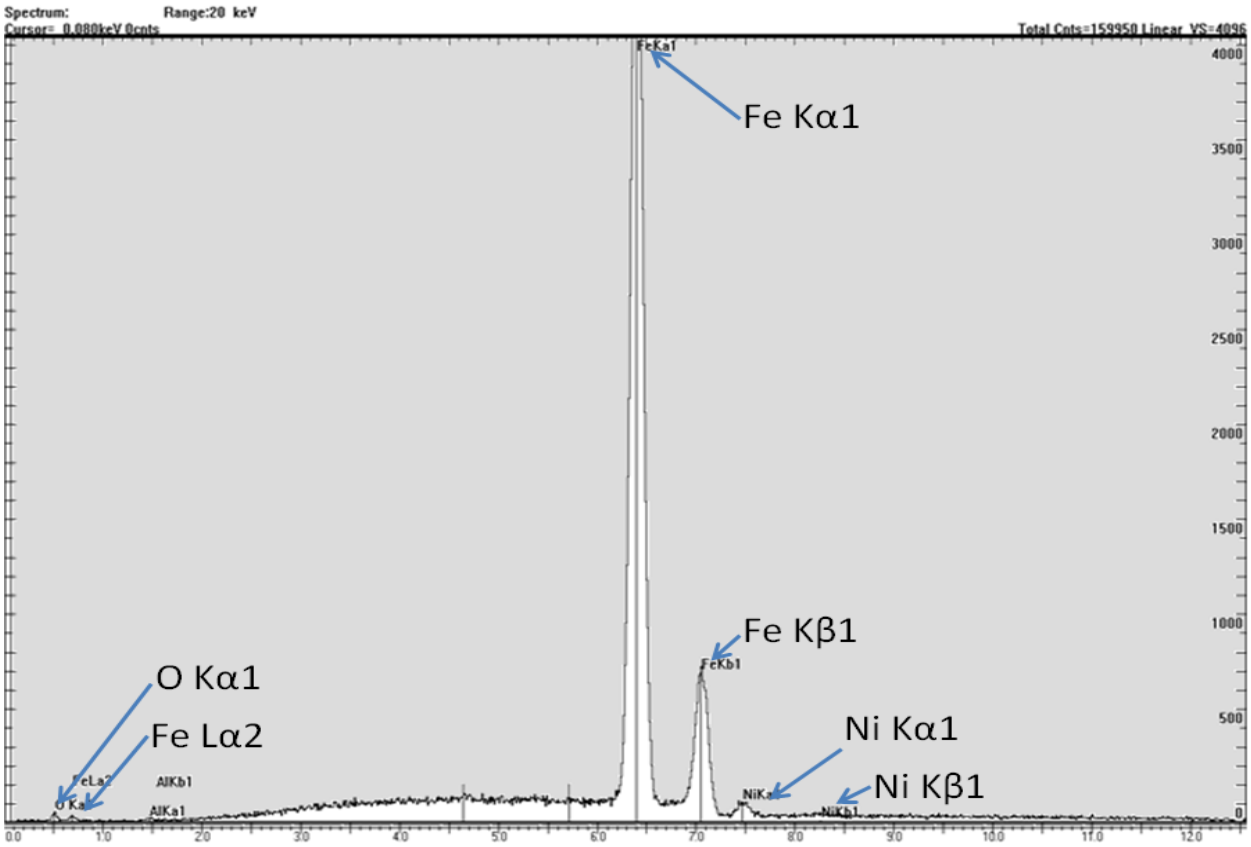

Figure 41: EDS of 20:1 [Fe-P:Ni-C] Mixture Degraded at 400°C

7.4 Compound Analysis by X-Ray Diffraction

X-ray diffraction was used to identify different phases of products of degradation. X-ray diffraction is ideal for compound analysis because of the ample database of known materials as well as its ability to identify different reflection planes within a given sample. X-ray diffraction results that contained iron were benchmarked against a calibrated iron specimen.

7.4.1 Calibration Versus Known Sources of Iron

X-ray diffraction analysis can include erroneous information if systems are not properly calibrated. This is especially important as the primary method of matching peaks to known materials relies on data collected on different equipment, substrate material and other factors. Experimental scans were conducted on bar form iron to assure that measured results correlated with accepted peak values as is available via JCPDs Powder Diffraction Files (PDFs). A small sample of 1018 Steel (C .15-.20%; Mn .60-

.90%; P <.04%, S<.05%) (1) was used in this study. Figure 42 describes experimental data collected compared to that collected for Alpha Iron information as provided on PDF # 98-000-0259.

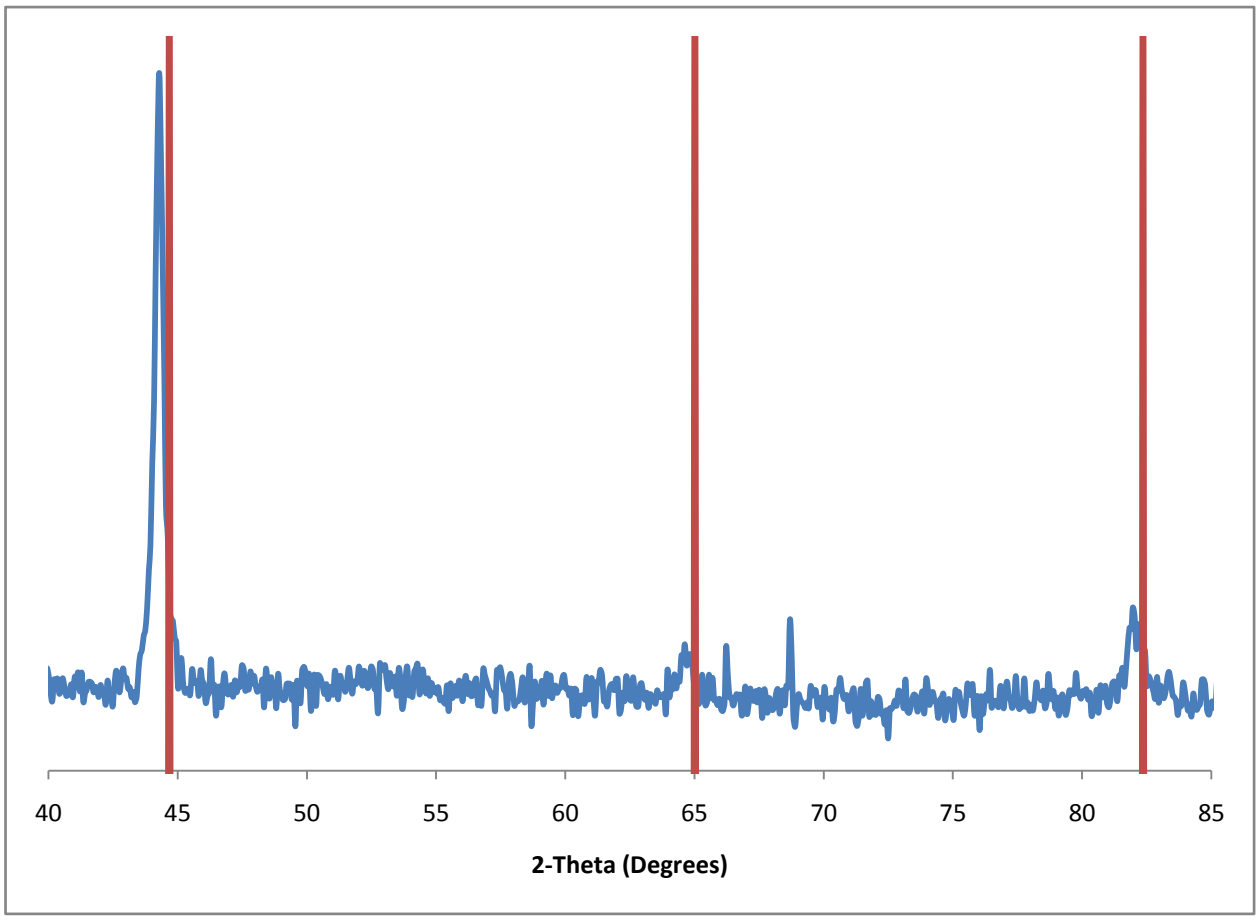

Figure 42: XRD of 1018 Steel Bar

Results observed from the comparison can be viewed in Table 5. Unidentified peaks were observed at angle values of 66.22° and 68.69°. These peaks were not identified, as suitable identification software was not available in the Washburn Laboratories x-ray diffraction lab. It is assumed that this reflection corresponds to one of the dissolved interstitial elements included in the Steel 1018 structure, such as carbon, manganese, phosphorus or sulfur. Peak shifting was observed by approximately 0.4° in all peak values; Error was tabulated by taking the quotient of the peak shift with accepted values. This shift can be contributed to stresses imparted in the steel lattice structure either caused by interstitial atoms or

residual stresses imparted during shaping operations. Data regarding Reflection plane were taken from information included in the Powder Diffraction File, which is included in the appendix of this report.

Table 5: Observations from Experimental Scan of Iron Bar

Measured Peaks (Degrees)	Accepted Peak Values (Degrees)	Peak Shift (Degrees)	Reflection Plane (hkl)	Relative Intensity (I./I)	Error [PS/A] (%)
44.28	44.68	-0.4	(110)	100	0.90
64.62	65.02	-0.4	(200)	13.7	0.62
81.92	82.36	-0.44	(211)	24.4	0.53

Judging by the relative proximity of observed peaks versus expected peaks, it can be said with reasonable accuracy that the Steel 1018 bar can be used as a satisfactory model as a benchmark for iron models. However, because this sample exists in bulk form, powder samples must be generated to guarantee that a powder sample can generate similar peaks when exposed to an x-ray scan.

Iron Powder sample was prepared by mechanical filing of the Steel 1018 sample using a hardened steel file available in the Washburn machine shops. Experimental runs were conducted at a step scan rate of .5°/s in a Rikagu X ray diffractometer. A silicon-based flexiglas sample holder was used for sample runs to mitigate background peaks. Scans were run between 2Θ values of 20° and 90°. Results from this experimental scan including software based peak matching can be viewed in Figure 43.

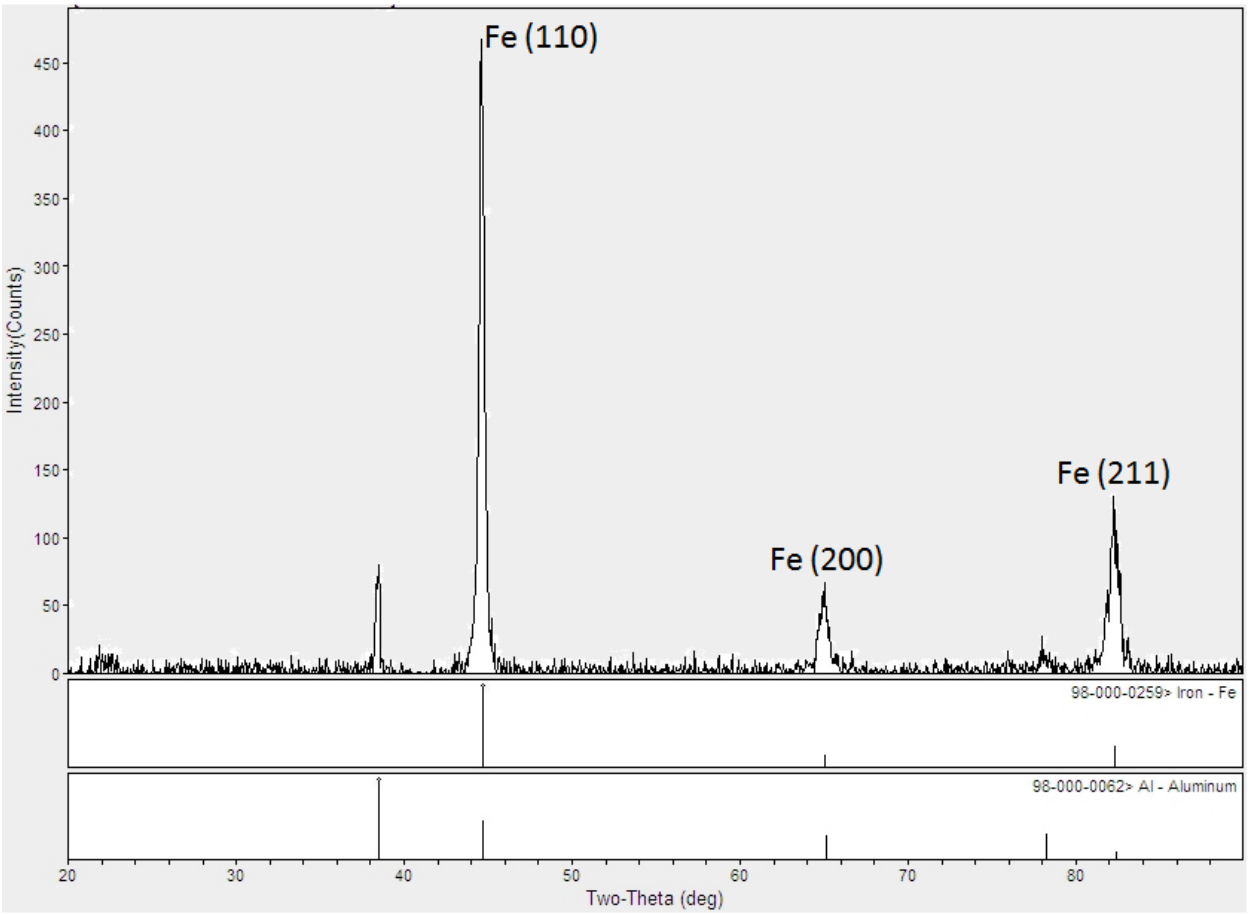

Figure 43: XRD of 1018 Steel Bar Mechanically Ground to Fine powder

In addition to the expected iron peaks, primary and secondary peaks for Aluminum (2Θ=38.5°,78.0°) were also observed in this sample. Whereas the steel sample used to generate powders does not contain aluminum, this contamination can be attributed to the use of machine shop steels which contributed small amounts of aluminum powder to the sample powder. Results from powder observations can be viewed in Table 6.

Table 6: Experimental Scan of Iron Powder versus Expected Peak 2-theta Values

Measured Values (Degrees)	Expected Values (Degrees)	Peak Shift (Degrees)	Reflection Planes	Relative Intensity (I./I)	Error [Peak Shift/ Accepted Value] %
38.5	-	-	-	-	-
44.7	44.68	0.02	(110)	100	0.04
65.0	65.02	-0.02	(200)	13.7	0.03
82.3	82.36	-0.05	(211)	24.4	0.07
78.0	-	-	-	-	-

7.4.2 Compound Analysis of Degraded Iron Carbonyl

Experimental scans of degraded iron pentacarbonyl powder sample degraded at 400°C were run using a Rikagu x-ray diffractometer using a flexiglas sample holder at a step rate of .5°/s at 2Θ ranges between 20° and 90°. Experimental data was compared against known powder diffraction peaks using JADE powder diffraction software. It was found that the degraded iron carbonyl powder was a mixture of Magnetite (Fe_3O_4), Hematite (Fe_2O_3) and Iron. Figure 44 describes the result of experimental rate scan conducted on the Iron Pentacarbonyl sample.

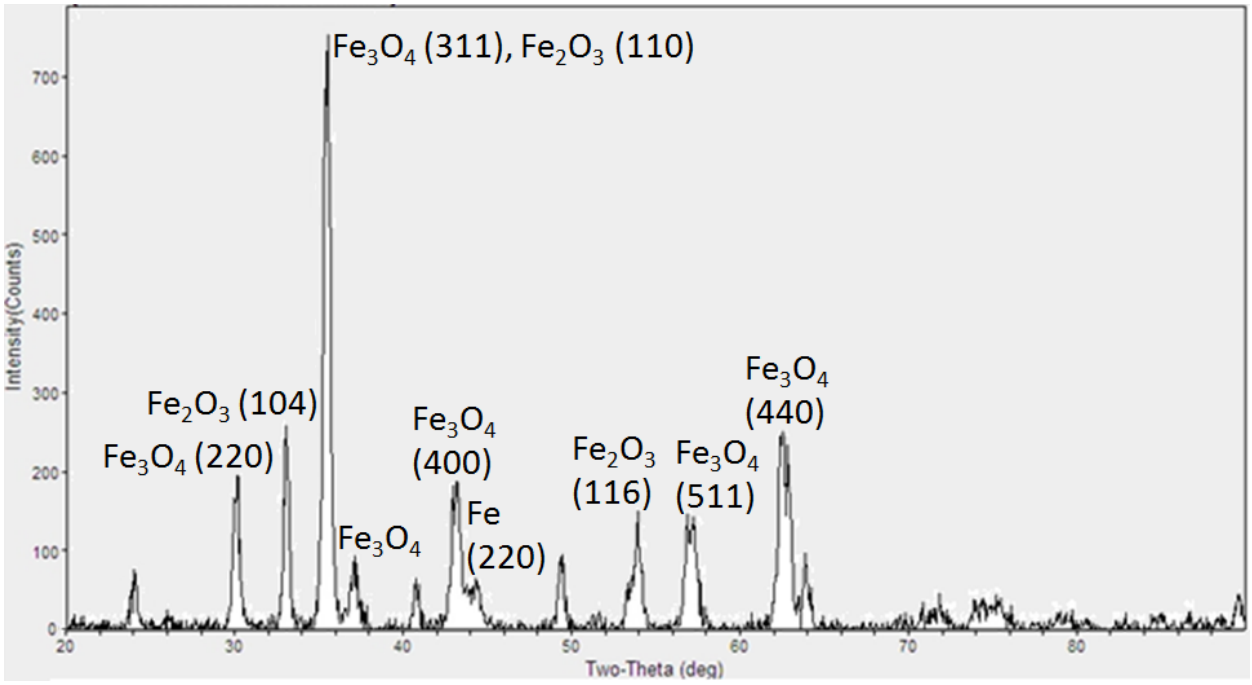

Figure 44: XRD of Iron Pentacarbonyl Degraded at 400°C

Table 7 describes in greater detail the findings of this experimental study as a function of relative accuracy of observed peaks versus matched values.

Table 7: Sample Peaks of Degraded Iron pentacarbonyl vs. Peaks of Known Materials

Measured Peaks (Degrees)	Relative Intensity	Magnetite Peaks (Degrees)	I(f)	Reflection Plane	Hematite Peaks (Degrees)	I(f)	Reflection Plane	Iron Peaks (Degrees)	I(f)	Reflection Plane
35.35	100.0	35.426	100.0	(311)	35.63	72.1	(110)	-	-	-
33.05	44.6	-	-	-	33.162	100.0	(104)	-	-	-
62.35	42.5	62.522	42.8	(440)	-	-	-	-	-	-
29.95	27.0	30.077	28.7	(220)	-	-	-	-	-	-
56.08	22.1	56.937	31.9	(511)	-	-	-	-	-	-
44.40	20.8	-	-	-	-	-	-	44.673	100.0	(220)
53.90	20.1	-	-	-	54.074	50.3	(116)	-	-	-
42.95	18.6	43.054	21.6	(400)	-	-	-	-	-	-
49.35	16.4	-	-	-	49.464	40.0	(024)	-	-	-
24.00	14.5	-	-	-	24.15	30.7	(012)	-	-	-
63.90	13.7	-	-	-	63.99	33.2	(214)	-	-	-
40.65	11.5	-	-	-	40.863	23.0	(113)	-	-	-
89.41	8.4	89.6	14.3	(731)	-	-	-	-	-	-
36.90	7.9	-	-	-	-	-	-	-	-	-
73.71	6.3	-	-	-	71.962	12.1	(1010)	-	-	-
71.91	6.0	-	-	-	69.604	32.6	(300)	-	-	-

Relative accuracy of sample data was compared for statistical error against proposed matches. Table 8 describes data generated based on comparison of measured and accepted powder diffraction file values.

Table 8: Accuracy of Experimental Scan of Degraded Iron Pentacarbonyl

Observed Peaks (Degrees)	Relative Intensity (I./Imax)	Magnetite	Hematite	Iron	Peak Shift (Degrees)	Error [Peak Shift/ Accepted Value] %
35.35	100.0	35.426	-	-	-0.08	0.21
35.35	100.0	-	35.63	-	-0.28	0.79
33.05	44.6	-	33.162	-	-0.11	0.34
62.35	42.5	62.522	-	-	-0.17	0.28
29.95	27.0	30.077	-	-	-0.13	0.42
56.08	22.1	56.937	-	-	-0.86	1.51
44.40	20.8	-	-	44.673	-0.27	0.61
53.90	20.1	-	54.074	-	-0.17	0.32
42.95	18.6	43.054	-	-	-0.10	0.24
49.35	16.4	-	-	49.464	-0.11	0.23
24.00	14.5	-	-	24.15	-0.15	0.62
63.90	13.7	-	-	63.99	-0.09	0.14
40.65	11.5	-	-	40.863	-0.21	0.52
89.41	8.4	89.6	-	-	-0.19	0.21
36.90	7.9	-	-	-	-	-
73.71	6.3	-	71.962	-	1.75	2.43
71.91	6.0	-	69.604	-	2.31	3.31

7.4.2 Compound Analysis of Degraded Nickelocene

Experimental scans of degraded nickelocene powder sample degraded at 400°C were run using a Riau x-ray diffractometer using a flexiglas sample holder at a step rate of .5°/s at 2Θ ranges between 20° and 90°. Experimental data was compared against known powder diffraction peaks using JADE powder diffraction software. It was found that the degraded nickelocene powder was a mixture of bunsenite (NiO) and elemental nickel (Ni). Figure 45 describes the result of experimental rate scan conducted on the Iron Pentacarbonyl sample.

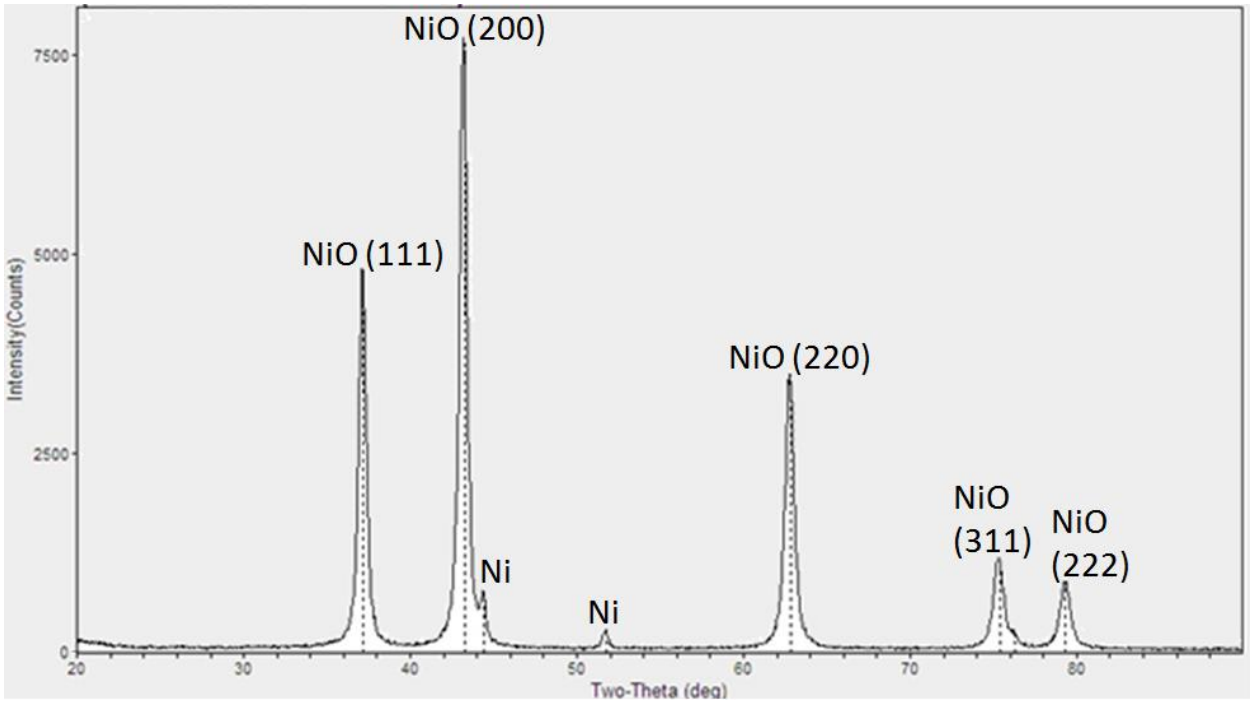

Figure 45: XRD of Nickelocene Degraded at 400°C

Relative accuracy of sample data was compared for statistical error against proposed matches. Table 9 describes data generated based on comparison of measured and accepted powder diffraction file values.

Table 9: Sample Peaks of Degraded Nickelocene vs. Peaks of Known Materials

2 Theta	I./I	Bunsenite	I./I	(hkl)	Nickel	I./I
43.25	100.0	43.276	100	(200)	-	-
37.15	62.4	37.246	64.7	(111)	-	-
62.8	45.3	62.863	51.3	(220)	-	-
75.4	15.4	75.394	18.9	(311)	-	-
79.3	11.6	79.386	14.2	(222)	-	-
44.4	10.0	-	-	-	44.508	100
51.8	3.8	-	-	-	51.847	40

7.5 Determination of Precursor Ratio

Based on experimental results of energy dispersive x-ray spectroscopy and x-ray diffraction analysis, it can be assumed that the primary degradation products formed by high temperature chemical vapor deposition are oxide structures for iron and nickel. Observed include Hematite (Fe_2O_3), Magnetite

(Fe_3O_4, $FeO\text{-}Fe_2O_3$) and Nickel (II) oxide (NiO). Based on literature, the formation of various spinel ceramic formations can be generated based on the atomic fraction of oxygen contained within a matrix that includes metal oxides, as can be viewed in Figure 46.

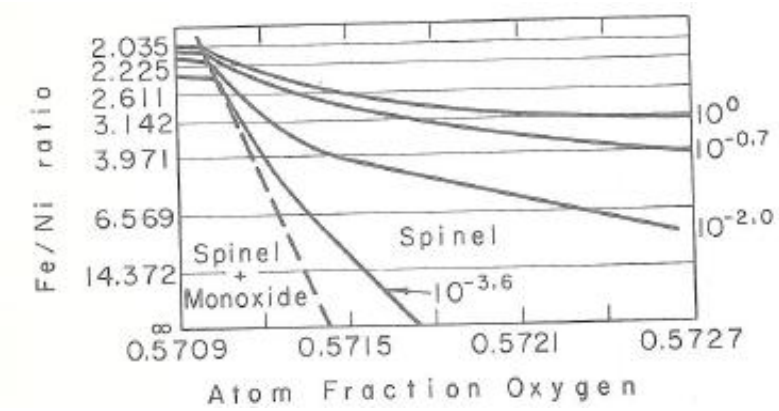

Figure 46: Atomic Fraction Oxygen vs. Fe/Ni Ratio

From the data suggested in this graph, calculations were performed to determine ratios of precursors that would provide three different atomic oxygen fractions: 0.5707, 0.5715 and 0.5727. Atomic fraction oxygen was taken as .5 for NiO, as one of two atoms is oxygen, and .6 for Fe_2O_3, as three of five atoms is oxygen. For oxygen fractions of 0.5707, 0.5715 and 0.5727, Fe/Ni ratios of 2.41, 2.51 and 2.66 were used respectively; calculations in Appendix 10.3 outline how ratios of NiO and Fe_2O_3 were used to generate relevant ratios. Using calculations that correlate precursor mass to anticipated degradation products [Appendix 10.2] these ratios were translated into needed precursor masses. Final ratios of Fe/Ni were determined to be 2.48, 2.59 and 2.74.

7.6 Compound Analysis of Degraded Mixture

Experimental scans of degraded iron pentacarbonyl/nickelocene powder sample degraded at 400°C were run using a Rikagu x-ray diffractometer using a flexiglas sample holder at a step rate of .5°/s at 2Θ ranges between 20° and 90°. Experimental data was compared against known powder diffraction peaks using JADE powder diffraction software. It was found that the degraded iron carbonyl powder was a mixture of magnetite (Fe_3O_4), hematite (Fe_2O_3) and bunsenite (NiO). Peaks of chromite ($FeCr_2O_4$) $Mn_{23}C_6$,

magnesiochromite ($MgCr_2O_4$) were also observed though it is hypothesized by the group that these matches are due to the relative similarity of these compounds with other observed compounds, namely magnetite.

7.6.1 Compound Analysis at Ratio 1:1 $Fe(CO)_5/Ni(C_5H_5)_2$

Iron pentacarbonyl/Nickelocene was prepared at a ratio of 1:1 and was degraded at 400°C by high temperature chemical vapor deposition. Products of reaction as detected by x-ray analysis included bunsenite (NiO), elemental nickel (Ni), magnesioferrite $Mg(Fe^{3+})_2O_4$, and hematite (Fe_2O_3). Figure 47 is the included information taken from the XRD scan.

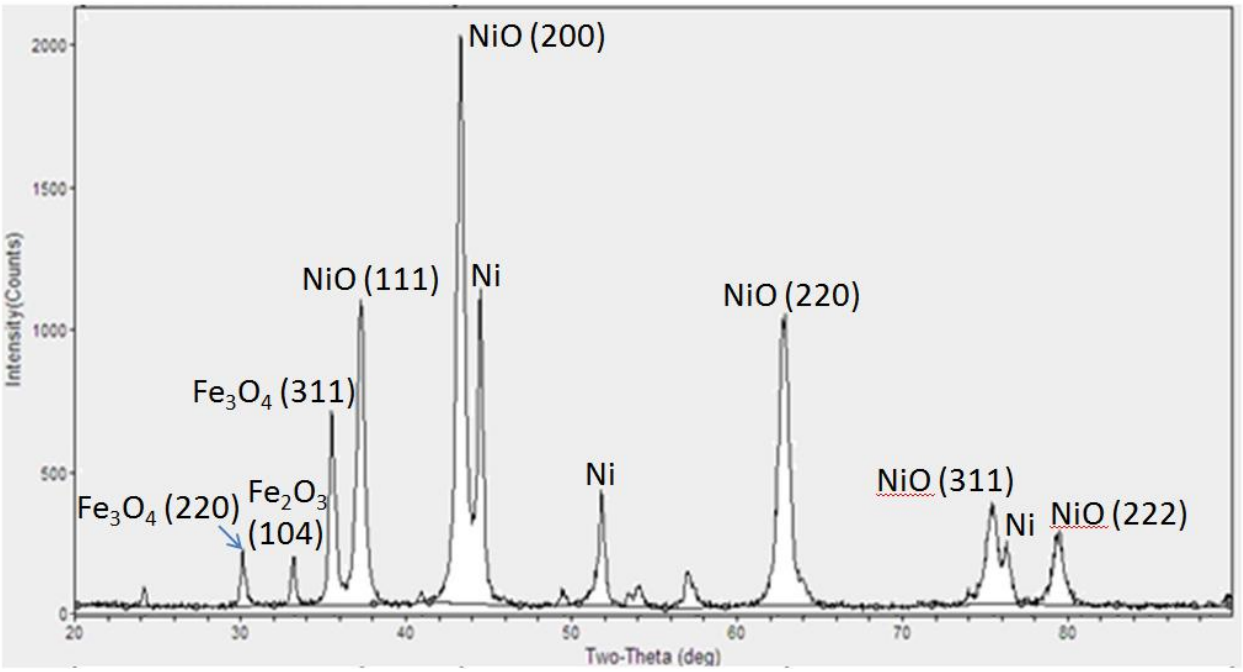

Figure 47: XRD of 1:1 [Fe-P:Ni-C] Mixture Degraded at 400°C

Relative accuracy of sample data was compared for statistical error against proposed matches. Table 10 describes data generated based on comparison of measured and accepted powder diffraction file values.

Table 10: Sample of 1:1 Ratio Mixture Peaks vs. Peaks of Known Materials

2 Theta	I./I	Bunsenite	I./I	(hkl)	Nickel	I./I	Magnesioferrite	I./I	(hkl)	Hematite	I./I	(hkl)
43.35	100.0	43.276	100	(200)	-	-	43.051	28.2	(400)	-	-	-
44.55	56.1	-	-	-	44.508	100	-	-	-	-	-	-
37.35	53.3	37.246	64.7	(111)	-	-	-	-	-	-	-	-
62.95	51.8	62.863	51.3	(220)	-	-	62.517	40.3	440	62.437	33.2	(214)
35.55	35.3	-	-	-	-	-	35.424	100	(331)	-	-	-
51.85	21.6	-	-	-	51.847	40	-	-	-	-	-	-
75.45	19.5	75.394	18.9	(311)	-	-	-	-	-	63.999	32.6	(300)
79.55	14.4	79.386	14.2	(222)	-	-	-	-	-	72.1	35.63	(110)
76.35	12.6	-	-	-	76.372	20	-	-	-	71.962	12.1	(1010)
30.2	11.4	-	-	-	-	-	30.075	26.5	(220)	-	-	-
33.25	10.1	-	-	-	-	-	-	-	-	33.162	100	(104)
57.05	7.6	-	-	-	-	-	56.932	28.1	(511)	-	-	-
54.15	5.1	-	-	-	-	-	-	-	-	54.074	50.3	(116)
24.25	4.9	-	-	-	-	-	-	-	-	24.15	30.7	(012)
49.45	4.7	-	-	-	-	-	-	-	-	49.464	40	(024)
41.05	4.1	-	-	-	-	-	-	-	-	40.863	23	(113)
53.55	3.7	-	-	-	-	-	-	-	-	-	-	-

Relative accuracy of sample data was compared for statistical error against proposed matches. Table 11 describes data generated based on comparison of measured and accepted powder diffraction file values.

Table 11: Accuracy of Experimental Scan of 1:1 [Fe-P:Ni-C]Ratio Mixture

2 Theta	I./I	Bunsenite	Nickel	Magnesioferrite	Hematite	Peak Shift	Error %
43.35	100	43.276	-		-	-0.074	-0.17
43.35	100	-	-	43.051		-0.299	-0.69
44.55	56.1	-	44.508	-	-	-0.042	-0.09
37.35	53.3	37.246	-	-	-	-0.104	-0.28
62.95	51.8	62.863	-	-	-	-0.087	0.00
62.95	51.8	-	-	62.517	-	-0.433	-0.69
62.95	51.8	-	-	-	62.437	-0.513	-0.82
35.55	35.3	-	-	35.424	-	-0.126	-0.36
51.85	21.6	-	51.847	-	-	-0.003	-0.01
75.45	19.5	75.394	-	-	-	-0.056	-0.07
79.55	14.4	79.386	-	-	-	-0.164	-0.21
76.35	12.6	-	76.372	-	-	0.022	0.03
30.2	11.4	-	-	30.075	-	-0.125	-0.42
33.25	10.1	-	-	-	33.162	-0.088	-0.27
57.05	7.6	-	-	56.932	-	-0.118	-0.21
54.15	5.1	-	-	-	54.074	-0.076	-0.14
24.25	4.9	-	-	-	24.15	-0.1	-0.41
49.45	4.7	-	-	-	49.464	0.014	0.03
41.05	4.1	-	-	-	40.863	-0.187	-0.46

7.6.2 Compound Analysis at Ratio 2.48:1 $Fe(CO)_5/Ni(C_5H_5)_2$

Iron pentacarbonyl/Nickelocene was prepared at a ratio of 2.48 and was degraded by high temperature chemical vapor deposition. Products of reaction as detected by x-ray analysis included magnetite (Fe_3O_4), Chromite ($FeCr_2O_4$), Bunsenite (NiO), Hematite (Fe_2O_3), $Mn_{23}C_6$, and Magnesiochromite ($MgCr_2O_4$). Figure 48 is the included information taken from the experimental scan.

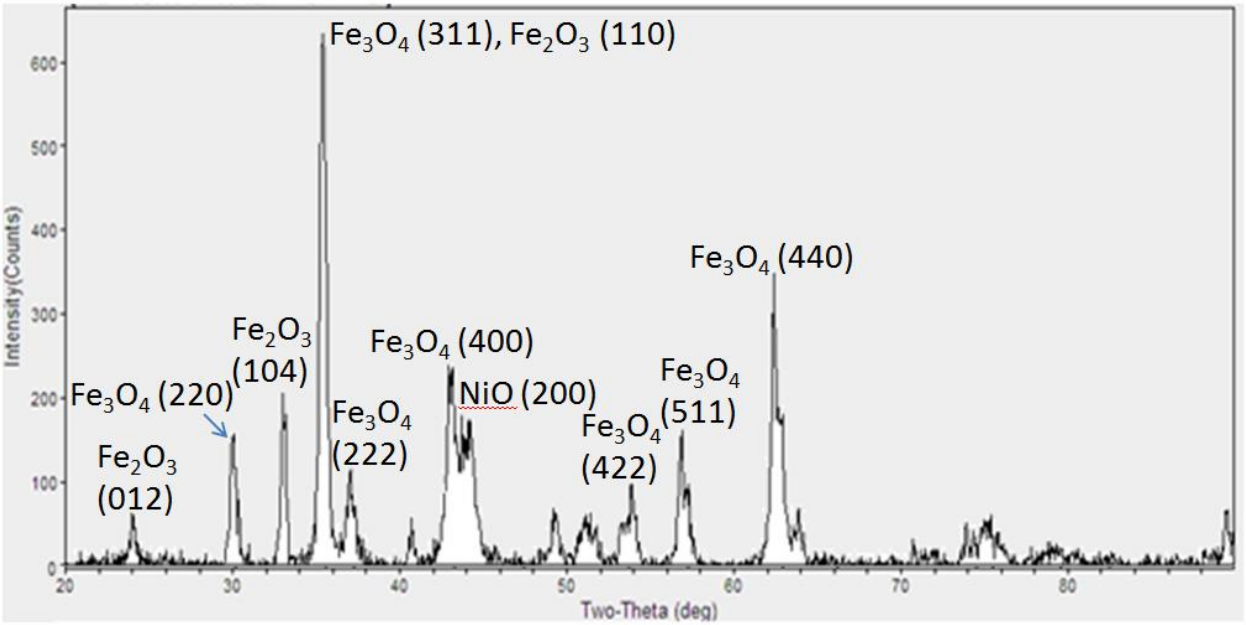

Figure 48: XRD of 2.48:1 [Fe-P:Ni-C] Mixture Degraded at 400°C

Table 12: Sample of 2.48 Ratio Mixture Peaks vs. Peaks of Known Materials

Measured Peaks (Degrees)	I./I	Magnetite	I(f)	(hkl)	Hematite	I(f)	(hkl)	Bunsenite	I(f)	(hkl)
35.45	100.00	35.426	100	(311)	35.63	72.1	(110)	-	-	-
62.45	46.85	62.522	42.8	(440)	-	-	-	62.863	51.3	(220)
43.25	38.45	43.054	21.6	(400)	-	-	-	43.276	100	(200)
33.2	30.99	-	-	-	33.162	100	(104)	-	-	-
44.25	27.63	-	-	-	-	-	-	-	-	-
30.1	27.00	30.077	28.7	(220)	-	-	-	-	-	-
56.95	25.11	56.937	31.9	(511)	-	-	-	-	-	-
37.1	20.06	-	-	-	-	-	-	37.246	64.7	(111)
53.9	15.02	-	-	-	54.074	50.3	(116)	-	-	-
24	11.55	-	-	-	24.15	30.7	(012)	-	-	-
51.25	11.13	-	-	-	-	-	-	-	-	-
75.45	10.82	-	-	-	-	-	-	75.394	18.9	(311)
40.8	10.19	-	-	-	40.863	23	(113)	-	-	-
49.25	10.19	-	-	-	49.464	40	(024)	-	-	-

Relative accuracy of sample data was compared for statistical error against proposed matches. Table 12 describes data generated based on comparison of measured and accepted powder diffraction file values.

Table 13: Accuracy of Experimental Scan of 2.48 [Fe-P:Ni-C] Ratio Mixture

Measured Peaks (Degrees)	I./I	Magnetite	Hematite	Bunsenite	Peak Shift	Error [Peak Shift /Accepted Value] %
35.45	100	35.426	-	-	-0.024	-0.07%
35.45	100	-	35.63	-	0.18	0.51%
62.45	46.85	62.522	-	-	0.072	0.12%
62.45	46.85	-	-	62.863	0.413	0.66%
43.25	38.45	43.054	-	-	-0.196	-0.46%
43.25	38.45	-	-	43.276	0.026	0.06%
33.2	30.99	-	33.162	-	-0.038	-0.11%
44.25	27.63	-	-	-	-	-
30.1	27	30.077	-	-	-0.023	-0.08%
56.95	25.11	56.937	-	-	-0.013	-0.02%
37.1	20.06	-	-	37.246	0.146	0.39%
53.9	15.02	-	54.074	-	0.174	0.32%
24	11.55	-	24.15	-	0.15	0.62%
51.25	11.13	-	-	-	-	-
75.45	10.82	-	-	75.394	-0.056	-0.07%
40.8	10.19	-	40.863	-	0.063	0.15%
49.25	10.19	-	49.464	-	0.214	0.43%

7.6.3 Compound Analysis at Ratio 2.59:1 $Fe(CO)_5/Ni(C_5H_5)_2$

Iron pentacarbonyl/Nickelocene was prepared at a ratio of 2.59 and was degraded by high temperature chemical vapor deposition. Products of reaction as detected by x-ray analysis included magnetite (Fe_3O_4), Chromite ($FeCr_2O_4$), Bunsenite (NiO), Hematite (Fe_2O_3), $Mn_{23}C_6$, and Magnesiochromite ($MgCr_2O_4$). Figure 49 is the included information taken from the experimental scan.

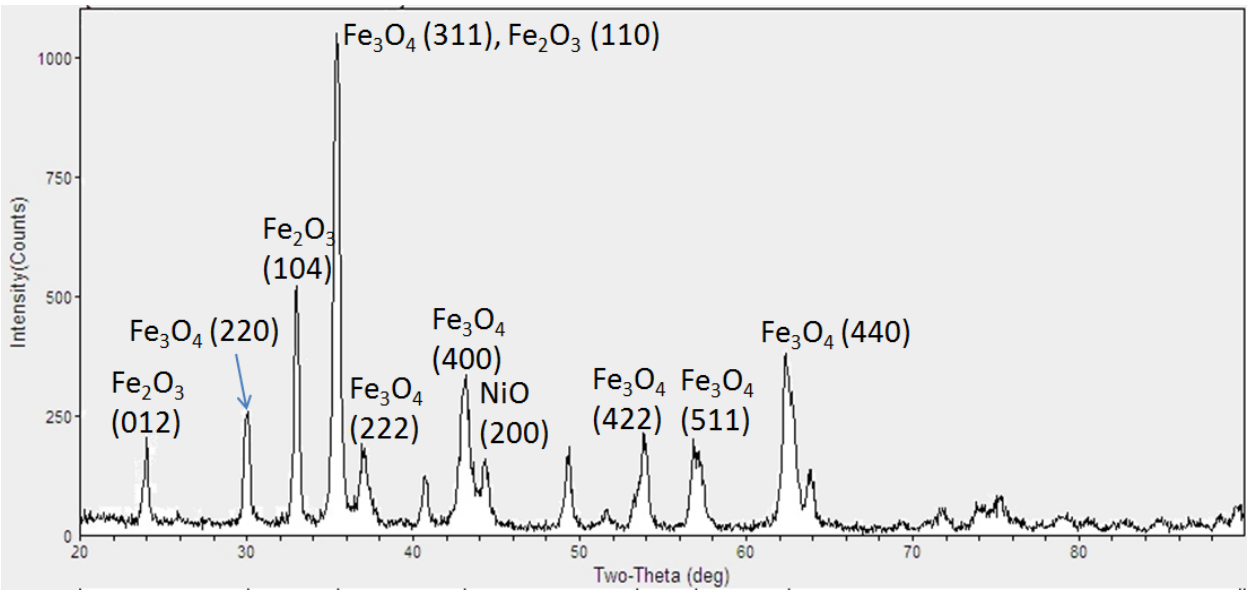

Figure 49: X-ray Scan of 2.59:1 [Fe-P:Ni-C] Mixture Degraded at 400°C

Table 14: Sample of 2.59 Ratio Mixture Peaks vs. Peaks of Known Materials

Measured Peaks (Degrees)	I./I	Magnetite	I(f)	(hkl)	Hematite	I(f)	(hkl)	Bunsenite	I(f)	(hkl)
35.45	100.00	35.426	100	(311)	35.63	72.1	(110)	-	-	-
33.05	50.14	-	-	-	33.162	100	(104)	-	-	-
62.45	36.25	62.522	42.8	(440)	62.437	33.2	(214)	62.863	51.3	(220)
43.2	32.06	43.054	21.6	(400)	-	-	-	43.276	100	(200)
30.1	24.74	30.077	28.7	(220)	-	-	-	-	-	-
53.9	20.55	-	-	-	54.074	50.3	(116)	-	-	-
24.05	19.51	-	-	-	24.15	30.7	(012)	-	-	-
56.9	19.41	56.937	31.9	(511)	-	-	-	-	-	-
37	18.27	-	-	-	-	-	-	37.246	64.7	(111)
49.4	17.89	-	-	-	49.464	40	(024)	-	-	-
63.95	13.23	-	-	-	63.999	32.6	(300)	-	-	-
40.8	11.99	-	-	-	40.863	23	(113)	-	-	-
75.35	8.09	-	-	-	-	-	-	75.394	18.9	(311)
71.65	5.71	-	-	-	71.962	12.1	(1,0,10)	-	-	-
51.75	5.33	-	-	-	-	-	-	-	-	-

Relative accuracy of sample data was compared for statistical error against proposed matches. Table 14 describes data generated based on comparison of measured and accepted powder diffraction file values.

Table 15: Accuracy of Experimental Scan of 2.59 [Fe-P:Ni-C] Ratio Mixture

2 Theta (Degrees)	I./I	Magnetite	Hematite	Bunsenite	Peak Shift	Error [Peak Shift /Accepted Value] %
35.45	100	35.426	-	-	-0.024	-0.07%
35.45	100	-	35.63		0.18	0.51%
33.05	50.14	-	33.162	-	0.112	0.34%
62.45	36.25	62.522	-	-	0.072	0.12%
62.45	36.25	-	62.437	-	-0.013	-0.02%
62.45	36.25	-	-	62.863	0.413	0.66%
43.2	32.06	43.054	-	-	-0.146	-0.34%
43.2	32.06	-	-	43.276	0.076	0.18%
30.1	24.74	30.077	-	-	-0.023	-0.08%
53.9	20.55	-	54.074	-	0.174	0.32%
24.05	19.51	-	24.15	-	0.1	0.41%
56.9	19.41	56.937	-	-	0.037	0.06%
37	18.27	-	-	37.246	0.246	0.66%
49.4	17.89	-	49.464	-	0.064	0.13%
63.95	13.23	-	63.999	-	0.049	0.08%
40.8	11.99	-	40.863	-	0.063	0.15%
75.35	8.09	-	-	75.394	0.044	0.06%
71.65	5.71	-	71.962	-	0.312	0.43%
51.75	5.33	-	-	-	-	-

7.6.4 Compound Analysis at Ratio 2.74:1 $Fe(CO)_5/Ni(C_5H_5)_2$

Iron pentacarbonyl/Nickelocene was prepared at a ratio of 2.74 and was degraded by high temperature chemical vapor deposition. Products of reaction as detected by x-ray analysis included magnetite (Fe_3O_4), chromite ($FeCr_2O_4$), and hematite (Fe_2O_3). Figure 50 is the included information taken from the XRD scan.

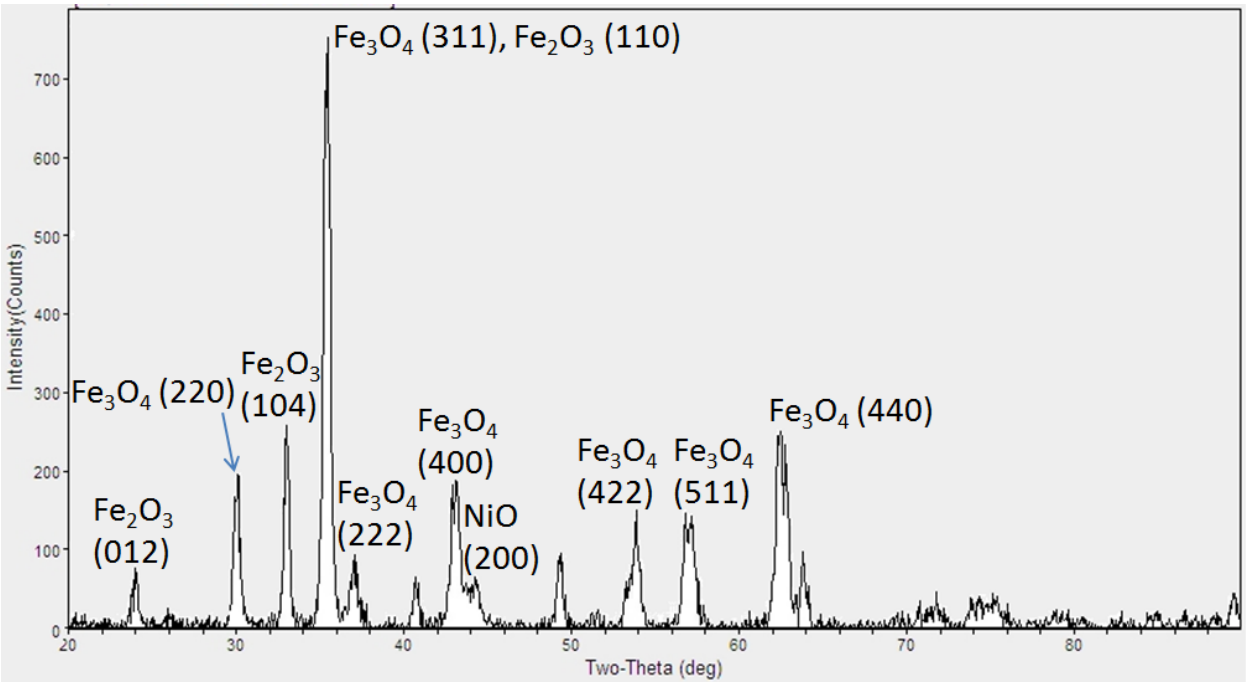

Figure 50: XRD of 2.74:1 [Fe-P:Ni-C] Mixture Degraded at 400°C

Table 16: Sample of 2.74 Ratio Mixture Peaks vs. Peaks of Known Materials

2 Theta (Degrees)	I./I	Magnetite	I(f)	(hkl)	Hematite	I(f)	(hkl)	Bunsenite	I(f)	(hkl)
35.50	100.00	35.426	100	(311)	35.63	72.1	(110)	-	-	-
33.10	36.96	-	-	-	33.162	100	(104)	-	-	-
62.56	35.59	62.522	42.8	(440)	62.437	33.2	(214)	62.863	51.3	(220)
30.20	28.27	30.077	28.7	(220)	-	-	-	-	-	-
43.25	26.53	43.054	21.6	(400)	-	-	-	43.276	100	(200)
53.96	19.21	-	-	-	54.074	50.3	(116)	-	-	-
57.26	19.85	56.937	31.9	(511)				-	-	-
24.05	11.80	-	-	-	24.15	30.7	(012)	-	-	-
57.26	19.85	-	-	-	-	-	-	-	-	-
37.10	13.54	-	-	-	-	-	-	37.246	64.7	(111)
49.46	14.36	-	-	-	49.464	40	(024)	-	-	-
63.91	12.81	-	-	-	63.999	32.6	(300)	-	-	-
40.80	10.06	-	-	-	40.863	23	(113)	-	-	-

Relative accuracy of sample data was compared for statistical error against proposed matches. Table 16 describes data generated based on comparison of measured and accepted powder diffraction file values.

Table 17: Accuracy of Experimental Scan of 2.74 [Fe-P:Ni-C] Ratio Mixture

2 Theta (Degrees)	I./I	Magnetite	Hematite	Bunsenite	Peak Shift	Error
35.5	100	35.426	-	-	-0.074	-0.21%
35.5	100	-	35.63	-	0.13	0.37%
33.1	36.96	-	33.162	-	0.062	0.19%
62.56	35.59	62.522	-	-	-0.038	-0.06%
62.56	35.59	-	62.437	-	-0.123	-0.20%
62.56	35.59	-	-	62.863	0.303	0.48%
30.2	28.27	30.077			-0.123	-0.41%
43.25	26.53	43.054	-	-	-0.196	-0.46%
43.25	26.53	-	-	43.276	0.026	0.06%
53.96	19.21	-	54.074	-	0.114	0.21%
57.26	19.85	56.937		-	-0.323	-0.57%
24.05	11.8		24.15	-	0.1	0.41%
37.1	13.54	-	-	37.246	0.146	0.39%
49.46	14.36	-	49.464	-	0.004	0.01%
63.91	12.81	-	63.999	-	0.089	0.14%
40.8	10.06	-	40.863	-	0.063	0.15%

7.6.5 Compound Analysis at Ratio 5:1 $Fe(CO)_5/Ni(C_5H_5)_2$

Iron pentacarbonyl/Nickelocene was prepared at a ratio of 5:1 and was degraded at 400°C by high temperature chemical vapor deposition. Products of reaction as detected by x-ray analysis included spinel structures, elemental nickel and Bunsenite (NiO). Figure 51 is the included information taken from the experimental scan.

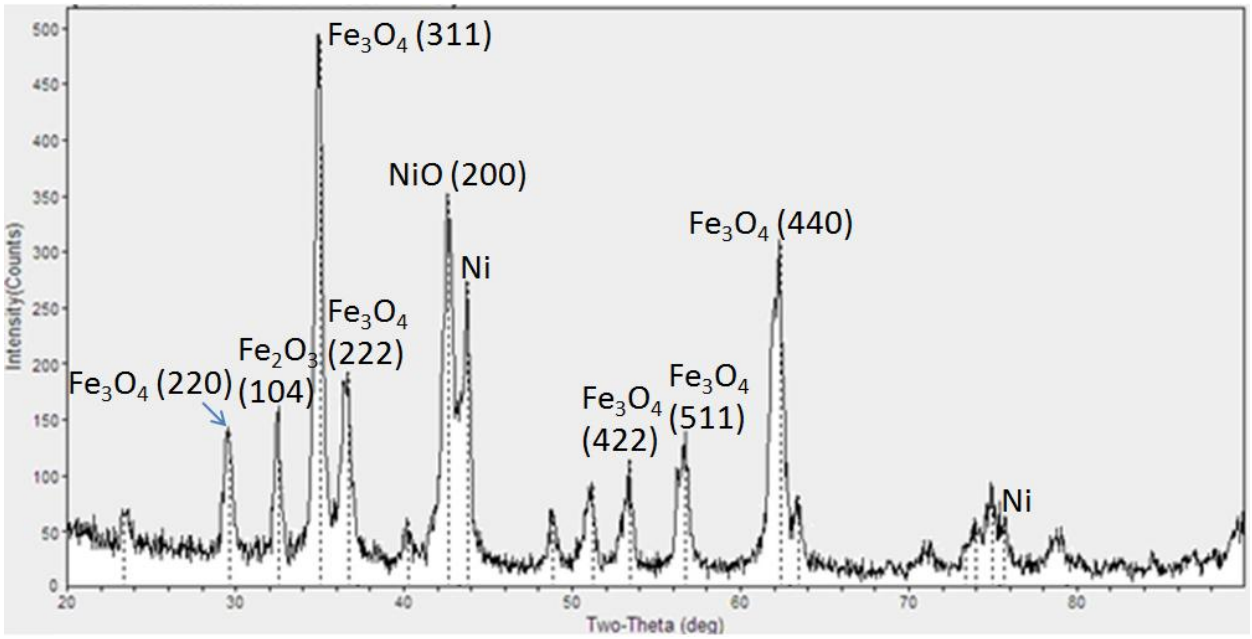

Figure 51: XRD of 5:1 [Fe-P:Ni-C] Mixture Degraded at 400°C

Table 18: Sample of 5:1 Ratio Mixture Peaks vs. Peaks of Known Materials

2 Theta	I./I	Franklinite	I./I	(hkl)	Ilmenite	I./I	(hkl)	Nickel	I./I	Bunsenite	I./I	(hkl)
34.95	100	-	-	-	35.258	65.9	(-110)	-	-	-	-	-
42.6	71.3	42.808	15.8	-400	-	-	-	-	-	43.276	100	-200
62.35	63	62.142	41.6	-440	61.559	34.2	-13	-	-	62.863	51.3	-220
43.8	55.3	-	-	-	-	-	-	44.508	100	-	-	-
36.55	37.4	-	-	-	-	-	-	-	-	37.246	64.7	-111
32.5	31.8	35.227	100	-311	32.526	100	-211	-	-	-	-	-
29.6	28.9	29.909	35.8	-511	-	-	-	-	-	-	-	-
56.75	28.1	56.598	35	-220	-	-	-	-	-	-	-	-
53.45	23.1	53.097	12.2	-422	53.043	40.1	-321	-	-	-	-	-
74.95	19.2	-	-	-	-	-	-	76.372	20	75.394	18.9	-311
51.2	19	-	-	-	-	-	-	51.947	40	-	-	-
23.3	14.2	-	-	-	23.805	27.3	-110	-	-	-	-	-
48.85	14.2	-	-	-	48.723	42.8	-220	-	-	-	-	-
40.25	12.6	-	-	-	40.295	25.8	-210	-	-	-	-	-
63.55	12.3	-	-	-	63.278	29.9	(-211)	-	-	-	-	-
79.1	11.1	-	-	-	-	-	-	-	-	79.386	14.2	-222
71.35	8.5	-	-	-	70.08	10.2	-443	-	-	-	-	-

Relative accuracy of sample data was compared for statistical error against proposed matches. Table 19 describes data generated based on comparison of measured and accepted powder diffraction file values.

Table 19: Accuracy of Experimental Scan of 5:1 [Fe-P:Ni-C] Ratio Mixture

2 Theta (Degrees)	I./I	Franklinite	Ilmenite	Nickel	Bunsenite	Peak Shift	Error %
34.95	100	-	35.258	-	-	0.308	0.87
42.6	71.3	42.808	-	-		0.208	0.49
42.6	71.3				43.276	0.676	1.56
62.35	63	62.142		-		-0.208	-0.33
62.35	63		61.559			-0.791	-1.28
62.35	63				62.863	0.513	0.82
43.8	55.3	-	-	44.508	-	0.708	1.59
36.55	37.4	-	-	-	37.246	0.696	1.87
32.5	31.8		32.526			0.026	0.08
29.6	28.9	29.909	-	-	-	0.309	1.03
56.75	28.1	56.598	-	-	-	-0.152	-0.27
53.45	23.1	53.097		-	-	-0.353	-0.66
53.45	23.1		53.043			-0.407	-0.77
74.95	19.2				75.394	0.444	0.59
51.2	19	-	-	51.947	-	0.747	1.44
23.3	14.2	-	23.805	-	-	0.505	2.12
48.85	14.2	-	48.723	-	-	-0.127	-0.26
40.25	12.6	-	40.295	-	-	0.045	0.11
63.55	12.3	-	63.278	-	-	-0.272	-0.43
79.1	11.1	-	-	-	79.386	0.286	0.36
71.35	8.5	-	70.08	-	-	-1.27	-1.81

7.7 Determination of Relative Amounts from X-ray Peak Intensities

In the interest of determining the relative amount of products formed by high temperature degradation, it was necessary to analyze recorded x-ray diffraction peak data to generate a rough estimate of sample composition.

7.7.1 Determination of Relative Amounts of Iron Pentacarbonyl

Due to the high similarity of primary peak observed in magnetite and secondary peak of hematite.

Omitting this peak from analysis yields the data reflected in the following table; previous data was modified to omit values recorded between 2Θ values between 33.75° and 36.00°. Percentage of materials was done by taking the quotient of the modified intensity with that of the sum of all modified intensities. Through this rough calculation it can be estimated that approximately 41% Fe_2O_3, 39% Fe_3O_4 and 20% Fe. Detailed results can be viewed in Table 20.

Table 20: Relative Amounts of Iron Carbonyl Products from Peak Intensities

Calculated Percent		
Magnetite (%)	Hematite (%)	Iron(%)
38.91	41.20	19.89

7.7.2 Determination of Relative Amounts of Iron Pentacarbonyl/Nickelocene Mixture

For determination of relative amounts of products, it is assumed that the correlation of peaks that does not contain base metals of either iron or nickel to be associated by coincidence and cannot be seriously considered as products generated by the degradation process. Omitting erroneous peak candidates, relative intensities of plots between Magnetite (Fe_3O_4), Hematite (Fe_2O_3), and Bunsenite (NiO) can be observed.

7.7.2.1 Relative amount of mixture at ratio 1:1 $Fe(CO)_5/Ni(C_5H_5)_2$

Relative intensity for mixture materials were calculated by taking the sum of the relative intensity peaks observed at 1:1 ratios omitting peak values that corresponded to more than one material. Specifically angle values of 43.35 and 51.80 were omitted. A modified intensity was instituted taking the intensity peak of 56.1 intensity as the maximum value. Relative percentage was calculated by taking the sum of observed intensities for each material versus the sum of all intensities. Table 21 outlines results taken from this exercise.

Table 21: Percentage of Relative Constituents for 1:1 [Fe-P:Ni-C] Ratio Mixture

Calculated Percent			
Bunsenite	Nickel	Magnesioferrite	Hematite
33.45%	34.64%	20.83%	11.09%

7.7.2.2 Relative amount of mixture at ratio 2.48:1 $Fe(CO)_5/Ni(C_5H_5)_2$

Relative intensity for mixture materials were calculated by taking the sum of the relative intensity peaks observed at 2.48:1 ratios omitting peak values that corresponded to more than one material. Specifically angle values of 35.45, 43.25 and 62.45 were omitted. Measured peak values at 44.25 and 51.25 were omitted because they did not correspond to a known peak. A modified intensity was instituted taking the intensity peak of 30.99 intensity as the maximum value. Relative percentage was calculated by taking the sum of observed intensities for each material versus the sum of all intensities. Table 22 outlines results taken from this exercise.

Table 22: Percentage of Relative Constituents for 2.48:1 [Fe-P:Ni-C] Ratio Mixture

Calculated Percent		
Magnetite	Hematite	Bunsenite
32.38%	48.43%	19.19%

7.7.2.3 Relative amount of mixture at ratio 2.59:1 $Fe(CO)_5/Ni(C_5H_5)_2$

Relative intensity for mixture materials were calculated by taking the sum of the relative intensity peaks observed at 2.48:1 ratios omitting peak values that corresponded to more than one material. Specifically angle values of 35.45, 43.20 and 62.45 were omitted. A modified intensity was instituted taking the intensity peak of 33.05 intensity as the maximum value. Relative percentage was calculated by taking the sum of observed intensities for each material versus the sum of all intensities. Table 23 outlines results taken from this exercise.

Table 23: Percentage of Relative Constituents for 2.59:1 [Fe-P:Ni-C] Ratio Mixture

Calculated Percent		
Magnetite	Hematite	Bunsenite
21.07%	66.35%	12.58%

7.7.2.4 Relative amount of mixture at ratio 2.74:1 $Fe(CO)_5/Ni(C_5H_5)_2$

Relative intensity for mixture materials were calculated by taking the sum of the relative intensity peaks observed at 2.48:1 ratios omitting peak values that corresponded to more than one material. Specifically angle values of 35.50, 43.25 and 62.56 were omitted. A modified intensity was instituted taking the intensity peak of 33.10 intensity as the maximum value. Relative percentage was calculated by taking the sum of observed intensities for each material versus the sum of all intensities. Table 24 outlines results taken from this exercise.

Table 24: Percentage of Relative Constituents for 2.74:1 [Fe-P:Ni-C] Ratio Mixture

Calculated Percent		
Magnetite	Hematite	Bunsenite
28.84%	63.05%	8.11%

7.7.2.5 Relative amount of mixture at ratio 5:1 $Fe(CO)_5/Ni(C_5H_5)_2$

Relative intensity for mixture materials were calculated by taking the sum of the relative intensity peaks observed at 5:1 ratios omitting peak values that corresponded to more than one material. Specifically angle values of 42.6, 62.35 and 53.45 were omitted. Relative percentage was calculated by taking the sum of observed intensities for each material versus the sum of all intensities. Table 25 outlines results taken from this exercise.

Table 25: Percentage of Relative Constituents for 5:1 [Fe-P:Ni-C] Ratio Mixture

Calculated Percent			
Franklinite	Ilmenite	Nickel	Bunsenite
14.52%	49.31%	18.93%	17.24%

8.0 Discussion

8.1 Detection of foreign materials within x-ray diffraction scans

Experimental x-ray diffraction peaks revealed matched peaks with unexpected materials, such as those containing chromite, magnesioferrite, franklinite, and ilmenite. While content of these materials is entirely possible due to metal substitutions and contamination from organometallic reagents, based on the data provided in the material data sheets for both organometallics, it is believed that background noise may be a factor in leading the peak matching software to identify these materials as the primary or secondary constituents of degradation. Additionally, relevant procedures performed on degraded singular species suggest that when either of the two organometallics is degraded by itself simple oxide and metal structures can be deposited at a relatively high purity by identifying characteristic x-rays by electron dispersive x-ray spectroscopy as well as x-ray diffraction of the singular degraded material. To confirm or refute data taken from x-ray diffraction scans more work is needed to establish the repeatability of product generation by this method.

8.2 Proposed reasoning for absence of elemental precursors in degraded mixture

When comparing product findings of the iron pentacarbonyl and nickelocene when degraded singularly against when the organometallic compounds are degraded as a mixture, it can be observed that when degraded unaccompanied, the organometallics will produce trace amounts of elemental metals; this was observed for both iron pentacarbonyl and nickelocene. The detection of elemental constituents after degradation was not observed in the mixture. It is postulated that a possible reasoning for this occurrence is the surplus of valence electrons of the nickelocene organometallic. To achieve valence stability, a metal compound will seek to have its outer valence shell completely filled. Most metallocene complexes fulfill this rule, notable exceptions being Nickel based compounds which exists in a 20 valence configurations. The effect of this valence surplus or debt is that the chemical stability of these

compounds is less than that of a similar compound with 18 valence electrons. This is demonstrated in the thermal stability of Ferrocene, which has a degradation temperature substantially higher than nickelocene while maintaining similar melting characteristics.

9.0 Conclusions and Future Work

Two organometallic species that met selection criteria were successfully chosen and analyzed. Degradation analysis revealed that peak mass retention was approximately 10% original sample mass for iron pentacarbonyl; this number corresponded to a substantial amount of vaporized organometallic escaping experimental systems and was greater than anticipated values. Nickel degradation studies were recorded within theoretical limits for formation of combinations of oxides and metal species. When combined, mixtures were measured to reflect weight losses that correspond to formation oxides and pure metals. Architecture of degraded organometallics using SEM concluded that fiber structures with submicron diameters iron pentacarbonyl/nickelocene mixtures can be generated depending on precursor ratio. From this atomic arrangement, it can be suggested that degraded organometallic compounds may assume a propensity to form fiber structures when degraded. Compound analysis by x-ray diffraction concluded that products of degradation of both pure organometallics contained mixtures of metal and oxides. Mixtures also were typically found to have combinations of oxides depending on the proportion of organometallics selected. Selecting different organometallic structures with better morphologies for producing metallic structures may be selected to form pure metallic alloy structures. Additionally, selection of precursor metals that do not as readily form oxides should be considered. Environmental parameters, such as degradation atmosphere, must be controlled to perform degradation studies where oxidation of deposited metals is avoided.

Future work should delve deeper into the effect of organometallic mixture ratios. In this work, large amounts of product reagents were lost during the reaction process. Future work should optimize degradation conditions in order to maximize generation of solid degradation products in a controlled atmosphere. Use of an electrostatic lab furnace is recommended. Loading of powder samples was limited due to the vertical loading mechanism of the x-ray diffractometer. Data was collected using horizontal loading x-ray diffractometers yielded better results than those taken from than the vertical

mounting x-ray diffractometer. Alternative methods for organometallic degradation including photodegradation microwave ablation, and laser ablation should be further investigated in future work. Additionally, the possibility of using organometallic compounds whose degradation products may form fibers should be applied to electrospinning as the inclination of forming fibers upon degradation may lead to high quality formation of fiber structures upon calcinations of electrospun fibers, fiber mats or membranes.

10.0 Bibliography

1. **Avner, Sidney H.** *Introduction to Physical Metallurgy.* New York, New York : McGraw-Hill Book Company, 1974.

2. **Ravi, B.** *Metal Casting - An Overview.* Bombay, India : s.n., 2004.

3. **Kalpakjian, Serope and Schmid, Steven R.** *Manufacturing Engineering and Technology.* Upper Saddle River : Pearson Prentice Hall, 2006.

4. **Hedge, Raghavendra R, Dahiya, Atul and Kamath, M. G.** Nanofiber Nonwovens. [Online] 6 13, 2005. [Cited: 10 1, 2008.] http://www.engr.utk.edu/mse/pages/Textiles/Nanofiber%20Nonwovens.htm.

5. Electrospinning. [Online] [Cited: 10 1, 2008.] http://www.che.vt.edu/Wilkes/electrospinning/electrspinning.html.

6. *Fabrication and magnetic properties of electrospun copper ferrite (CuFe2O4) nanofibers.* **Ponhan, Wichaid and Maensiri, Wichaid.** 2009, Solid State Sciences, pp. 479-484.

7. *Fabrication and characterization of cobalt ferrite (CoFe2O4) nanofibers by electrospinning.* **Ju, Young-Wan, et al.** 2008, Material Science and Engineering B 147, pp. 7-12.

8. *Thermoelectric oxide NaCo2O4 nanofibers fabricated by electrospinning.* **Maensiri, Santi and Nuansing, Wiwat.** 2006, Material Chemistry and Physics 99, pp. 104-108.

9. **Koch, Carl C.** Synthesis of Nanustrectured materials by Electrodeposition. *Nanostructured Materials - Processing, Properties and Applications (2nd Edition).* s.l. : William Andrew Publsihing, 2007.

10. *Electrodeposition of zinc composite zinc-yttria stabilized zirconia coatings.* **Xia, Xuli, Zhitomirsky, Igor and McDermid, Joseph R.** 2009, Jornal of Materials Processing Technology 209, pp. 2632-2640.

11. *Hard coatings based on thermal sparay and laser cladding.* **Khanna, A.S., et al.** 2009, Int. Journal of Refractory Metals & Hard Materials, pp. 485-491.

12. *Evaluating Zn, Al, Al-Zn coatings on carbon steel in a special atmosphere.* **de Rincon, O., et al.** 2009, Construction and Building materials, pp. 1465-1471.

13. **Eisch, John J.** *The Chemistry of Organometallic Compounds.* New York : The Macmillan Company, 1967.

14. **G.E. Coates, M. L. H. Green, P. Powell,.** *Principles of Organometallic Chemistry.* London : Chapman and Hall, 1988.

15. **Lukehart, Charles M.** *Fundamental Transition Metal Organometallic Chemsitry.* Belmont, CA : Brooks/Cole Publishing Company, 1985.

16. *The synthesis of iron and nickel carbnonyl as calibration material for spectroscopic systems.* **Tepe, Reha K., Vassallo, David and Jacksier, Tracey.** 1999, Spectrochimica Acta Part B, pp. 165-175.

17. *From nickelocene to novel organonickel compounds.* **Pasyniewicz, Stanislaw and Pietrzykowski, Antoni.** 2002, Coordination Chemistry Reviews, pp. 196-202.

18. **Welipitiya, D., et al.** 1997, Surf. Sci, p. 393.

19. **Pierson, H.O.** *Handbook of CHemical Vapor Deposition (CVD) - Principles, Technology and Applications.* 1999.

20. *OMCVD Processes and Precursor Chemistry.* **Thurier, Cyril and Doppelt, Pascal.** 2008, Cordination Chemistry Reviews, pp. 155-169.

21. *Synthesis, Properties, and applications of iron oxide nanoparticles.* **Teja, Amyn S and Koh, Peu-Yoong.** 2008, Progress in Crystal Growth and Characterization of Materials, pp. 1-24.

22. **Sheshan, K.** *Handbook of thin-film deposition processes and techniques: principes, methods and applications.* 2002.

23. *The adsorption of nickelocene Part 2: decomposition and selective area deposition.* **Welipitiya, D., et al.** 1998, Surface Science 418, pp. 466-478.

24. *The removal of carbon monoxide by iron oxide nanoparticles.* **Li, Ping, et al.** 2003, Applied Catalysis B, pp. 151-162.

25. **Hosford, Williiam F.** *Physical Metallurgy.* Boca Raton, FL : CRC Press, 2005.

26. **Cao, Guozhong.** *Nanostructures and Nanomatials: Synthesis, Properties and Applications.* s.l. : Imperial College Press, 2004.

27. **Toreki, Rob.** The organometallic hypertextbook. *www.chemglas.* [Online] 6 28, 2008. [Cited: 10 15, 2008.] http://www.ilpi.com/organomet/index.html.

28. *Synthesis of nickelocene containing polyimides with low-dielectric constants.* **Koytepe, Suleyman, Adiguzel, Ibrahim and Seckin, Turgay.** 2009, Journal of Alloys and Compounds, pp. 347-353.

29. *c-C5H5 on a Ni (111) surface: Theoretical study of adsorption, electronic structure and bonding.* **German, E., et al.** 2008, Applied Surface Chemistry, pp. 5831-5836.

30. **Housecraft, Catherine E. and Sharpe, Alan G.** *Inorganic Chemistry: 2nd Edition.* Essex, England : Pearson, 2004.

31. **Tisza, M.** *Physical Metallurgy for Engineers.* London : ASM International, 2001.

11.0 Appendix

Supplementary information for this report can be viewed in the following subsections.

11.1 Mass Estimation by Theoretical Modeling

Prior to degradation studies, theoretical mass loss calculations were conducted to determine products form by relative weights of elemental metals and their oxides for degradation of individual species and combined mixture. Data surrounding determination of expected degraded products are included below.

Iron Pentacarbonyl

$Fe(Co)5 = 195.90$ g/mol

Anticipated Reactions and recoverable solids

$Fe(CO)5 = Fe + 5CO$
$1(195.90) = 1(55.85)$

$195.90 = 55.85$

$\frac{55.85}{195.90} = 28.509\text{-}\%$

$2Fe(CO)5 + 5O2 = 2Fe + 10CO2$
$2(195.90) = 2(55.85)$

$391.8 = 111.7$

$\frac{111.7}{391.8} = 28.509\text{-}\%$

$2Fe(CO)5 + 6O2 = 2FeO + 10CO2$
$2(195.90) = 2(71.85)$

$391.8 = 143.7$

$\frac{143.7}{391.8} = 36.677\text{-}\%$

$6Fe(CO)5 + 17O2 = 2Fe3O4 + 30CO2$

$6(195.90) = 2(231.53)$

$1175.4 = 463.06$

$\frac{463.06}{1175.4} = 39.396\text{-}\%$

$4Fe(CO)5 + 13O2 = 2Fe2O3 + 20CO2$

$4(195.90) = 2(159.69)$

$783.6 = 319.38$

$\frac{319.38}{783.6} = 40.758\text{-}\%$

$2Fe(CO)5 = 2Fe + 5CO2 + 5C$

$2(195.90) = 2(55.85) + 5(12.01)$

$391.8 = 111.7 + 60.05$

$391.8 = 171.75$

$\frac{171.75}{391.8} = 43.836\text{-}\%$

$Fe(CO)5 + O2 = FeO2 + 5CO$

$(195.90) = (87.85)$

$\frac{87.85}{195.9} = 44.844\text{-}\%$

$2Fe(CO)5 + 7O2 = 2FeO2 + 10CO2$
$2(195.90) = 2(87.85)$

$391.8 = 175.7$

$\frac{175.7}{391.8} = 44.844\text{-}\%$

$Fe(CO)5 = FeO + 2CO2 + 3C$
$2(195.90) = 2(71.85) + 3(12.01)$

$391.8 = 143.7 + 36.03$

$391.8 = 179.73$

$\frac{179.73}{391.8} = 45.873\text{-}\%$

$2Fe(CO)5 = Fe2O3 + 7CO + 3C$

$2(195.90) = (159.69) + 3(12.01)$

$391.8 = 159.69 + 36.03$

$391.8 = 195.72$

$\frac{195.72}{391.8} = 49.954\text{-}\%$

$3Fe(CO)5 + 14O2 = Fe3C + 14CO2$
$3(195.90) = 2(179.56)$

$587.7 = 359.12$

$\frac{359.12}{587.7} = 61.106\text{-}\%$

$2Fe(CO)5 = 2FeO2 + 3CO2 + 7C$
$2(195.90) = 2(87.85) + 7(12.01)$

$391.8 = 175.7 + 84.07$

$391.8 = 259.77$

$\frac{259.77}{391.8} = 66.302\text{-}\%$

Nickelocene

$Ni(C5H5)2 = 188.88$ g/mol

$Ni(C5H5)2 = Ni + 2(C5H5)$
$1(188.88) = (58.69)$

$188.88 = 58.69$

$\frac{58.69}{188.88} = 31.073\text{-}\%$

$2Ni(C5H5)2 + 15O2 = 2Ni + 20CO2 + 10H2O$

$2(188.88) = 2(58.69)$

$377.76 = 117.38$

$\frac{117.38}{377.38} = 31.104\text{-}\%$

$6Ni(C5H5)2 + 69O2 = 2Ni3C + 54CO2 + 30H2O$

$6(188.88) = 2(188.08)$

$1133.28 = 376.16$

$\frac{376.16}{1133.28} = 33.192\text{-}\%$

$2Ni(C5H5)2 + 16O2 = 2NiO + 20CO2 + 10H2O$
$2(188.88) = 2(74.69)$

$377.76 = 149.38$

$\frac{149.38}{377.76} = 39.544\text{-}\%$

$4Ni(C5H5)2 + 53O2 = 2Ni2O3 + 40CO2 + 20H2O$

$4(188.88) = 2(165.39)$

$755.52 = 330.78$

$\frac{330.78}{755.52} = 43.782\text{-}\%$

11.2 Estimation of Ratio of Degraded Products from Precursor Masses

$Fe(Co)_5$ = 195.90 g/mol

Fe_2O_3 = 159.69 g/mol

$4Fe(CO)_5 + 13O_2 = 2Fe_2O_3 + 20CO_2$

4(195.90) = 2(159.69)

783.6 = 319.38

$\frac{319.38}{783.6} = 40.758\cdot\%$

$Ni(C_5H_5)_2$ = 188.88 g/mol

NiO = 74.69 g/mol

$2Ni(C_5H_5)_2 + 16O_2 = 2NiO + 20CO_2 + 10H_2O$
2(188.88) = 2(74.69)

377.76 = 149.38

$\frac{149.38}{377.76} = 39.544\cdot\%$

Case 1

1:1, Iron to Nickel precursor ratio

Mass Nickelocene	Mass Nickelocene
1000mg or 1g	1000mg
Expected degraded mass	
407.58 mg	395.44 mg

Degraded ratio

$\frac{407.58}{395.44} = 1.031$

Case 2

10:1, Iron to Nickel precursor ratio

Mass Nickelocene	Mass Nickelocene
1000mg or 1g	100mg
Expected degraded mass	
407.58 mg	39.544 mg

Degraded ratio

$\frac{407.58}{39.544} = 10.307$

Case 3

20:1, Iron to Nickel precursor ratio

Mass Nickelocene	Mass Nickelocene
1000mg or 1g	50mg
Expected degraded mass	
407.58 mg	19.772 mg

Case 4

30:1, Iron to Nickel precursor ratio

Mass Nickelocene	Mass Nickelocene
1000mg or 1g	33.3mg

Expected degraded mass

407.58 mg	13.050 mg

Degraded ratio

$$\frac{407.58}{13.050} = 31.232$$

Case 5

40:1, Iron to Nickel precursor ratio

Mass Nickelocene	Mass Nickelocene
1000mg or 1g	25 mg

Expected degraded mass

407.58 mg	9.886 mg

Degraded ratio

$$\frac{407.58}{9.886} = 41.228$$

Case 1

1:1, Final ratio

Mass Nickelocene		Mass Nickelocene	
1000mg or 1g		1030.7mg	

Expected degraded mass

407.58 mg		407.58 mg	

Degraded ratio

$\frac{407.58}{407.58} = 1$ Precursor Ratio must be: $\frac{1000}{1030.7} = 0.97$ 0.97:1

Case 2

10:1, Iron to Nickel precursor ratio

Mass Nickelocene	Mass Nickelocene	
1000mg or 1g	103mg	
Expected degraded mass		
407.58 mg	40.758 mg	
Degraded ratio		
$\frac{407.58}{40.758} = 10$	$\frac{1000}{103} = 9.709$	9.71:1

Case 3

20:1, Iron to Nickel precursor ratio

Mass Nickelocene	Mass Nickelocene	
1000mg or 1g	51.53mg	
Expected degraded mass		
407.58 mg	20.379 mg	
Degraded ratio		
$\frac{407.58}{20.379} = 20$	$\frac{1000}{51.53} = 19.406$	19.41:1

Case 4

30:1, Iron to Nickel precursor ratio

Mass Nickelocene	Mass Nickelocene	
1000mg or 1g	34.36mg	
Expected degraded mass		
407.58 mg	13.586 mg	
Degraded ratio		
$\frac{407.58}{13.586} = 30$	$\frac{1000}{34.36} = 29.104$	29.1:1

Case 5

40:1, Iron to Nickel precursor ratio

Mass Nickelocene

1000mg or 1g

Mass Nickelocene

25.767 mg

Expected degraded mass

407.58 mg

10.1895 mg

Degraded ratio

$$\frac{407.58}{10.1895} = 40$$

$$\frac{1000}{25.767} = 38.809$$

38.8:1

11.3 Calculations for Iron Carbonyl/Nickel Ratios

Atomic Fraction Oxygen

Upper limit of available graph = .5727

NiO = 1/2 atoms

$\frac{1}{2} = 0.5$

Fe2O3=

$\frac{3}{5} = 0.6$

Lower limit of available graph = .5707

NiO + Fe2O3 assuming one mole of each

$$\frac{1(.5) + 1(.6)}{2} = 0.55$$

NiO + Fe2O3 assuming 2 mole Fe2O3 to 1 mole NiO

$$\frac{1(.5) + 2(.6)}{3} = 0.567$$

NiO + Fe2O3 assuming 10 mole Fe2O3 to 1 mole NiO

$$\frac{1(.5) + 10(.6)}{11} = 0.591$$

1*(.5)+x(.6)/(x+1) = .5727

Upper limit of available graph = .5727

.5727*(x+1) = .5+.6x

.5727*x+.5727 = .5+.6x

.5727-.5 = (.6-.5727)x

.0727= .0273x

.0727/(.0273) = x

x = 2.66

.5707*x+.5707 = .5+.6x

Lower limit of available graph = .5707

.5707-.5 = (.6-.5707)x

.0707 = .0293 x

.0707/.0293 = x

x = 2.41

Choose middle value that should expect different phase

$.5715*x+.5715 = .5+.6x$

$.5715-.5 = (.6-.5715)x$

$.0715 = .0285\ x$

$.0715/.0285 = x$

$x = 2.51$

Using the conversion factors that correlate precursor mass to degraded mass we can yield the following data.

$$\frac{\text{Degraded}}{\text{Undegraded}} \equiv \frac{.971}{1} \qquad \frac{\text{Undegraded}}{\text{Degraded}} \equiv \frac{1}{.971} \qquad \frac{1}{.971} = 1.03$$

desired x values	required x values for ratio	
$x_1 := 2.41$	$1.03 \cdot x_1 = 2.482$	2.48
$x_2 := 2.51$	$1.03 \cdot x_2 = 2.585$	2.59
$x_3 := 2.66$	$1.03 \cdot x_3 = 2.74$	2.74

11.4 Estimation of Reaction Rate

MathCAD analytical software was used to generate data regarding rates of reaction.

$$k = A \cdot e^{\frac{-Q}{R \cdot t}} \qquad R_1 := 8.31447215 \cdot \frac{J}{mol}$$

$$Q = R \cdot t \cdot \ln\left(\frac{k}{A}\right)$$

$$k_{80} := 7.5713 \cdot 10^{20} \frac{1}{min} \qquad T_{80} := 353K \qquad A_1 := \frac{10^6}{min}$$

$$k_{100} := 1.3692 \cdot 10^{21} \frac{1}{min} \qquad T_{100} := 373K$$

$$k_{200} := 2.6799 \cdot 10^{21} \frac{1}{min} \qquad T_{200} := 473K$$

$$k_{300} := 2.6544 \cdot 10^{21} \frac{1}{min} \qquad T_{300} := 573K$$

$$k_{400} := 2.6959 \cdot 10^{21} \frac{1}{min} \qquad T_{400} := 673K$$

$$Q_{80} := R_1 \cdot T_{80} \cdot \ln\left(\frac{k_{80}}{A_1}\right)$$

$$Q_{80} = 1.006 \times 10^5 K \cdot \frac{J}{mol}$$

$$Q_{100} := R_1 \cdot T_{100} \cdot \ln\left(\frac{k_{100}}{A_1}\right) \qquad Q_{100} = 1.081 \times 10^5 K \cdot \frac{J}{mol} \qquad Q_{100} = 10.9 \frac{kJ}{mol}$$

$$Q_{200} := R_1 \cdot T_{200} \cdot \ln\left(\frac{k_{200}}{A_1}\right) \qquad Q_{200} = 1.397 \times 10^5 K \cdot \frac{J}{mol} \qquad Q_{200} = 14.0 \frac{kJ}{mol}$$

$$Q_{300} := R_1 \cdot T_{300} \cdot \ln\left(\frac{k_{300}}{A_1}\right) \qquad Q_{300} = 1.692 \times 10^5 K \cdot \frac{J}{mol} \qquad Q_{300} = 16.9 \frac{kJ}{mol}$$

$$Q_{400} := R_1 \cdot T_{400} \cdot \ln\left(\frac{k_{400}}{A_1}\right) \qquad Q_{400} = 1.988 \times 10^5 K \cdot \frac{J}{mol} \qquad Q_{400} = 19.9 \frac{kJ}{mol}$$

11.5 Avrami Kinetics

Avrami kinetics is a method of analysis that can be applied to better understand growth factors generated in the crystallization process of solids. The generalized form of this equation seen in Equation 31 (25)

$$f = 1 - e^{-bt^n} \tag{32}$$

represents the fraction of crystallized mass. In our case, that which has changed forms from liquid. By manipulation this form can be modified to reflect a logarithmic relationship as follows between two points, as seen in Equation 32.

$$n = \frac{\ln\left(\frac{ln(1-f2)}{ln(1-f1)}\right)}{\ln\left(\frac{t2}{t1}\right)} \tag{33}$$

The practical significance of this expression is that n can be determined by finding the slope of the plot of $f_{solidus}$ versus time in the form displayed in Equation 33; note that the term ln(b) is a constant and thus does not define slope.

$$\ln\left[\ln(1/(1-f))\right] = \ln(b) + n(\ln(t) \tag{34}$$

11.6 Phase Diagrams of Transition Metals Considered for Investigation

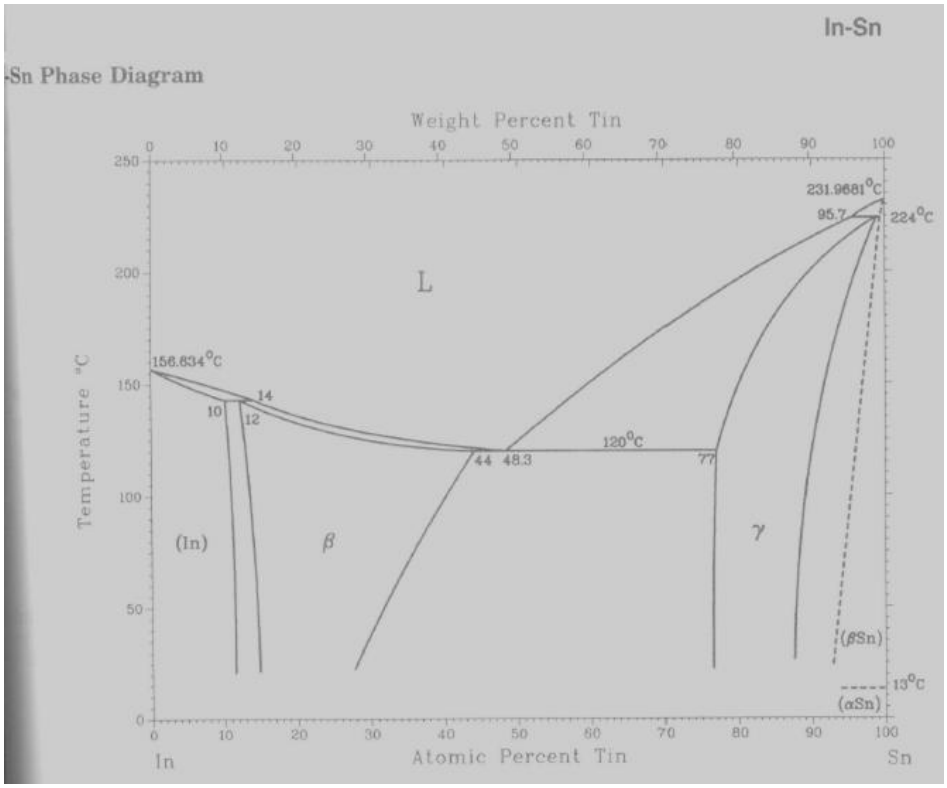

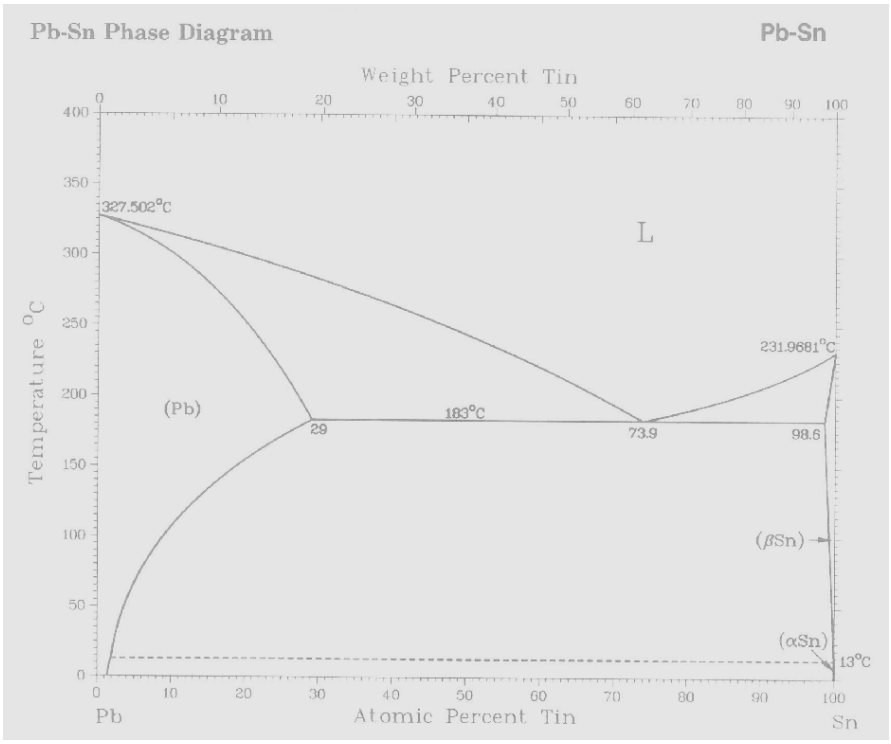

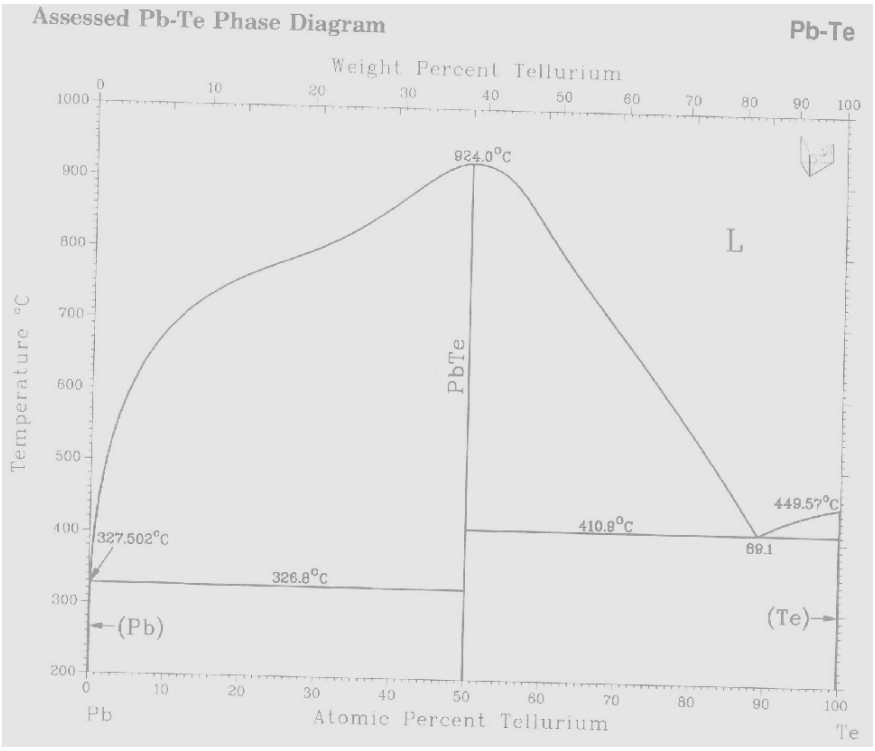
Assessed Pb-Te Phase Diagram
Pb-Te
Weight Percent Tellurium
Temperature °C
Atomic Percent Tellurium
Pb
Te
924.0°C
L
PbTe
327.502°C
326.8°C
410.9°C
449.57°C
89.1
(Pb)
(Te)

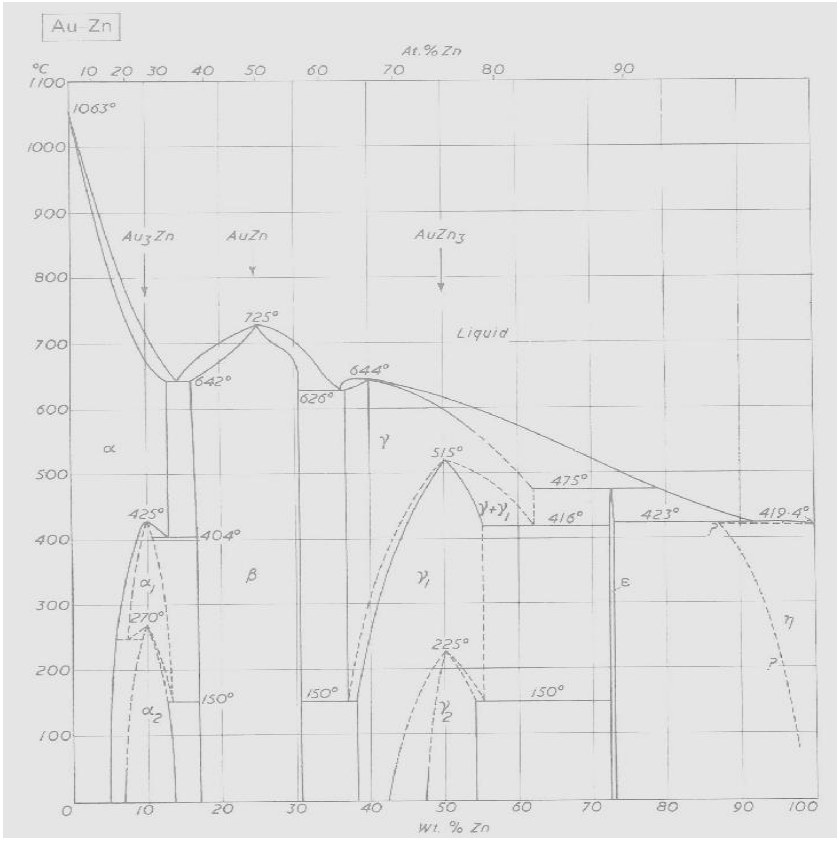
Au-Zn
At.% Zn
Wt. % Zn
1063°
Au3Zn
AuZn
AuZn3
725°
Liquid
642°
644°
626°
α
γ
515°
475°
425°
404°
416°
423°
419.4°
β
γ1
ε
η
270°
225°
150°
α1
α2
γ2

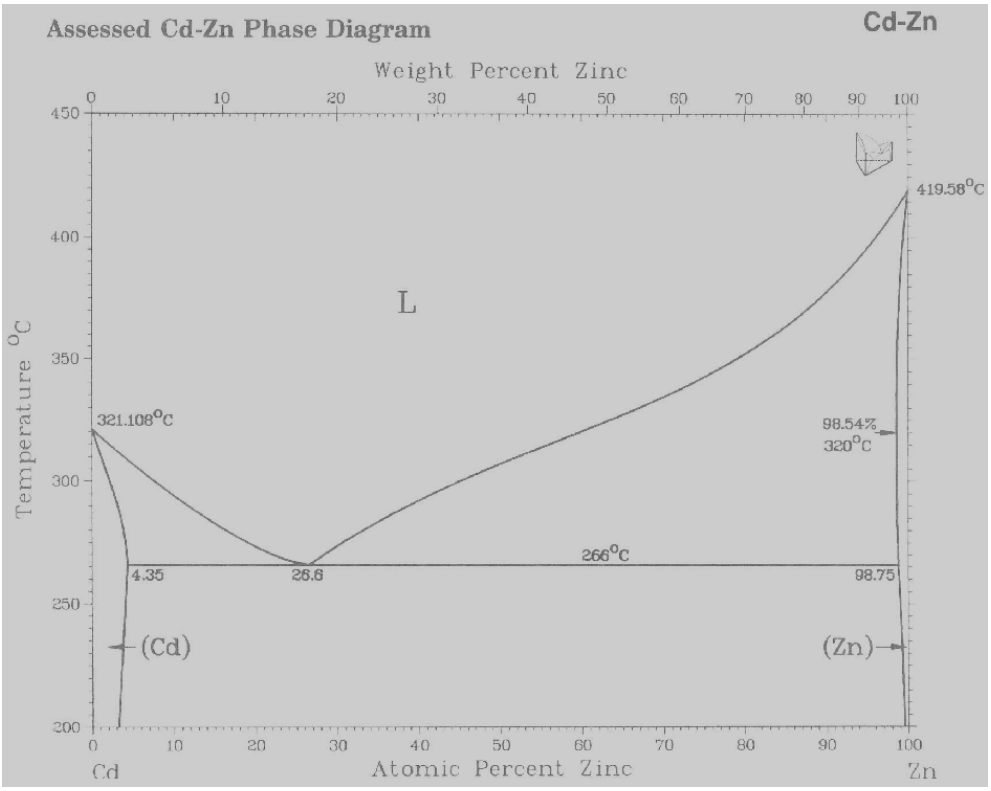
Assessed Cd-Zn Phase Diagram
Cd-Zn
Weight Percent Zinc
Temperature °C
Atomic Percent Zinc
Cd
Zn
L
321.108°C
419.58°C
98.54%
320°C
266°C
4.35
26.6
98.75
(Cd)
(Zn)

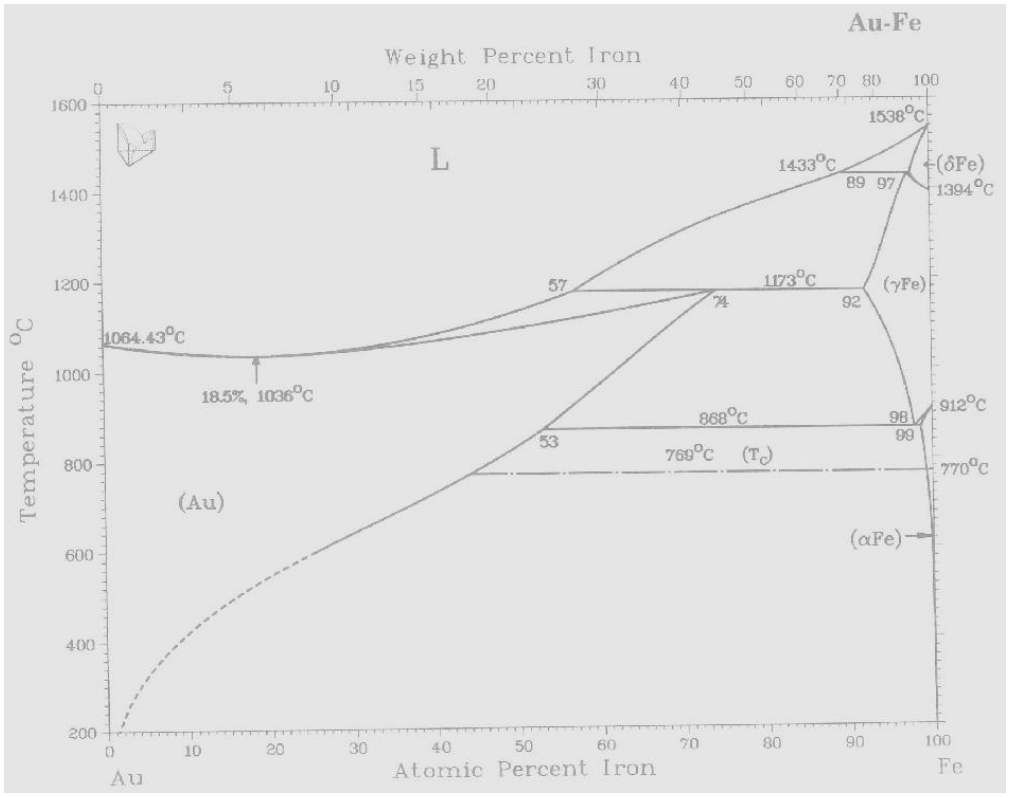
Au-Fe
Weight Percent Iron
Temperature °C
Atomic Percent Iron
Au
Fe
L
1538°C
1433°C
(δFe)
1394°C
89
97
57
1173°C
(γFe)
74
92
1064.43°C
18.5%, 1036°C
868°C
98
912°C
53
99
769°C
(T_c)
770°C
(Au)
(αFe)

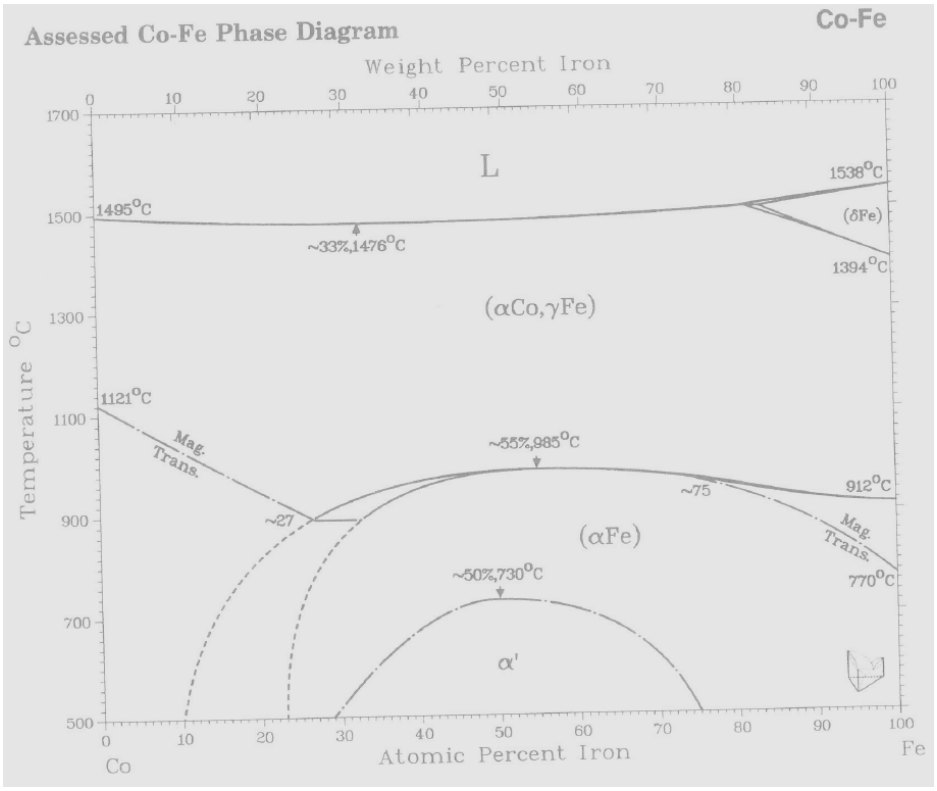
Assessed Co-Fe Phase Diagram
Co-Fe
Weight Percent Iron
Temperature °C
L
1538°C
1495°C
(δFe)
~33%,1476°C
1394°C
(αCo,γFe)
1121°C
Mag. Trans.
~55%,985°C
912°C
~27
~75
Mag. Trans.
(αFe)
770°C
~50%,730°C
α'
Co
Atomic Percent Iron
Fe

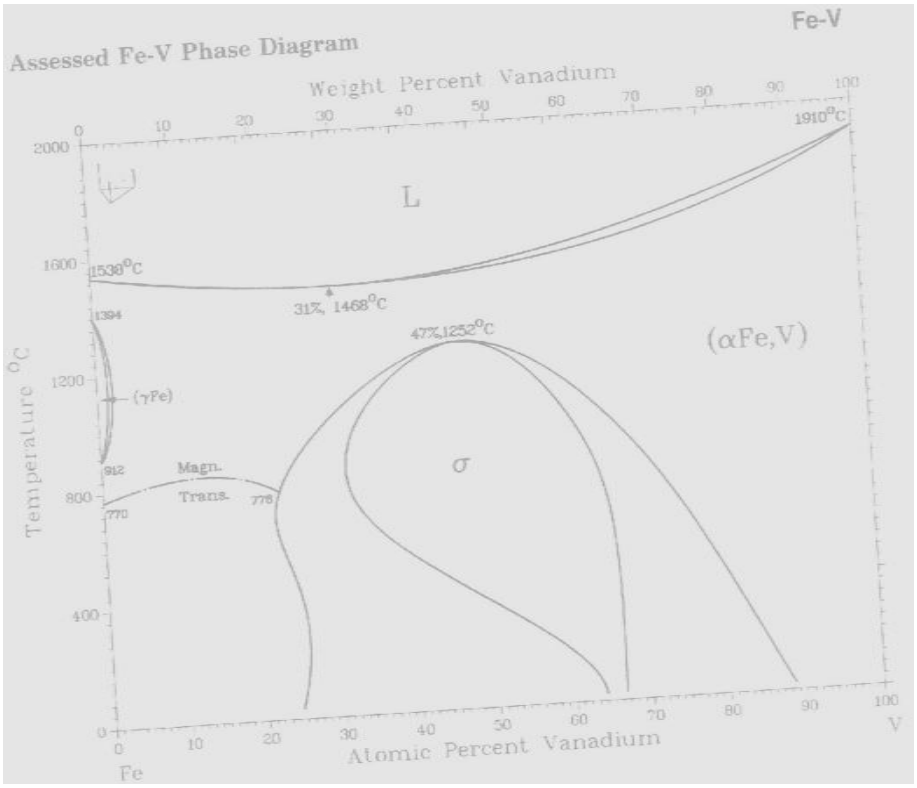
Assessed Fe-V Phase Diagram
Fe-V
Weight Percent Vanadium
Temperature °C
1910°C
L
1538°C
1394
31%, 1468°C
47%,1252°C
(αFe,V)
(γFe)
912
Magn. Trans.
776
770
σ
Fe
Atomic Percent Vanadium
V

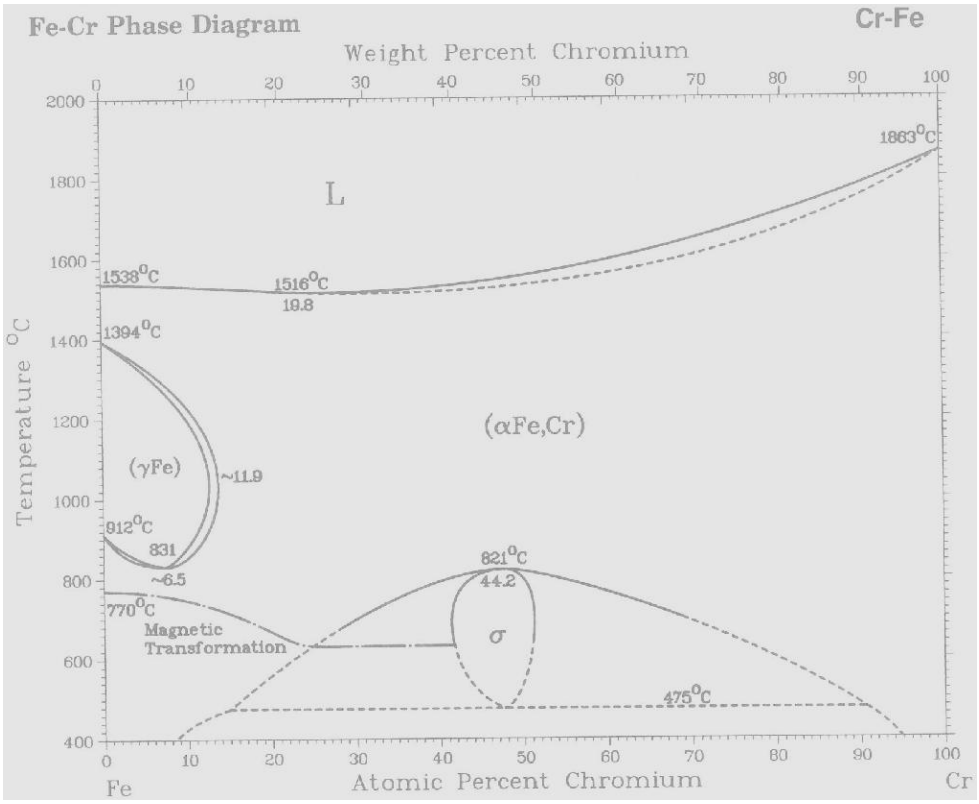
Fe-Cr Phase Diagram
Cr-Fe
Weight Percent Chromium
Temperature °C
Atomic Percent Chromium
Fe
Cr
L
1863°C
1538°C
1516°C
19.8
1394°C
(αFe,Cr)
(γFe)
~11.9
912°C
831
~6.5
770°C
Magnetic Transformation
821°C
44.2
σ
475°C

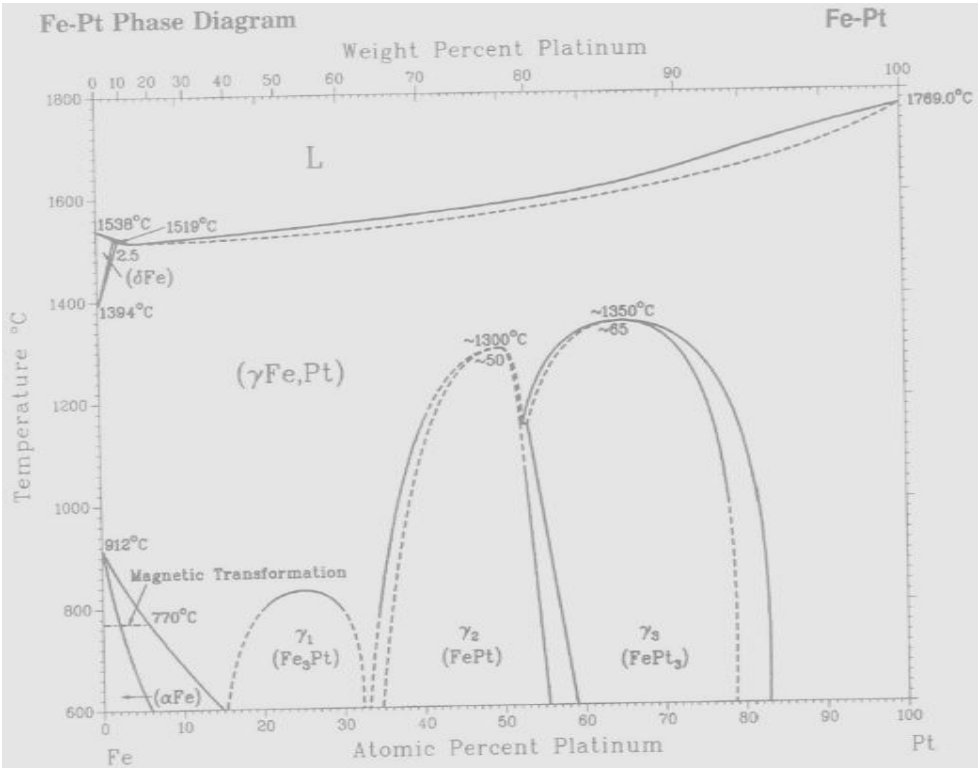
Fe-Pt Phase Diagram
Fe-Pt
Weight Percent Platinum
Temperature °C
Atomic Percent Platinum
Fe
Pt
L
1769.0°C
1538°C
1519°C
2.5
(δFe)
1394°C
(γFe,Pt)
~1300°C
~50
~1350°C
~65
912°C
Magnetic Transformation
770°C
(αFe)
γ1 (Fe3Pt)
γ2 (FePt)
γ3 (FePt3)

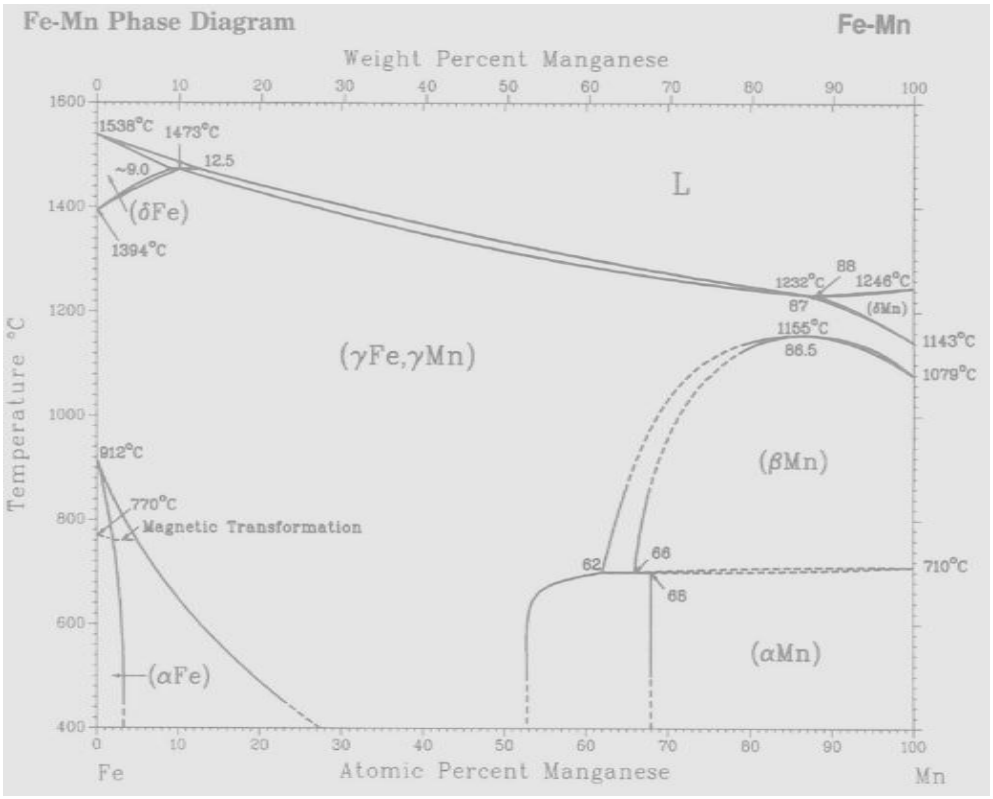
Fe-Mn Phase Diagram
Fe-Mn
Weight Percent Manganese
Temperature °C
Atomic Percent Manganese
Fe
Mn
1538°C
1473°C
12.5
~9.0
(δFe)
1394°C
L
88
1232°C
1246°C
87
(δMn)
1155°C
86.5
1143°C
1079°C
(γFe,γMn)
912°C
770°C
Magnetic Transformation
(βMn)
62
66
710°C
65
(αMn)
(αFe)

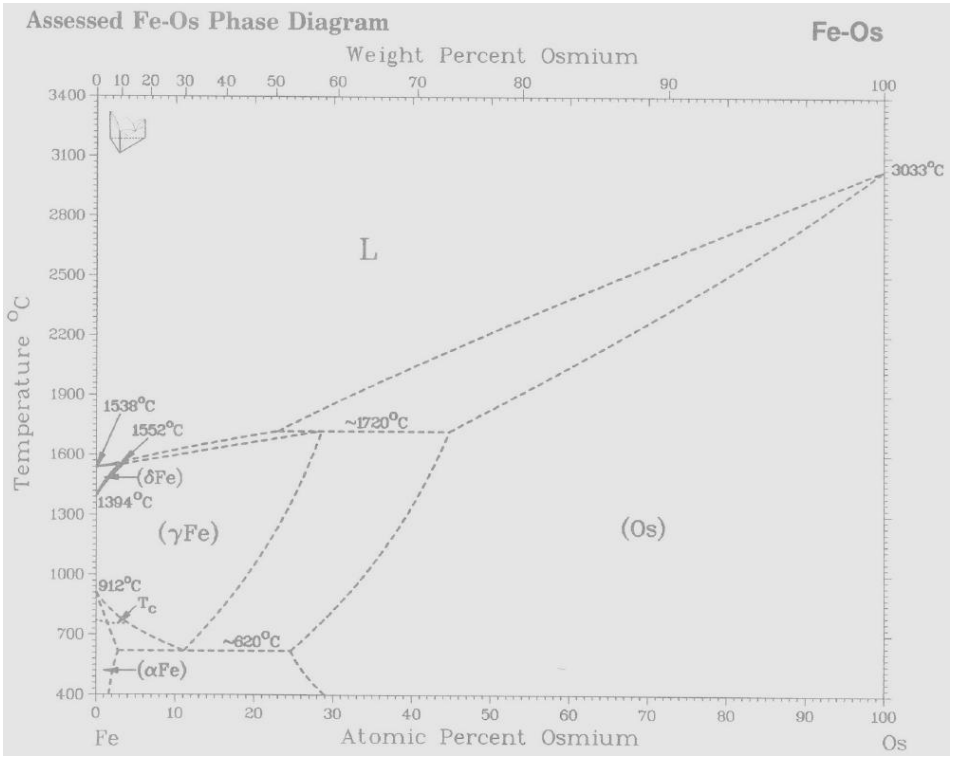
Assessed Fe-Os Phase Diagram
Fe-Os
Weight Percent Osmium
Temperature °C
Atomic Percent Osmium
Fe
Os
3033°C
L
1538°C
1552°C
~1720°C
(δFe)
1394°C
(γFe)
(Os)
912°C
Tc
~620°C
(αFe)

Fe–Ni–O

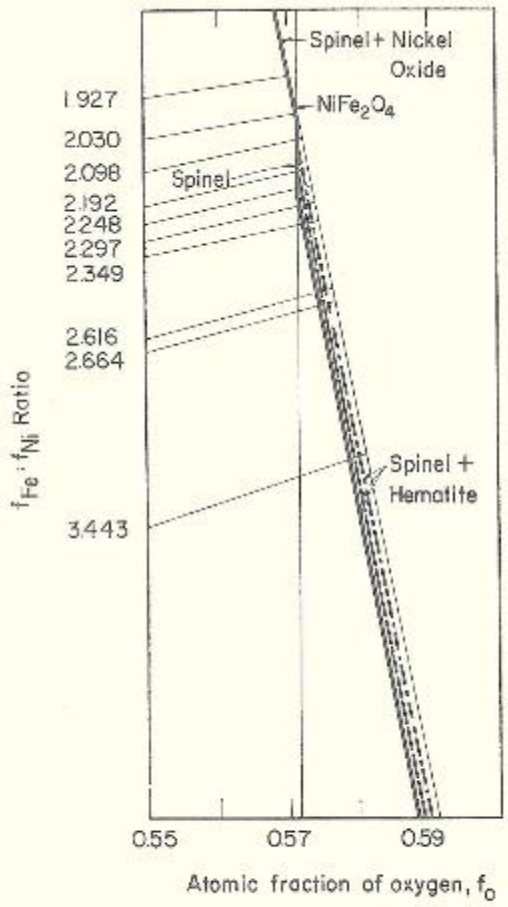

FIG. 75.—System Fe–Ni–O; ferrite region at 1000°C. Solid line = 1.0×10^{-2} isobar, dashed line = 2.1×10^{-1} isobar, dash dot line = 1.0×10^{0} isobar.

A. E. Paladino, Jr., *J. Am. Ceram. Soc.*, **42** [4] 173 (1959).

11.7 Generation of Scan Artifacts

For experimental scans for iron powder, undegraded nickelocene or degraded nickelocene, packing was exceptionally poor, thus a piece of single tape was affixed to keep the sample mass from falling out once mounted in the machine. Rate scans were conducted at step values of .4°/step between 2Θ values of 10° and 165°. Experimental Data collected using the alumina sample holder contained significant background distortion of peaks. Broadening within the scan does not allow for suitable analysis, as can be viewed in Figure 52, which describes convoluted data that was omitted from experimental analysis.

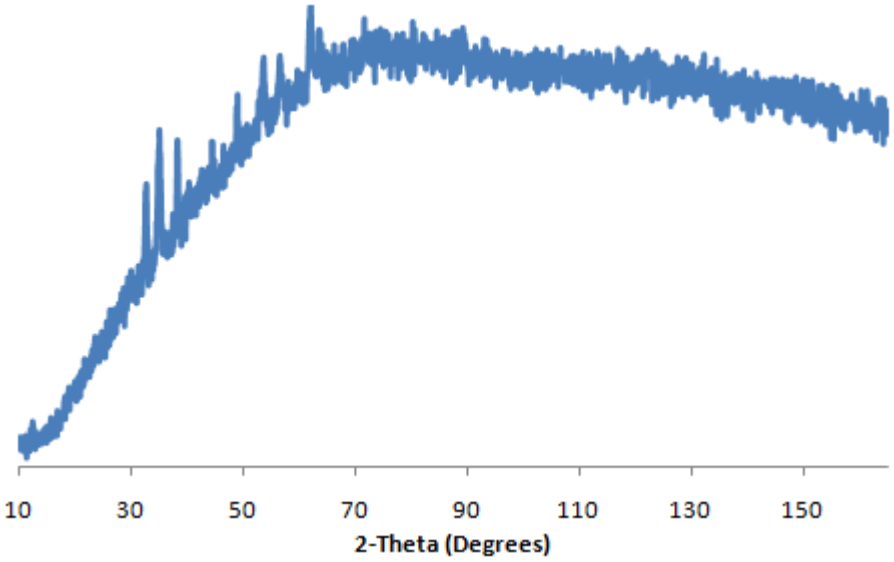

Figure 52: XRD Containing Generalized Broadening

Additionally, low-angle peak artifacts were viewed within experimental scans. One these scan (undegraded nickelocene) can be viewed in Figure 53.

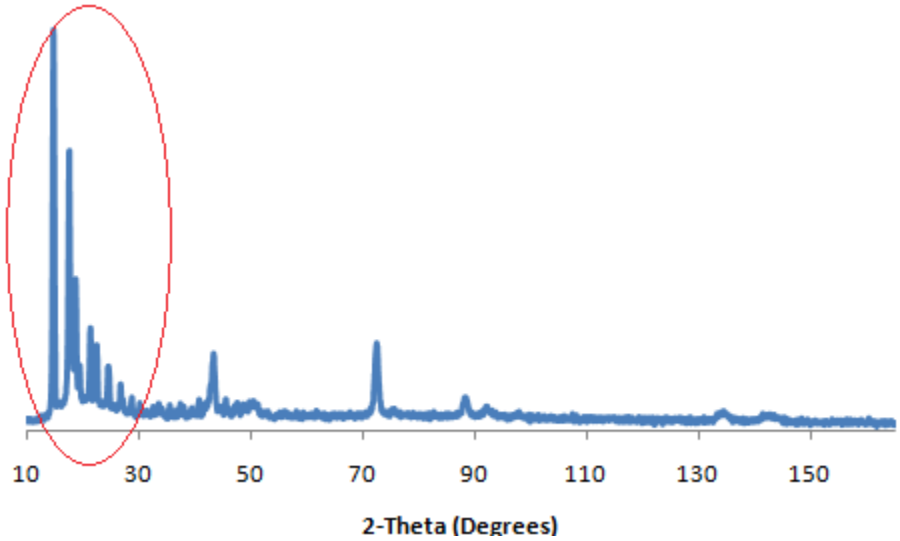

Figure 53: XRD Containing Artifacts at Low 2-theta Values

11.5 Primary X-ray Diffraction Peaks for Anticipated Products

Table 26: Four Major 2-theta Peaks for Expected Products

entry #	Formula	Major Peaks (2Θ)			
60696	Fe	44.71	82.41	65.08	116.53
340529	Fe	49.54	46.07	42.65	87.68
851410	Fe	44.39	81.74	64.58	-
340001	Fe_3C	43.77	42.9	45.89	49.14
350772	Fe_3C	45.03	43.78	42.92	44.61
60615	FeO	41.96	36.07	60.82	72.81
60711	FeO	61.3	60.75	106.26	107.28
160653	Fe_2O_3	32.83	67.75	60.95	29.98
210920	Fe_2O_3	24.73	20.37	14.74	29.78
761849	Fe_3O_4	35.44	62.55	30.09	58.96
771545	Fe_3O_4	35.45	62.58	30.1	56.99
60675	C	43.95	75.37	91.59	140.85
190268	C	43.95	41.22	75.44	47.35
40850	Ni	44.54	51.89	76.44	93.04
451027	Ni	44.56	41.56	39.13	58.47
441159	NiO	44.32	37.28	62.91	62.97
471049	NiO	43.31	37.28	62.93	75.48
951977	NiO_2	18.57	44.74	37.15	58.71
1410481	Ni_2O_3	31.96	44.87	51.64	56.83
60697	Ni_3C	44.9	86.25	71.29	78.28
180877	(Fe,Ni)	26.69	31.06	35.54	20.96
260790	(Fe,Ni)	48.69	45.58	42.23	75.44
370474	(Fe,Ni)	44.68	82.36	65.04	137.23
471417	(Fe,Ni)	43.53	50.72	74.61	90.55
380419	$FeNi_3$	44.31	51.58	92.3	75.94

11.8 Powder Diffraction Files for Detected Materials

```
PDF#98-000-0062: QM=Calculated; d=Calculated; I=(Unknown)
Aluminum
Al
Radiation=CuKa1 Lambda=1.5406   Filter=
Calibration=    2T=38.474-116.578       I/Ic(RIR)=4.47
Ref: Calculated from CSD#62 (MDI-500.csd) by Jade

Cubic, Fm-3m (225)      Z=4     mp=
CELL: 4.0494 x 4.0494 x 4.0494 <90.0 x 90.0 x 90.0>     P.S=
Density(c)=2.699        Density(m)=     Mwt=    Vol=66.4
Ref: Ibid.

Strong Lines: 2.34/X 2.02/5 1.22/3 1.43/3 0.93/2 0.91/2 1.17/1
NOTE: NBS Circ 359 (1953) 1, Swanson H E, Tatge E, See also PDF 4-787.
[Aluminum.csf]

2-Theta    d(Å)   I(f)  ( h k l)   Theta  1/(2d)   2pi/d  n^2
 38.474  2.3379  100.0  ( 1 1 1)  19.237  0.2139  2.6875    3
 44.723  2.0247   47.7  ( 2 0 0)  22.362  0.2470  3.1033    4
 65.100  1.4317   28.8  ( 2 2 0)  32.550  0.3492  4.3887    8
 78.234  1.2209   32.0  ( 3 1 1)  39.117  0.4095  5.1462   11
 82.441  1.1690    9.2  ( 2 2 2)  41.220  0.4277  5.3750   12
 99.087  1.0124    4.5  ( 4 0 0)  49.543  0.4939  6.2065   16
112.027  0.9290   16.1  ( 3 3 1)  56.014  0.5382  6.7634   19
116.578  0.9055   16.0  ( 4 2 0)  58.289  0.5522  6.9391   20
PDF#98-000-0133: QM=Calculated; d=Calculated; I=(Unknown)
Bunsenite
NiO
Radiation=CuKa1 Lambda=1.5406   Filter=
Calibration=    2T=37.246-111.081       I/Ic(RIR)=5.19
Ref: Calculated from CSD#133 (MDI-500.csd) by Jade

Cubic, Fm3m (225)       Z=4     mp=
CELL: 4.178 x 4.178 x 4.178 <90.0 x 90.0 x 90.0>        P.S=
Density(c)=6.803        Density(m)=     Mwt=    Vol=72.9
Ref: Ibid.

Strong Lines: 2.09/X 2.41/6 1.48/5 0.93/2 1.26/2 1.21/1 0.96/1 1.04/1
NOTE: Proc.
Jap.
Acad.
55 (1979), 43, Sasaki et.
al., See also PDF 47-1049, ICSD 9866.
[Bunsenite.csf]

2-Theta    d(Å)   I(f)  ( h k l)   Theta  1/(2d)   2pi/d  n^2
 37.246  2.4122   64.7  ( 1 1 1)  18.623  0.2073  2.6048    3
 43.276  2.0890  100.0  ( 2 0 0)  21.638  0.2393  3.0077    4
 62.863  1.4771   51.3  ( 2 2 0)  31.431  0.3385  4.2536    8
 75.394  1.2597   18.9  ( 3 1 1)  37.697  0.3969  4.9878   11
 79.386  1.2061   14.2  ( 2 2 2)  39.693  0.4146  5.2096   12
 95.034  1.0445    6.2  ( 4 0 0)  47.517  0.4787  6.0155   16
106.960  0.9585    7.4  ( 3 3 1)  53.480  0.5216  6.5552   19
111.081  0.9342   19.4  ( 4 2 0)  55.540  0.5352  6.7255   20
```

PDF#98-000-0161: QM=Calculated; d=Calculated; I=(Unknown)
Chromite
FeCr2O4
Radiation=CuKa1 Lambda=1.5406 Filter=
Calibration= 2T=18.324-119.169 I/Ic(RIR)=4.71
Ref: Calculated from CSD#161 (MDI-500.csd) by Jade

Cubic, Fd3m (227) Z=8 mp=
CELL: 8.3792 x 8.3792 x 8.3792 <90.0 x 90.0 x 90.0> P.S=
Density(c)=5.054 Density(m)= Mwt= Vol=588.3
Ref: Ibid.

Strong Lines: 2.53/X 1.48/4 1.61/4 2.96/3 2.09/2 1.09/1 4.84/1 1.71/1
NOTE: Smyth J.R., Bish D.L.
(1988), Crystal structures and cation sites of the rock-forming, minerals.
Boston., See also PDF 34-140.
[Chromite.csf]

2-Theta	d(Å)	I(f)	(h k l)	Theta	1/(2d)	2pi/d	n^2
18.324	4.8377	12.0	(1 1 1)	9.162	0.1034	1.2988	3
30.142	2.9625	32.4	(2 2 0)	15.071	0.1688	2.1209	8
35.504	2.5264	100.0	(3 1 1)	17.752	0.1979	2.4870	11
37.139	2.4189	5.9	(2 2 2)	18.569	0.2067	2.5976	12
43.150	2.0948	21.1	(4 0 0)	21.575	0.2387	2.9994	16
53.534	1.7104	10.3	(4 2 2)	26.767	0.2923	3.6735	24
57.068	1.6126	35.7	(5 1 1)	28.534	0.3101	3.8964	27
62.669	1.4812	42.5	(4 4 0)	31.334	0.3376	4.2418	32
65.894	1.4163	1.1	(5 3 1)	32.947	0.3530	4.4362	35
71.100	1.3249	3.5	(6 2 0)	35.550	0.3774	4.7425	40
74.144	1.2778	8.9	(5 3 3)	37.072	0.3913	4.9171	43
75.149	1.2632	4.2	(6 2 2)	37.574	0.3958	4.9740	44
79.123	1.2094	2.4	(4 4 4)	39.561	0.4134	5.1951	48
82.068	1.1733	0.8	(5 5 1)	41.034	0.4261	5.3550	51
86.934	1.1197	4.5	(6 4 2)	43.467	0.4465	5.6114	56
89.841	1.0909	13.7	(7 3 1)	44.920	0.4583	5.7597	59
94.688	1.0474	5.2	(8 0 0)	47.344	0.4774	5.9988	64
102.530	0.9875	2.4	(8 2 2)	51.265	0.5063	6.3627	72
105.525	0.9675	9.2	(7 5 1)	52.762	0.5168	6.4939	75
106.532	0.9612	2.3	(6 6 2)	53.266	0.5202	6.5371	76
110.620	0.9368	3.2	(8 4 0)	55.310	0.5337	6.7069	80
119.169	0.8932	1.0	(6 6 4)	59.584	0.5598	7.0343	88

PDF#98-000-0240: QM=Calculated; d=Calculated; I=(Unknown)
Hematite
Fe2O3
Radiation=CuKa1 Lambda=1.5406 Filter=
Calibration= 2T=24.150-118.710 I/Ic(RIR)=3.18
Ref: Calculated from CSD#240 (MDI-500.csd) by Jade

Hexagonal, R-3c (167) Z=6 mp=
CELL: 5.0355 x 5.0355 x 13.7471 <90.0 x 90.0 x 120.0> P.S=
Density(c)=5.27 Density(m)= Mwt= Vol=301.9
Ref: Ibid.

Strong Lines: 2.70/X 2.52/7 1.69/5 1.84/4 1.49/3 1.45/3 3.68/3 2.21/2
NOTE: Acta Cryst B50 (1994) 435, Maslen E N, Streltsov V A, Streltsova N R, Ishizawa N, See also PDF 33-664.
[Hematite.csf]

2-Theta	d(Å)	I(f)	(h k l)	Theta	1/(2d)	2pi/d	n^2
24.150	3.6823	30.7	(0 1 2)	12.075	0.1358	1.7063	
33.162	2.6993	100.0	(1 0 4)	16.581	0.1852	2.3277	
35.630	2.5178	72.1	(1 1 0)	17.815	0.1986	2.4956	
39.291	2.2912	1.9	(0 0 6)	19.646	0.2182	2.7423	
40.863	2.2066	23.0	(1 1 3)	20.431	0.2266	2.8474	
43.508	2.0784	2.0	(2 0 2)	21.754	0.2406	3.0231	
49.464	1.8412	40.0	(0 2 4)	24.732	0.2716	3.4126	
54.074	1.6946	50.3	(1 1 6)	27.037	0.2951	3.7078	
56.158	1.6365	0.6	(2 1 1)	28.079	0.3055	3.8393	
57.448	1.6028	2.6	(1 2 2)	28.724	0.3120	3.9201	
57.608	1.5987	8.8	(0 1 8)	28.804	0.3127	3.9301	
62.437	1.4862	33.2	(2 1 4)	31.219	0.3364	4.2277	
63.999	1.4536	32.6	(3 0 0)	32.000	0.3440	4.3224	
69.604	1.3496	3.2	(2 0 8)	34.802	0.3705	4.6555	
71.962	1.3111	12.1	(1,0,10)	35.981	0.3814	4.7923	
72.292	1.3059	2.1	(1 1 9)	36.146	0.3829	4.8113	
75.453	1.2589	7.6	(2 2 0)	37.726	0.3972	4.9911	
77.741	1.2274	2.9	(0 3 6)	38.871	0.4074	5.1190	
78.775	1.2139	1.2	(2 2 3)	39.387	0.4119	5.1760	
80.581	1.1912	1.8	(3 1 2)	40.290	0.4197	5.2747	
80.717	1.1895	4.5	(1 2 8)	40.359	0.4203	5.2821	
82.967	1.1629	6.4	(0,2,10)	41.483	0.4300	5.4031	
84.934	1.1409	9.6	(1 3 4)	42.467	0.4383	5.5072	
88.560	1.1033	9.2	(2 2 6)	44.280	0.4532	5.6949	
91.349	1.0768	1.0	(0 4 2)	45.675	0.4644	5.8353	
93.713	1.0557	10.1	(2,1,10)	46.856	0.4736	5.9516	
95.247	1.0427	0.6	(1,1,12)	47.623	0.4795	6.0257	
95.676	1.0392	3.1	(4 0 4)	47.838	0.4811	6.0463	
102.304	0.9891	3.7	(3 1 8)	51.152	0.5055	6.3527	
104.919	0.9715	0.6	(2 2 9)	52.459	0.5147	6.4678	
106.625	0.9606	9.2	(3 2 4)	53.312	0.5205	6.5410	
107.048	0.9580	4.4	(0,1,14)	53.524	0.5219	6.5590	
108.086	0.9516	7.5	(4 1 0)	54.043	0.5254	6.6026	
111.528	0.9317	1.0	(4 1 3)	55.764	0.5366	6.7435	
113.598	0.9206	2.2	(0 4 8)	56.799	0.5431	6.8253	
116.051	0.9081	10.1	(1,3,10)	58.025	0.5506	6.9193	
117.766	0.8998	0.6	(3,0,12)	58.883	0.5557	6.9832	
118.710	0.8953	5.2	(2,0,14)	59.355	0.5584	7.0177	

PDF#98-000-0259: QM=Calculated; d=Calculated; I=(Unknown)
Iron
Fe
Radiation=CuKa1 Lambda=1.5406 Filter=
Calibration= 2T=44.673-116.381 I/Ic(RIR)=11.91
Ref: Calculated from CSD#259 (MDI-500.csd) by Jade

Cubic, Im-3m (229) Z=2 mp=
CELL: 2.8664 x 2.8664 x 2.8664 <90.0 x 90.0 x 90.0> P.S=
Density(c)=7.875 Density(m)= Mwt= Vol=23.6
Ref: Ibid.

Strong Lines: 2.03/X 1.17/2 0.91/1 1.43/1 1.01/1
NOTE: NBS Circ 539 (1955) 4-4, Swanson H E, Tatge E, See also PDF 6-696.
[Iron.csf]

2-Theta	d(Å)	I(f)	(h k l)	Theta	1/(2d)	2pi/d	n^2
44.673	2.0269	100.0	(1 1 0)	22.336	0.2467	3.1000	2
65.022	1.4332	13.7	(2 0 0)	32.511	0.3489	4.3840	4
82.334	1.1702	24.4	(2 1 1)	41.167	0.4273	5.3693	6
98.944	1.0134	7.8	(2 2 0)	49.472	0.4934	6.1999	8
116.381	0.9064	13.9	(3 1 0)	58.191	0.5516	6.9318	10

PDF#98-000-0289: QM=Calculated; d=Calculated; I=(Unknown)
Magnesiochromite
MgCr2O4
Radiation=CuKa1 Lambda=1.5406 Filter=
Calibration= 2T=18.426-114.738 I/Ic(RIR)=3.29
Ref: Calculated from CSD#289 (MDI-500.csd) by Jade

Cubic, Fd-3m (227) Z=8 mp=
CELL: 8.333 x 8.333 x 8.333 <90.0 x 90.0 x 90.0> P.S=
Density(c)=4.414 Density(m)= Mwt= Vol=578.6
Ref: Ibid.

Strong Lines: 2.51/X 4.81/7 2.08/6 1.47/6 1.60/4 1.08/1 2.95/1 0.93/1
NOTE: Phys and Chem of Min.
(Germany) 20 (1994) 541, O'Neill H, Dollase W, See also PDF 10-0351, ICSD 75623.
[Magnesiochromite.csf]

2-Theta	d(Å)	I(f)	(h k l)	Theta	1/(2d)	2pi/d	n^2
18.426	4.8111	73.1	(1 1 1)	9.213	0.1039	1.3060	3
30.313	2.9462	13.0	(2 2 0)	15.157	0.1697	2.1327	8
35.707	2.5125	100.0	(3 1 1)	17.854	0.1990	2.5008	11
37.352	2.4055	9.9	(2 2 2)	18.676	0.2079	2.6120	12
43.401	2.0833	58.6	(4 0 0)	21.701	0.2400	3.0161	16
47.523	1.9117	4.9	(3 3 1)	23.762	0.2615	3.2867	19
53.854	1.7010	3.9	(4 2 2)	26.927	0.2940	3.6939	24
57.414	1.6037	39.7	(5 1 1)	28.707	0.3118	3.9180	27
63.056	1.4731	56.4	(4 4 0)	31.528	0.3394	4.2653	32
66.306	1.4085	9.0	(5 3 1)	33.153	0.3550	4.4608	35
71.555	1.3176	1.2	(6 2 0)	35.777	0.3795	4.7688	40
74.625	1.2708	9.7	(5 3 3)	37.313	0.3935	4.9444	43
75.638	1.2562	7.3	(6 2 2)	37.819	0.3980	5.0016	44
79.649	1.2028	7.8	(4 4 4)	39.824	0.4157	5.2240	48
82.622	1.1669	4.9	(5 5 1)	41.311	0.4285	5.3847	51
87.538	1.1135	2.1	(6 4 2)	43.769	0.4490	5.6425	56
90.476	1.0849	14.9	(5 5 3)	45.238	0.4609	5.7917	59
95.380	1.0416	7.4	(8 0 0)	47.690	0.4800	6.0321	64
103.325	0.9821	1.2	(8 2 2)	51.663	0.5091	6.3980	72
106.365	0.9622	11.0	(7 5 1)	53.182	0.5196	6.5299	75
107.388	0.9559	4.4	(6 6 2)	53.694	0.5231	6.5733	76
111.543	0.9317	12.1	(8 4 0)	55.771	0.5367	6.7441	80
114.738	0.9147	4.0	(9 1 1)	57.369	0.5466	6.8694	83

PDF#98-000-0291: QM=Calculated; d=Calculated; I=(Unknown)
Magnesioferrite
Mg(Fe3+)2O4
Radiation=CuKa1 Lambda=1.5406 Filter=
Calibration= 2T=18.284-113.376 I/Ic(RIR)=4.67
Ref: Calculated from CSD#291 (MDI-500.csd) by Jade

Cubic, Fd-3m (227) Z=8 mp=
CELL: 8.3975 x 8.3975 x 8.3975 <90.0 x 90.0 x 90.0> P.S=
Density(c)=5.173 Density(m)= Mwt= Vol=592.2
Ref: Ibid.

Strong Lines: 2.53/X 1.48/4 2.10/3 1.62/3 2.97/3 1.09/1 4.85/1 0.94/1
NOTE: AC C40 (1984) 1491, Fleet, M.E., See also PDF 19-0629.
[Magnesioferrite.csf]

2-Theta	d(Å)	I(f)	(h k l)	Theta	1/(2d)	2pi/d	n^2
18.284	4.8483	8.9	(1 1 1)	9.142	0.1031	1.2960	3
30.075	2.9690	26.5	(2 2 0)	15.037	0.1684	2.1163	8
35.424	2.5319	100.0	(3 1 1)	17.712	0.1975	2.4816	11
37.055	2.4241	7.2	(2 2 2)	18.527	0.2063	2.5919	12
43.051	2.0994	28.2	(4 0 0)	21.526	0.2382	2.9929	16
47.136	1.9265	1.8	(3 3 1)	23.568	0.2595	3.2614	19
53.408	1.7141	6.2	(4 2 2)	26.704	0.2917	3.6655	24
56.932	1.6161	28.1	(5 1 1)	28.466	0.3094	3.8879	27
62.517	1.4845	40.3	(4 4 0)	31.258	0.3368	4.2326	32
65.732	1.4194	3.3	(5 3 1)	32.866	0.3523	4.4265	35
70.922	1.3278	1.5	(6 2 0)	35.461	0.3766	4.7322	40
73.956	1.2806	6.8	(5 3 3)	36.978	0.3904	4.9064	43
74.957	1.2660	4.3	(6 2 2)	37.478	0.3950	4.9631	44
78.917	1.2121	4.7	(4 4 4)	39.458	0.4125	5.1838	48
81.851	1.1759	2.1	(5 5 1)	40.925	0.4252	5.3434	51
86.698	1.1222	1.2	(6 4 2)	43.349	0.4456	5.5992	56
89.592	1.0933	9.8	(7 3 1)	44.796	0.4573	5.7472	59
94.417	1.0497	4.5	(8 0 0)	47.209	0.4763	5.9858	64
105.197	0.9697	5.7	(7 5 1)	52.598	0.5156	6.4798	75
106.198	0.9633	2.2	(6 6 2)	53.099	0.5191	6.5228	76
110.260	0.9389	7.8	(8 4 0)	55.130	0.5326	6.6923	80
113.376	0.9217	2.2	(7 5 3)	56.688	0.5424	6.8166	83

PDF#98-000-0294: QM=Calculated; d=Calculated; I=(Unknown)
Magnetite
Fe3O4
Radiation=CuKa1 Lambda=1.5406 Filter=
Calibration= 2T=18.285-118.758 I/Ic(RIR)=5.22
Ref: Calculated from CSD#294 (MDI-500.csd) by Jade

Cubic, Fd-3m (227) Z=8 mp=
CELL: 8.3969 x 8.3969 x 8.3969 <90.0 x 90.0 x 90.0> P.S=
Density(c)=5.195 Density(m)= Mwt= Vol=592.0
Ref: Ibid.

Strong Lines: 2.53/X 1.48/4 1.62/3 2.97/3 2.10/2 1.09/1 1.71/1 0.97/1
NOTE: J Solid State Chem 62 (1986) 75-82, Fleet M E, See also PDF 19-629.
[Magnetite.csf]

2-Theta	d(Å)	I(f)	(h k l)	Theta	1/(2d)	2pi/d	n^2
18.285	4.8480	6.9	(1 1 1)	9.143	0.1031	1.2960	3
30.077	2.9688	28.7	(2 2 0)	15.038	0.1684	2.1164	8
35.426	2.5318	100.0	(3 1 1)	17.713	0.1975	2.4817	11
37.058	2.4240	6.6	(2 2 2)	18.529	0.2063	2.5921	12
43.054	2.0992	21.6	(4 0 0)	21.527	0.2382	2.9931	16
47.140	1.9264	0.6	(3 3 1)	23.570	0.2596	3.2617	19
53.412	1.7140	9.8	(4 2 2)	26.706	0.2917	3.6658	24
56.937	1.6160	31.9	(5 1 1)	28.468	0.3094	3.8881	27
62.522	1.4844	42.8	(4 4 0)	31.261	0.3368	4.2329	32
65.737	1.4193	1.0	(5 3 1)	32.869	0.3523	4.4269	35
70.927	1.3277	3.5	(6 2 0)	35.464	0.3766	4.7325	40
73.962	1.2805	8.8	(5 3 3)	36.981	0.3905	4.9068	43
74.963	1.2659	3.9	(6 2 2)	37.482	0.3950	4.9635	44
78.924	1.2120	2.7	(4 4 4)	39.462	0.4125	5.1842	48
81.858	1.1758	0.5	(5 5 1)	40.929	0.4252	5.3437	51
86.705	1.1221	3.9	(6 4 2)	43.353	0.4456	5.5996	56
89.600	1.0932	14.3	(7 3 1)	44.800	0.4574	5.7476	59
94.426	1.0496	5.5	(8 0 0)	47.213	0.4764	5.9862	64
102.229	0.9896	2.1	(8 2 2)	51.115	0.5053	6.3493	72
105.207	0.9696	8.9	(7 5 1)	52.604	0.5157	6.4802	75
106.209	0.9632	2.0	(6 6 2)	53.105	0.5191	6.5233	76
110.271	0.9388	3.8	(8 4 0)	55.136	0.5326	6.6928	80
118.758	0.8951	1.2	(6 6 4)	59.379	0.5586	7.0194	88

PDF#98-000-0312: QM=Calculated; d=Calculated; I=(Unknown)
Mn23C6
Mn23C6
Radiation=CuKa1 Lambda=1.5406 Filter=
Calibration= 2T=14.423-118.084 I/Ic(RIR)=5.1
Ref: Calculated from CSD#312 (MDI-500.csd) by Jade

Cubic, Fm-3m (225) Z=1 mp=
CELL: 10.62831 x 10.62831 x 10.62831 <90.0 x 90.0 x 90.0> P.S=
Density(c)=7.389 Density(m)= Mwt= Vol=1200.6
Ref: Ibid.

Strong Lines: 2.05/X 2.17/3 1.80/3 2.38/2 1.88/2 1.25/2 1.08/1 1.77/1
NOTE: Acta Chem Scan d45 (1991) 549, Karen et.
al., See also PDF 28-0646, ICSD 69536.
[Mn23C6.csf]

2-Theta	d(Å)	I(f)	(h k l)	Theta	1/(2d)	2pi/d	n^2
14.423	6.1363	0.9	(1 1 1)	7.211	0.0815	1.0239	3
27.817	3.2046	1.7	(3 1 1)	13.909	0.1560	1.9607	11
29.081	3.0681	1.2	(2 2 2)	14.540	0.1630	2.0479	12
33.704	2.6571	4.9	(4 0 0)	16.852	0.1882	2.3647	16
36.832	2.4383	0.8	(3 3 1)	18.416	0.2051	2.5769	19
37.825	2.3766	23.0	(4 2 0)	18.912	0.2104	2.6438	20
41.594	2.1695	28.0	(4 2 2)	20.797	0.2305	2.8962	24
44.246	2.0454	100.0	(3 3 3)	22.123	0.2444	3.0718	27
48.408	1.8788	21.9	(4 4 0)	24.204	0.2661	3.3442	32
50.779	1.7965	26.4	(5 3 1)	25.390	0.2783	3.4974	35
51.552	1.7714	12.9	(6 0 0)	25.776	0.2823	3.5470	36
54.565	1.6805	2.2	(6 2 0)	27.282	0.2975	3.7389	40
56.752	1.6208	3.0	(5 3 3)	28.376	0.3085	3.8766	43
57.469	1.6023	7.4	(6 2 2)	28.734	0.3121	3.9214	44
62.340	1.4883	0.7	(7 1 1)	31.170	0.3360	4.2218	51
63.018	1.4739	0.8	(6 4 0)	31.509	0.3392	4.2630	52
70.874	1.3285	4.0	(8 0 0)	35.437	0.3764	4.7294	64
73.404	1.2889	5.5	(6 4 4)	36.702	0.3879	4.8750	68
75.901	1.2526	18.2	(6 6 0)	37.950	0.3992	5.0163	72
77.755	1.2273	10.8	(7 5 1)	38.878	0.4074	5.1197	75
80.819	1.1883	4.5	(8 4 0)	40.409	0.4208	5.2876	80
82.643	1.1666	5.9	(9 1 1)	41.322	0.4286	5.3859	83
85.669	1.1330	0.6	(6 6 4)	42.834	0.4413	5.5457	88
87.478	1.1142	2.7	(9 3 1)	43.739	0.4488	5.6394	91
90.488	1.0847	13.2	(8 4 4)	45.244	0.4609	5.7923	96
92.295	1.0682	7.4	(9 3 3)	46.147	0.4681	5.8821	99
92.897	1.0628	1.1	(8 6 0)	46.449	0.4704	5.9117	100
97.735	1.0227	2.1	(6 6 6)	48.867	0.4889	6.1437	108
102.013	0.9911	1.5	(9 5 3)	51.006	0.5045	6.3396	115
102.629	0.9868	2.7	(10,4,0)	51.314	0.5067	6.3671	116
105.109	0.9702	2.7	(10,4,2)	52.555	0.5153	6.4760	120
106.988	0.9583	3.3	(11,1,1)	53.494	0.5217	6.5564	123
110.164	0.9394	1.3	(8 8 0)	55.082	0.5322	6.6884	128
112.100	0.9286	6.4	(9 5 5)	56.050	0.5384	6.7663	131
112.751	0.9251	1.9	(10,4,4)	56.375	0.5405	6.7921	132
115.388	0.9114	0.9	(10,6,0)	57.694	0.5486	6.8942	136
117.404	0.9015	1.7	(9 7 3)	58.702	0.5546	6.9698	139
118.084	0.8983	2.0	(10,6,2)	59.042	0.5566	6.9949	140

PDF#98-000-0221: QM=Calculated; d=Calculated; I=(Unknown)
Franklinite
ZnFe2O4
Radiation=CuKa1 Lambda=1.5406 Filter=
Calibration= 2T=18.184-117.709 I/Ic(RIR)=5.62
Ref: Calculated from CSD#221 (MDI-500.csd) by Jade

Cubic, Fd-3m (227) Z=8 mp=
CELL: 8.443 x 8.443 x 8.443 <90.0 x 90.0 x 90.0> P.S=
Density(c)=5.321 Density(m)= Mwt= Vol=601.9
Ref: Ibid.

Strong Lines: 2.55/X 1.49/4 2.99/4 1.62/3 2.11/2 1.10/1 1.72/1 1.29/1
NOTE: Rev Modern Phys 25 (1953) 114, Hastings, J.M., Corliss, L.M.,, See also PDF 22-1012, ICSD 28511-4, 66854, 76178, 280055.
[Franklinite.csf]

2-Theta	d(Å)	I(f)	(h k l)	Theta	1/(2d)	2pi/d	n^2
18.184	4.8746	5.4	(1 1 1)	9.092	0.1026	1.2890	3
29.909	2.9851	35.8	(2 2 0)	14.954	0.1675	2.1049	8
35.227	2.5457	100.0	(3 1 1)	17.613	0.1964	2.4682	11
36.848	2.4373	6.0	(2 2 2)	18.424	0.2051	2.5779	12
42.808	2.1108	15.8	(4 0 0)	21.404	0.2369	2.9768	16
53.097	1.7234	12.2	(4 2 2)	26.549	0.2901	3.6458	24
56.598	1.6249	35.0	(5 1 1)	28.299	0.3077	3.8669	27
62.142	1.4925	41.6	(4 4 0)	31.071	0.3350	4.2098	32
65.334	1.4271	0.6	(5 3 1)	32.667	0.3504	4.4027	35
70.482	1.3350	4.3	(6 2 0)	35.241	0.3745	4.7067	40
73.492	1.2875	9.1	(5 3 3)	36.746	0.3883	4.8800	43
74.484	1.2728	3.8	(6 2 2)	37.242	0.3928	4.9364	44
78.409	1.2186	1.9	(4 4 4)	39.205	0.4103	5.1559	48
81.317	1.1823	0.5	(5 5 1)	40.658	0.4229	5.3146	51
86.116	1.1282	5.2	(6 4 2)	43.058	0.4432	5.5690	56
88.980	1.0992	14.0	(7 3 1)	44.490	0.4549	5.7162	59
93.752	1.0554	5.2	(8 0 0)	46.876	0.4738	5.9535	64
101.457	0.9950	2.7	(8 2 2)	50.728	0.5025	6.3147	72
104.393	0.9749	9.0	(7 5 1)	52.196	0.5129	6.4449	75
105.380	0.9685	1.9	(6 6 2)	52.690	0.5163	6.4877	76
109.378	0.9440	2.6	(8 4 0)	54.689	0.5297	6.6562	80
117.709	0.9000	1.2	(6 6 4)	58.855	0.5555	6.9811	88

PDF#98-000-0255: QM=Calculated; d=Calculated; I=(Unknown)
Ilmenite
FeTiO3
Radiation=CuKa1 Lambda=1.5406 Filter=
Calibration= 2T=18.886-119.963 I/Ic(RIR)=2.95
Ref: Calculated from CSD#255 (MDI-500.csd) by Jade

Rhombohedral, R-3 (148) Z=2 mp=
CELL: 5.538 x 5.538 x 5.538 <54.68 x 54.68 x 54.68> P.S=
Density(c)=4.789 Density(m)= Mwt= Vol=105.2
Ref: Ibid.

Strong Lines: 2.75/X 2.54/7 1.87/4 1.73/4 1.51/3 1.47/3 3.73/3 2.24/3
NOTE: J Phys and Chem of Solids 10 (1959) 35, Shirane G, Pickart S J, Nathans R, Ishikawa Y, See also PDF 29-0733.
[Ilmenite.csf]

2-Theta	d(Å)	I(f)	(h k l)	Theta	1/(2d)	2pi/d	n^2
18.886	4.6951	1.8	(1 1 1)	9.443	0.1065	1.3382	
21.113	4.2045	0.9	(1 0 0)	10.557	0.1189	1.4944	
23.805	3.7349	27.3	(1 1 0)	11.902	0.1339	1.6823	
32.526	2.7506	100.0	(2 1 1)	16.263	0.1818	2.2843	
35.258	2.5434	65.9	(-1 1 0)	17.629	0.1966	2.4704	
40.295	2.2364	25.8	(2 1 0)	20.148	0.2236	2.8095	
41.459	2.1762	1.0	(-1 1 1)	20.730	0.2298	2.8872	
42.989	2.1023	0.8	(2 0 0)	21.495	0.2378	2.9888	
48.723	1.8674	42.8	(2 2 0)	24.361	0.2677	3.3646	
49.777	1.8303	0.5	(3 2 2)	24.889	0.2732	3.4329	
53.043	1.7251	40.1	(3 2 1)	26.521	0.2898	3.6423	
55.529	1.6536	1.2	(0-1 2)	27.765	0.3024	3.7998	
56.218	1.6349	13.1	(3 3 2)	28.109	0.3058	3.8431	
56.767	1.6204	1.5	(-1 1 2)	28.384	0.3086	3.8776	
61.559	1.5053	34.2	(0 1 3)	30.779	0.3322	4.1741	
63.278	1.4685	29.9	(-2 1 1)	31.639	0.3405	4.2788	
65.012	1.4334	0.5	(0 2 3)	32.506	0.3488	4.3834	
68.124	1.3753	4.3	(4 2 2)	34.062	0.3636	4.5686	
70.080	1.3416	10.2	(4 3 3)	35.040	0.3727	4.6833	
70.607	1.3329	2.2	(2 3 4)	35.303	0.3751	4.7139	
74.560	1.2717	7.0	(-2 2 0)	37.280	0.3932	4.9407	
76.448	1.2450	1.6	(3 3 0)	38.224	0.4016	5.0469	
77.738	1.2275	1.1	(-1 1 3)	38.869	0.4073	5.1187	
79.097	1.2098	6.1	(1 3 4)	39.548	0.4133	5.1937	
79.563	1.2038	1.6	(0-1 3)	39.782	0.4153	5.2193	
80.952	1.1867	4.7	(4 4 2)	40.476	0.4214	5.2949	
83.721	1.1543	8.9	(3 2-1)	41.860	0.4332	5.4432	
87.083	1.1182	6.6	(0 2 4)	43.541	0.4472	5.6191	
90.131	1.0881	0.9	(-2 2 2)	45.066	0.4595	5.7744	
91.501	1.0754	7.5	(5 3 2)	45.750	0.4650	5.8428	
92.567	1.0658	2.1	(5 4 3)	46.283	0.4691	5.8955	
94.248	1.0511	2.6	(4 0 0)	47.124	0.4757	5.9776	
100.238	1.0038	5.1	(5 2 1)	50.119	0.4981	6.2594	
103.505	0.9808	3.9	(5 5 4)	51.752	0.5098	6.4059	
104.923	0.9714	9.0	(4 1-1)	52.461	0.5147	6.4679	
106.506	0.9613	6.8	(1 2-3)	53.253	0.5201	6.5359	
109.751	0.9418	0.7	(0-1 4)	54.876	0.5309	6.6715	
111.173	0.9337	2.9	(4 4 0)	55.586	0.5355	6.7292	
113.146	0.9230	7.8	(1 4 5)	56.573	0.5417	6.8076	
114.643	0.9151	4.7	(6 4 4)	57.322	0.5464	6.8657	
119.963	0.8896	8.2	(4 3-1)	59.982	0.5620	7.0627	

PDF#99-000-2639: QM=Uncommon(?); d=Other/Unknown; I=(Unknown)
Nickel
Ni
Radiation=CuKa1 Lambda=1.5406 Filter=
Calibration= 2T=44.508-155.663 I/Ic(RIR)=
Ref: JADE's Userfile

Cubic, Fm-3m (225) Z=4 mp=
CELL: 3.524 x 3.524 x 3.524 <90.0 x 90.0 x 90.0> P.S=
Density(c)=8.9 Density(m)= Mwt= Vol=43.8
Ref: Ibid.

Strong Lines: 2.03/X 1.76/4 1.06/2 1.25/2 0.81/1 0.79/1 1.02/1
NOTE: = IMA 1966-039.
Locality: Bogota, Canala, New Caledonia.
Metallic white.
Min-Group: Nickel.
PDF: 04-0850.
Ref: Mineralogical Magazine 40 (1975), 247.
Ref: USA National Bureau of Standards Circular 539, 1 (1953), 13.
Ref: Handbook of Mineralogy (Anthony et al.), 1 (1990), 349.
Ref: Canadian Mineralogist 38 (2000), 585.
Ref: Neues Jahrbuch für Mineralogie, Abhandlungen 107 (1967), 241.
Ref: Transactions (Doklady) of the USSR Academy of Sciences, Earth Science Sections 389 (2003), 278.

2-Theta	d(Å)	I(f)	(h k l)	Theta	1/(2d)	2pi/d	n^2
44.508	2.0340	100.0		22.254	0.2458	3.0891	0
51.847	1.7620	40.0		25.924	0.2838	3.5659	0
76.372	1.2460	20.0		38.186	0.4013	5.0427	0
92.992	1.0620	20.0		46.496	0.4708	5.9164	0
98.474	1.0170	10.0		49.237	0.4916	6.1782	0
144.855	0.8080	10.0		72.427	0.6188	7.7762	0
155.663	0.7880	10.0		77.831	0.6345	7.9736	0

11.9 Material Safety Data Sheets (MSDS)

11.9.1 MSDS for Iron Pentacarbonyl

SIGMA-ALDRICH

MATERIAL SAFETY DATA SHEET

Date Printed: 03/19/2009
Date Updated: 02/23/2009
Version 1.7

Section 1 - Product and Company Information

Product Name	IRON(0)PENTACARBONYL, 99.999 % METALS BASIS PURITY
Product Number	481718
Brand	ALDRICH
Company	Sigma-Aldrich
Address	3050 Spruce Street SAINT LOUIS MO 63103 US
Technical Phone:	800-325-5832
Fax:	800-325-5052
Emergency Phone:	314-776-6555

Section 2 - Composition/Information on Ingredient

Substance Name	CAS #	SARA 313
IRON PENTACARBONYL	13463-40-6	Yes

Formula	Fe(CO)5
Synonyms	FER pentacarbonyle (French) * Iron carbonyl (Fe(CO)5), (TB-5-11) (9CI) * Iron, pentacarbonyl- * Iron pentacarbonyl (ACGIH) * Pentacarbonyliron
RTECS Number:	NO4900000

Section 3 - Hazards Identification

EMERGENCY OVERVIEW

Flammable (USA) Highly Flammable (EU). Highly Toxic (USA) Very Toxic (EU).
Toxic in contact with skin. Very toxic by inhalation and in contact with skin
Readily absorbed through skin. Target organ(s): Liver. Kidneys.

HMIS RATING

HEALTH: 3*
FLAMMABILITY: 3
REACTIVITY: 2

NFPA RATING

HEALTH: 3
FLAMMABILITY: 3
REACTIVITY: 2

*additional chronic hazards present.

For additional information on toxicity, please refer to Section 11.

Section 4 - First Aid Measures

ORAL EXPOSURE

If swallowed, wash out mouth with water provided person is conscious. Call a physician immediately.

INHALATION EXPOSURE
If inhaled, remove to fresh air. If not breathing give artificial respiration. If breathing is difficult, give oxygen.

DERMAL EXPOSURE
In case of skin contact, flush with copious amounts of water for at least 15 minutes. Remove contaminated clothing and shoes. Call a physician.

EYE EXPOSURE
In case of contact with eyes, flush with copious amounts of water for at least 15 minutes. Assure adequate flushing by separating the eyelids with fingers. Call a physician.

Section 5 - Fire Fighting Measures

EXPLOSION HAZARDS
Vapor may travel considerable distance to source of ignition and flash back.

FLASH POINT
5 °F - 15.0 °C Method: closed cup

AUTOIGNITION TEMP
50 °C

FLAMMABILITY
N/A

EXTINGUISHING MEDIA
Suitable: Water spray. Carbon dioxide, dry chemical powder, or appropriate foam.

FIREFIGHTING
Protective Equipment: Wear self-contained breathing apparatus and protective clothing to prevent contact with skin and eyes.
Specific Hazard(s): Emits toxic fumes under fire conditions.

Section 6 - Accidental Release Measures

PROCEDURE TO BE FOLLOWED IN CASE OF LEAK OR SPILL
Evacuate area.

PROCEDURE(S) OF PERSONAL PRECAUTION(S)
Wear self-contained breathing apparatus, rubber boots, and heavy rubber gloves.

METHODS FOR CLEANING UP
Cover with dry-lime, sand, or soda ash. Place in covered containers using non-sparking tools and transport outdoors. Ventilate area and wash spill site after material pickup is complete.

Section 7 - Handling and Storage

HANDLING
User Exposure: Do not breathe dust. Do not get in eyes, on skin, on clothing. Avoid prolonged or repeated exposure.
Fire: Under fire conditions, material may decompose to form flammable and/or explosive mixtures in air.

STORAGE
Suitable: Keep tightly closed. Keep away from heat, sparks, and open flame. Store in a dry area. Handle and store under nitrogen.
Unsuitable: Air.
Incompatible Materials: Oxidizing agents
Store at 2-8°C

SPECIAL REQUIREMENTS
Heat- and air-sensitive. Light sensitive. Handle and store under inert gas.

Section 8 - Exposure Controls / PPE

ENGINEERING CONTROLS
Safety shower and eye bath. Use only in a chemical fume hood.

PERSONAL PROTECTIVE EQUIPMENT
Respiratory: Use respirators and components tested and approved under appropriate government standards such as NIOSH (US) or CEN (EU). Where risk assessment shows air-purifying respirators are appropriate use a full-face respirator with multi-purpose combination (US) or type ABEK (EN 14387) respirator cartridges as a backup to engineering controls. If the respirator is the sole means of protection, use a full-face supplied air respirator.
Hand: Compatible chemical-resistant gloves.
Eye: Chemical safety goggles.

GENERAL HYGIENE MEASURES
Wash contaminated clothing before reuse. Wash thoroughly after handling.

EXPOSURE LIMITS, RTECS

Country	Source	Type	Value
USA	ACGIH	STEL	0.2 PPM
USA	ACGIH	TWA	0.1 PPM
USA	MSHA Standard-air	TWA	0.01 PPM (0.08 MG/M3)
New Zealand OEL			
Remarks: check ACGIH TLV			
USA	NIOSH	TWA	0.1 PPM
		STEL	0.2 PPM

Section 9 - Physical/Chemical Properties

Appearance — Physical State: Clear liquid

Property	Value	At Temperature or Pressure
Molecular Weight	195.9 AMU	
pH	N/A	
BP/BP Range	103 °C	
MP/MP Range	- 20.0 °C	
Freezing Point	N/A	
Vapor Pressure	40 mmHg	30.3 °C
Vapor Density	6.74 g/l	
Saturated Vapor Conc.	N/A	
SG/Density	1.45 g/cm3	
Bulk Density	N/A	
Odor Threshold	N/A	
Volatile%	N/A	
VOC Content	N/A	
Water Content	N/A	
Solvent Content	N/A	

Evaporation Rate	N/A
Viscosity	N/A
Surface Tension	N/A
Partition Coefficient	N/A
Decomposition Temp.	N/A
Flash Point	5 °F - 15.0 °C Method: closed cup
Explosion Limits	N/A
Flammability	N/A
Autoignition Temp	50 °C
Refractive Index	1.5196
Optical Rotation	N/A
Miscellaneous Data	N/A
Solubility	N/A

N/A = not available

Section 10 - Stability and Reactivity

STABILITY
Stable: Unstable.
Conditions of Instability: May decompose on exposure to air and moisture.
Conditions to Avoid: Air. Heat. Light.
Materials to Avoid: Strong oxidizing agents, Strong bases, Amines, Halogens.

HAZARDOUS DECOMPOSITION PRODUCTS
Hazardous Decomposition Products: Carbon monoxide, Carbon dioxide.

HAZARDOUS POLYMERIZATION
Hazardous Polymerization: Will not occur

Section 11 - Toxicological Information

ROUTE OF EXPOSURE
Skin Contact: May cause skin irritation.
Skin Absorption: Toxic if absorbed through skin.
Eye Contact: May cause eye irritation.
Inhalation: Material may be irritating to mucous membranes and upper respiratory tract. May be fatal if inhaled.
Ingestion: May be fatal if swallowed.

TARGET ORGAN(S) OR SYSTEM(S)
Kidneys. Central nervous system. Liver.

SIGNS AND SYMPTOMS OF EXPOSURE
Damage to the kidneys. Chemical pneumonitis. Inhalation may result in spasm, inflammation and edema of the larynxand bronchi, chemical pneumonitis, and pulmonary edema. Symptoms of exposure may include burning sensation, coughing, wheezing, laryngitis, shortness of breath, headache, nausea, and vomiting.
Exposure can cause: Cyanosis. Damage to the liver.

TOXICITY DATA

Oral
Rat
25 mg/kg
LD50

Inhalation
Rat

10 ppm
LC50
Remarks: Behavioral:Somnolence (general depressed activity). Lungs, Thorax, or Respiration:Dyspnea. Nutritional and Gross Metabolic:Weight loss or decreased weight gain.

Oral
Mouse
62 mg/kg
LD50

Inhalation
Mouse
2,190 mg/m3
LC50

Intraperitoneal
Mouse
60 MG/KG
LD50

Oral
Cat
100 mg/kg
LD50

Oral
Rabbit
12 mg/kg
LD50

Skin
Rabbit
56 mg/kg
LD50
Remarks: Lungs, Thorax, or Respiration:Dyspnea. Lungs, Thorax, or Respiration:Cyanosis. Nutritional and Gross Metabolic:Weight loss or decreased weight gain.

Subcutaneous
Rabbit
240 MG/KG
LD50

Intravenous
Rabbit
11 MG/KG
LD50

Oral
Guinea pig
22 mg/kg
LD50

---

ction 12 - Ecological Information

---

data available.

---

ction 13 - Disposal Considerations

PROPRIATE METHOD OF DISPOSAL OF SUBSTANCE OR PREPARATION
Contact a licensed professional waste disposal service to dispose

of this material. Dissolve or mix the material with a combustible solvent and burn in a chemical incinerator equipped with an afterburner and scrubber. Observe all federal, state, and local environmental regulations.

Section 14 - Transport Information

DOT
Proper Shipping Name: Iron pentacarbonyl
UN#: 1994
Class: 6.1
Packing Group: Packing Group I
Hazard Label: Poison inhalation hazard
Hazard Label: Flammable liquid
PIH: Zone A

IATA
Proper Shipping Name: Iron pentacarbonyl
IATA UN Number: 1994
Hazard Class: 6.1
Packing Group: I
Not Allowed - Aircraft: Not permitted for air transport.

Section 15 - Regulatory Information

EU ADDITIONAL CLASSIFICATION
Symbol of Danger: F-T+
Indication of Danger: Highly Flammable. Very toxic.
R: 11-24-26/28
Risk Statements: Highly flammable. Toxic in contact with skin. Very toxic by inhalation and if swallowed.
S: 16-26-28-36/37/39-45
Safety Statements: Keep away from sources of ignition - no smoking. In case of contact with eyes, rinse immediately with plenty of water and seek medical advice. After contact with skin, wash immediately with plenty of water. Wear suitable protective clothing, gloves, and eye/face protection. In case of accident or if you feel unwell, seek medical advice immediately (show the label where possible).

US CLASSIFICATION AND LABEL TEXT
Indication of Danger: Flammable (USA) Highly Flammable (EU). Highly Toxic (USA) Very Toxic (EU).
Risk Statements: Toxic in contact with skin. Very toxic by inhalation and in contact with skin
Safety Statements: Keep away from sources of ignition - no smoking. In case of contact with eyes, rinse immediately with plenty of water and seek medical advice. After contact with skin, wash immediately with plenty of water. Wear suitable protective clothing, gloves, and eye/face protection. In case of accident or if you feel unwell, seek medical advice immediately (show the label where possible).
US Statements: Readily absorbed through skin. Target organ(s): Liver. Kidneys.

UNITED STATES REGULATORY INFORMATION
SARA LISTED: Yes
NOTES: This product is subject to SARA section 313 reporting requirements.
TSCA INVENTORY ITEM: Yes

CANADA REGULATORY INFORMATION

WHMIS Classification: This product has been classified in accordance with the hazard criteria of the CPR, and the MSDS contains all the information required by the CPR.

DSL: Yes

NDSL: No

Section 16 - Other Information

DISCLAIMER

For R&D use only. Not for drug, household or other uses.

WARRANTY

The above information is believed to be correct but does not purport to be all inclusive and shall be used only as a guide. The information in this document is based on the present state of our knowledge and is applicable to the product with regard to appropriate safety precautions. It does not represent any guarantee of the properties of the product. Sigma-Aldrich Inc., shall not be held liable for any damage resulting from handling or from contact with the above product. See reverse side of invoice or packing slip for additional terms and conditions of sale.

11.9.2 MSDS for Nickelocene (Bis(cyclopentadienyl)nickel(II))

SIGMA-ALDRICH

Material Safety Data Sheet

Version 3.0
Revision Date 12/29/2008
Print Date 03/19/2009

1. PRODUCT AND COMPANY IDENTIFICATION

Product name	:	Bis(cyclopentadienyl)nickel(II)
Product Number	:	N7524
Brand	:	Aldrich
Company	:	Sigma-Aldrich 3050 Spruce Street SAINT LOUIS MO 63103 USA
Telephone	:	+1 800-325-5832
Fax	:	+1 800-325-5052
Emergency Phone #	:	(314) 776-6555

2. COMPOSITION/INFORMATION ON INGREDIENTS

Synonyms	:	Nickelocene Di(cyclopentadienyl)nickel(II)
Formula	:	$C_{10}H_{10}Ni$
Molecular Weight	:	188.88 g/mol

CAS-No.	EC-No.	Index-No.	Concentration
Bis(η5-2,4-cyclopentadien-1-yl)nickel			
1271-28-9	215-039-0	-	-

3. HAZARDS IDENTIFICATION

Emergency Overview

OSHA Hazards
Flammable Solid, Target Organ Effect, Toxic by ingestion, Skin sensitizer, Carcinogen

Target Organs

Lungs

HMIS Classification

Health Hazard:	2
Chronic Health Hazard:	*
Flammability:	0
Physical hazards:	3

NFPA Rating

Health Hazard:	2
Fire:	0
Reactivity Hazard:	3

Potential Health Effects

Inhalation	May be harmful if inhaled. May cause respiratory tract irritation.
Skin	May be harmful if absorbed through skin. May cause skin irritation.
Eyes	May cause eye irritation.
Ingestion	Toxic if swallowed.

4. FIRST AID MEASURES

General advice
Consult a physician. Show this safety data sheet to the doctor in attendance.Move out of dangerous area.

If inhaled
If breathed in, move person into fresh air. If not breathing give artificial respiration Consult a physician.

In case of skin contact
Wash off with soap and plenty of water. Consult a physician.

In case of eye contact
Rinse thoroughly with plenty of water for at least 15 minutes and consult a physician.

If swallowed
Do NOT induce vomiting. Never give anything by mouth to an unconscious person. Rinse mouth with water. Consult a physician.

5. FIRE-FIGHTING MEASURES

Flammable properties

Flash point	no data available
Ignition temperature	no data available

Suitable extinguishing media
Use water spray, alcohol-resistant foam, dry chemical or carbon dioxide.

Special protective equipment for fire-fighters
Wear self contained breathing apparatus for fire fighting if necessary.

Further information
Use water spray to cool unopened containers.

6. ACCIDENTAL RELEASE MEASURES

Personal precautions
Use personal protective equipment. Avoid dust formation. Avoid breathing dust. Ensure adequate ventilation. Remove all sources of ignition. Evacuate personnel to safe areas.

Environmental precautions
Prevent further leakage or spillage if safe to do so. Do not let product enter drains.

Methods for cleaning up
Contain spillage, and then collect with an electrically protected vacuum cleaner or by wet-brushing and place in container for disposal according to local regulations (see section 13). Keep in suitable, closed containers for disposal.

7. HANDLING AND STORAGE

Handling
Avoid exposure - obtain special instructions before use. Avoid formation of dust and aerosols.
Provide appropriate exhaust ventilation at places where dust is formed. Keep away from sources of ignition - No smoking. Take measures to prevent the build up of electrostatic charge.

Storage
Keep container tightly closed in a dry and well-ventilated place. Store in cool place.

Handle and store under inert gas. Light sensitive.

8. EXPOSURE CONTROLS/PERSONAL PROTECTION

Components with workplace control parameters

Components	CAS-No.	Value	Control parameters	Update	Basis
Bis(η5-2,4-cyclopentadien-1-yl)nickel	1271-28-9	TWA	1 mg/m3	1993-06-30	US. Department of Labor - Occupational Safety and Health Administration (OSHA) Permissible Exposure Limits (PEL) 29 CFR 1910.1000 Air Contaminants.
		TWA	1 mg/m3	1989-03-01	US. Department of Labor - Occupational Safety and Health Administration (OSHA) 29 CFR 1910.1000 Z-1-A
		TWA	0.2 mg/m3	1998-09-01	US. American Conference of Governmental and Industrial Hygienists Threshold Limit Values for Chemical Substances in the Work Environment; Annual Reports for the Year 2004:Committees on Threshold Limit Values (TLVs) and Biological Exposure Indices (BEIs)
Remarks	Confirmed human carcinogen. Adopted Values enclosed are those for which changes are proposed. Consult the Notice of Intended Changes for current proposal. See Notice of Intended Changes. Substance identified by other sources as a suspected or confirmed human carcinogen.				

Personal protective equipment

Respiratory protection
Where risk assessment shows air-purifying respirators are appropriate use a full-face particle respirator type N100 (US) or type P3 (EN 143) respirator cartridges as a backup to engineering controls. If the respirator is the sole means of protection, use a full-face supplied air respirator. Where risk assessment shows air-purifying respirators are appropriate use a full-face particle respirator type N99 (US) or type P2 (EN 143) respirator cartridges as a backup to engineering controls. If the respirator is the sole means of protection, use a full-face supplied air respirator. Use respirators and components tested and approved under appropriate government standards such as NIOSH (US) or CEN (EU).

Hand protection
Handle with gloves.

Eye protection
Safety glasses

Skin and body protection
Choose body protection according to the amount and concentration of the dangerous substance at the work

place.

Hygiene measures
Avoid contact with skin, eyes and clothing. Wash hands before breaks and immediately after handling the product.

9. PHYSICAL AND CHEMICAL PROPERTIES

Appearance

Form	solid

Safety data

pH	no data available
Melting point	171 - 173 °C (340 - 343 °F)
Boiling point	no data available
Flash point	no data available
Ignition temperature	no data available
Lower explosion limit	no data available
Upper explosion limit	no data available
Water solubility	no data available

10. STABILITY AND REACTIVITY

Storage stability
Stable under recommended storage conditions.

Conditions to avoid
Heat, flames and sparks.

Materials to avoid
Strong oxidizing agents

Hazardous decomposition products
Hazardous decomposition products formed under fire conditions. - Carbon oxides, Nickel/nickel oxides

11. TOXICOLOGICAL INFORMATION

Acute toxicity

LD50 Oral - rat - 490 mg/kg

Irritation and corrosion

no data available

Sensitisation

May cause allergic skin reaction.

Chronic exposure

Carcinogenicity - rat - Intramuscular
Tumorigenic:Neoplastic by RTECS criteria. Blood:Lymphomas including Hodgkin's disease. Tumorigenic:Tumors at site or application.

Carcinogenicity - rat - Intramuscular

Tumorigenic:Equivocal tumorigenic agent by RTECS criteria. Musculoskeletal:Tumors. Skin and Appendages: Other: Tumors.

This is or contains a component that has been reported to be carcinogenic based on its IARC, OSHA, ACGIH, NTP, or EPA classification.

IARC: Group 1 - Carcinogenic to humans (Bis(η5-2,4-cyclopentadien-1-yl)nickel)

NTP: NTP known to be carcinogenic (Bis(η5-2,4-cyclopentadien-1-yl)nickel)

OSHA: No component of this product present at levels greater than or equal to 0.1% is identified as a carcinogen or potential carcinogen by OSHA.

Signs and Symptoms of Exposure

To the best of our knowledge, the chemical, physical, and toxicological properties have not been thoroughly investigated.

Potential Health Effects

Inhalation	May be harmful if inhaled. May cause respiratory tract irritation.
Skin	May be harmful if absorbed through skin. May cause skin irritation.
Eyes	May cause eye irritation.
Ingestion	Toxic if swallowed.
Target Organs	Lungs,

Additional Information
RTECS: QR6500000

12. ECOLOGICAL INFORMATION

Elimination information (persistence and degradability)

no data available

Ecotoxicity effects

no data available

Further information on ecology

no data available

13. DISPOSAL CONSIDERATIONS

Product
Burn in a chemical incinerator equipped with an afterburner and scrubber but exert extra care in igniting as this material is highly flammable. Observe all federal, state, and local environmental regulations. Contact a licensed professional waste disposal service to dispose of this material.

Contaminated packaging
Dispose of as unused product.

14. TRANSPORT INFORMATION

DOT (US)
UN-Number: 1325 Class: 4.1 Packing group: II
Proper shipping name: Flammable solids, organic, n.o.s. (Bis(η5-2,4-cyclopentadien-1-yl)nickel)
Marine pollutant: No
Poison Inhalation Hazard: No

IMDG
UN-Number: 1325 Class: 4.1 Packing group: II EMS-No: F-A, S-G

Proper shipping name: FLAMMABLE SOLID, ORGANIC, N.O.S. (Bis(η5-2,4-cyclopentadien-1-yl)nickel)
Marine pollutant: No

IATA
UN-Number: 1325 Class: 4.1 Packing group: II
Proper shipping name: Flammable solid, organic n.o.s. (Bis(η5-2,4-cyclopentadien-1-yl)nickel)

15. REGULATORY INFORMATION

OSHA Hazards
Flammable Solid, Target Organ Effect, Toxic by ingestion, Skin sensitizer, Carcinogen

DSL Status
This product contains the following components listed on the Canadian NDSL list. All other components are on the Canadian DSL list.

	CAS-No.
Bis(η5-2,4-cyclopentadien-1-yl)nickel	1271-28-9

SARA 302 Components
SARA 302: No chemicals in this material are subject to the reporting requirements of SARA Title III, Section 302.

SARA 313 Components

	CAS-No.	Revision Date
Bis(η5-2,4-cyclopentadien-1-yl)nickel	1271-28-9	1991-07-01

SARA 311/312 Hazards
Fire Hazard, Acute Health Hazard, Chronic Health Hazard

Massachusetts Right To Know Components

	CAS-No.	Revision Date
Bis(η5-2,4-cyclopentadien-1-yl)nickel	1271-28-9	1991-07-01

Pennsylvania Right To Know Components

	CAS-No.	Revision Date
Bis(η5-2,4-cyclopentadien-1-yl)nickel	1271-28-9	1991-07-01

New Jersey Right To Know Components

	CAS-No.	Revision Date
Bis(η5-2,4-cyclopentadien-1-yl)nickel	1271-28-9	1991-07-01

California Prop. 65 Components

	CAS-No.	Revision Date
WARNING! This product contains a chemical known in the State of California to cause cancer. Bis(η5-2,4-cyclopentadien-1-yl)nickel	1271-28-9	1989-10-01

16. OTHER INFORMATION

Further information

The above information is believed to be correct but does not purport to be all inclusive and shall be used only as a guide. The information in this document is based on the present state of our knowledge and is applicable to the product with regard to appropriate safety precautions. It does not represent any guarantee of the properties of the product. Sigma-Aldrich Co., shall not be held liable for any damage resulting from handling or from contact with the above product. See reverse side of invoice or packing slip for additional terms and conditions of sale.

11.10 Schematic for XRD Sample Holder

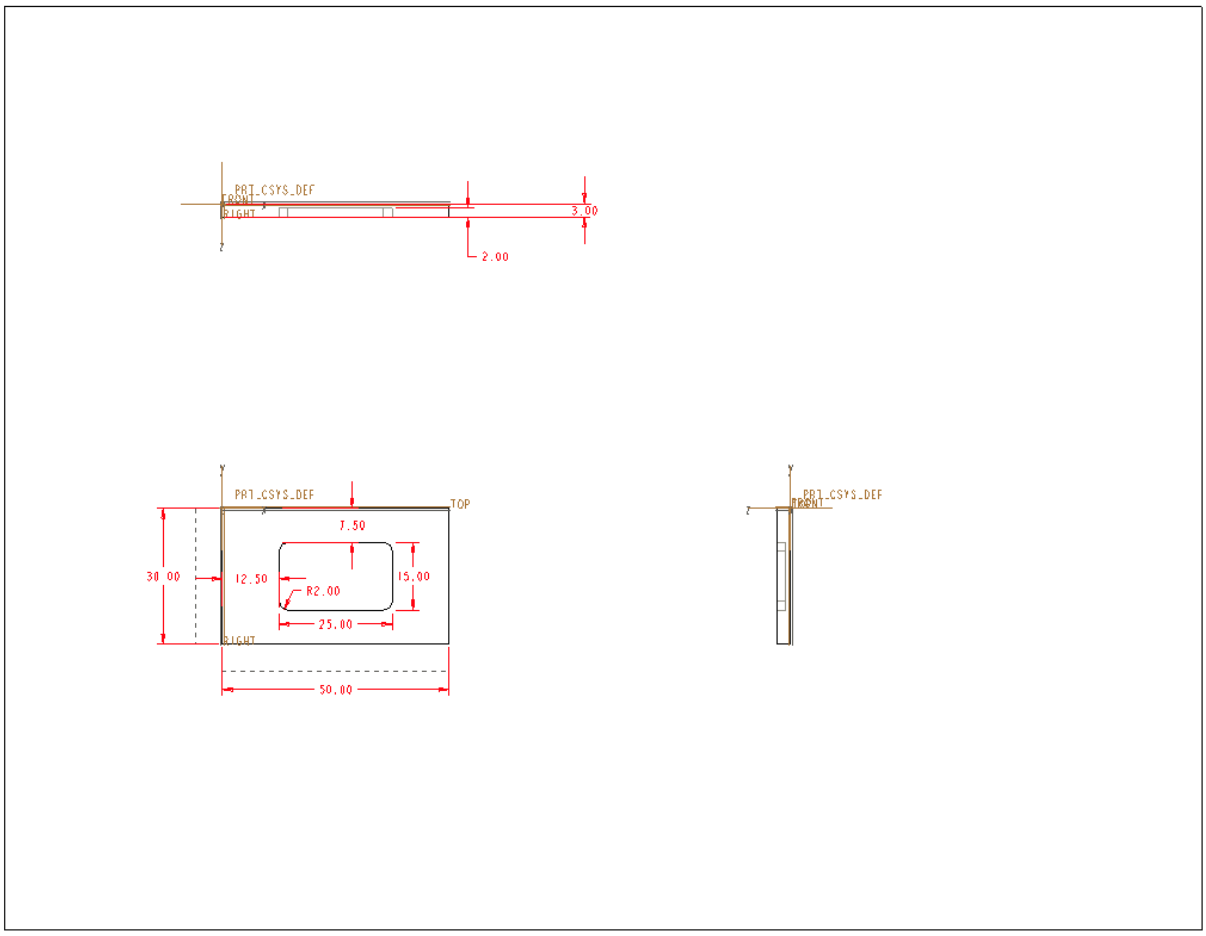

11.11 Acknowledgements

We would like to extend our thanks to the many people that made the completion of this project possible. These individuals include Dr. Boquan Li, Professor Engin Ayturk, Huanan Duan, who assisted the group in lab training and acquisition of X-ray Diffraction data, and Xiaoshu Dai, who assisted the group with the collection of SEM and EDS data.